Order Number 9405607

Long chain molecules in the molten state: Surface adsorption, near surface structure, and mutual-diffusion

Zhao, Xiaofeng, Ph.D.

City University of New York, 1993

U·M·I
300 N. Zeeb Rd.
Ann Arbor, MI 48106

Long Chain Molecules in the Molten State: Surface Adsorption, Near Surface Structure, and Mutual-Diffusion

by

XIAOFENG ZHAO

A dissertation submitted to the Graduate Faculty
in Physics
in partial fulfillment of the requirements for the degree of
Doctor of Philosophy,
The City University of New York.

1993

This manuscript has been read and accepted for the Graduate Faculty in Physics in satisfaction of the dissertation requirement for the degree of Doctor of Philosophy.

9/03/93
Date

Professor Azriel Z. Genack
Chair of Examining Committee

9/22/93
Date

Professor Joseph B. Krieger
Executive Officer

Professor Miriam H. Rafailovich, Advisor

Professor Jonathan C. Sokolov

Professor Ronald Dickman
Department of Physics, Herbert H. Lehman College

Dr. Steven A. Schwarz
Bellcore

Supervisory Committee

The City University of New York

To my parents,
Zhonghong Zhao *and* **Guigu Wharng,**
for the gift of the life they gave me.

—

献给我生命的创造、养育者
我的亲爱的父母：赵宗鸿、黄桂菊

Preface

The interaction between a surface and a polymer melt is the primary focus of this thesis. In Chapters 2, the segregation of the component of lower surface energy in a binary mixture of polymers is studied. The surface segregation profile is compared with the mean-field prediction, and the process of surface segregation is found to be controlled by the diffusion in the bulk. In Chapter 3, the end grafted chain in a melt matrix is profiled. The thermodynamic balance between the end grafted chains and the free chain is analyzed. The end-labeling of chains strengthens the ability of the chain to bind to the surface, and the stretching of the end grafted chain is proved to be a controlling fact limiting the brush density. The growth of the grafted layer as a function of time is studied in Chapter 4. In order to graft more chains to a surface with high coverage, the chain must penetrate the existing brush, and this becomes a controlling process.

The structure of a chain near a surface needs to be known in order to make more quantitative analysis. Such knowledge is currently not available although a reflecting surface model is proposed in Chapter 5.

Chapter 6 deals with the mutual-diffusion of compatible linear chains. It is observed that the broadening of the interfacial width scales as the 1/4 power of the diffusion time for a time scale much longer than the reptation time. Attempts are made to rule out several possible side effects. It is speculated that the anomalous behavior is either due to small molecular residue in the sample or due to the long chain nature of the polymer itself. If the former possibility can be ruled out, the validity of applying the reptation model to polymer diffusion over small distances might be under challenge.

The technique of dynamic secondary ion mass spectrometry (SIMS) is used in all experimental studies. SIMS is an established technique and its application in polymer science has been around for quite some time. The quantitative application in depth profiling was not very successful until recently. In Chapter 1, the technique is reviewed and procedures that ensure correct extraction of depth profiles from raw SIMS data are discussed.

Acknowledgements

First of all, I want to express my sincere gratitude and deep appreciation to my dissertation advisor, Professor Miriam H. Rafailovich and my co-advisor, Professor Jonathan C. Sokolov, who step by step, led me to explore the scientific community in general and to study the entangled spaghetti-like macromolecule in specific. Starting with little research experience, to become capable of working independently, I learned a great deal from their patient teachings and instructions.

I am deeply indebted to our long time collaborator Dr. Steven A. Schwarz of Bellcore for his generous help in doing the SIMS experiments. He taught me how to operate the SIMS instrument and helped me, from his expertise in SIMS, getting good understanding of the technique. I am deeply indebted to Dr. Barry Wilkens of Bellcore for his help in doing RBS and FRES experiments. I would also like to express my

gratitude towards Bellcore for its broad support of scientific research.

The final form of the dissertation benefitted significantly from discussions with the members of Examining Committee. I would like to especially acknowledge my advisors and Dr. Steven A. Schwarz for carefully correcting the English mistakes.

My thanks goes to Dr. T. D. Lee for organizing the CUSPEA program that opened the door of opportunity to me.

I can't help but mention those of my friends with whom we have stayed "under the same roof" for a long period of time. They are Cheng-Ming Ma and Shu-ling Wu, C. W. Liao and Lei Ke, Yan Wei and Yizi Cai, to name a few. We spent a lot of our leisure time together. We tried to share some knowledge with each other in different disciplines. I want also to thank the long time friend of our family, George Xiaoye Wu and Hongbin Ge and their adorable little daughter Ann☺. Having these friends with the same culture background, I never had to sacrifice any fun to be in a foreign country, or to "forget my native language yet failing to master the English language spoken here".

The importance of the influence of my parents and sisters in my life can never be overstated. The caring, understanding, and encouragement from my parents helped me resist temptations and achieve success. My sisters inspired me to read all kind of books and reading in turn build my confidence that I will benefit for my whole life.

Finally, I want to express my thanks to my dearest lady, my wife, my ♥, Weizhong Zhao. Through all these years, she supported me, spiritually and materially, with her whole heart.

Contents

List of Tables

List of Figures

CHAPTER 1

Depth Profiling of Polymer Concentrations with Ion Scattering Techniques

Energetic ion beams are powerful tools for probing the surface or near surface properties of solids. Depending on their mass, charge, and energy, ion beams interact differently with solid materials. A light particle with high energy, such as an α particle with energy of a few MeV, can penetrate a few microns in an organic sample. A heavier particle with lower energy ($\sim$ 1 keV), however, is stopped within a few nanometers. Either type of ion beam is useful in probing the concentration profile of a sample. Coulombic elastic scattering from different depths of ion penetration is used in Rutherford backscattering spectrometry (RBS) and forward recoil elastic spectrometry (FRES) to map out the concentration profiles in a sample. The erosion of the sample surface by low energy heavy ion beams is the basis of the secondary ion mass spectrometry (SIMS) technique.

RBS, FRES, and SIMS are standard and widely available techniques. These are the main techniques used in this thesis work. FRES and RBS have been extensively described elsewhere[1,2] and hence only a brief discussion is presented. The quantitative analysis of SIMS profiles was developed specifically for the analysis of data in this thesis and will be described in more detail.[3]

1.1 RUTHERFORD BACKSCATTERING SPECTROMETRY AND FORWARD RECOIL ELASTIC SPECTROMETRY

The interaction of α particles with solids is well characterized. A high energy (2 - 3 MeV) α particle can penetrate deeply into a solid target (a few microns in organic solids). It loses energy as it passes by electrons in the target (electronic energy loss).† Since the mass of the electron is much smaller, the collisions with the electrons do not alter the path of the α particle significantly. A small cross section for elastic collision with target nuclei (Rutherford scattering) results in a small fraction of the incident particles deflected to large scattering angles.

When a particle of mass M_1 and energy E_0 makes an elastic collision with a target nucleus of mass M_2, the energy it retains after the collision is given by

$$K \equiv \frac{E_1}{E_0} = 1 - \frac{2M_1M_2}{(M_1+M_2)^2}(1-\cos\theta_c) \ , \qquad (1.1)$$

where θ_c is the scattering angle of the incident particle in the center of mass reference

†The ratio between the energy loss to nuclei and to electrons is estimated to be approximately 1/3600, the ratio of masses between electron and proton.

frame, which is related to the scattering angle of the incident particle in the laboratory reference frame, θ, by

$$\tan\theta = \frac{\sin\theta_c}{\cos\theta_c + M_1/M_2}. \tag{1.2}$$

If the target nucleus is located a distance z underneath the surface, the energy loss of the α particle in penetrating in and out of the material is

$$E(z) - E(0) = K\frac{dE}{dx}\bigg|_{E_{in}} \frac{z}{\cos\alpha} + \frac{dE}{dx}\bigg|_{E_{out}} \frac{z}{\cos\beta}, \tag{1.3}$$

where K is the kinetic factor defined by equation (1.1), dE/dx is the stopping power of the α particle in the material, α and β are the angles of the incident and scattering direction with respect to the normal of the surface ($\alpha + \beta = 180° - \theta$). dE/dx values for various elements are well known and tabulated by Anderson and Ziegler etc.[4] For energy loss in compounds, Bragg's rule essentially says that the energy loss to each constituent element is not effected by the presence of other elements.

In Rutherford backscattering spectrometry (RBS), the energy spectrum of backward scattered (θ close to 180°) α particles is used to analyze the depth concentration profile of the sample. Taking the spectrum at a large (back) scattering angle has several advantages. It can be seen from equation (1.1) that the energy loss is most sensitive to the mass of the target particle when the incident particle is backward scattered ($\cos\theta_c = -1$) and is less sensitive to the scattering angle, allowing a larger detector acceptance solid angle. The backward direction is free of the recoiled target particles. And (with the incident and scattering angle $\alpha = \beta = \theta/2$) the path length of the α particle in the material is minimized for a given penetration depth and less prone to

misalignment.

Polymers, where mass contrast is frequently obtained by deuterium substitution, can not be profiled by RBS since deuterium and protons do not scatter α particles to large angles. To profile deuterium and hydrogen, forward recoiled deuterium and hydrogen atoms are detected as a function of their emitted energy. The technique is called forward recoil elastic spectrometry (FRES). Since the scattering cross section of α particles (which would create a large background) is very large at forward angles, they must be blocked. This can be done by placing a mylar foil ($\simeq 10\,\mu$m thick) in front of the detector.[1] The stopping power of hydrogen or deuterium in mylar is considerably lower than that of α particles, since the protons and deuterons have only half of the charge and move faster than α particles. However, the straggling of the protons and deuterons as they penetrate the mylar foil significantly broadens the energy resolution, leading to an uncertainty in the emission depth of approximately 800 Å.[1]

Since α particles and other heavier particles have larger masses than hydrogen or deuterium, then with the same energy, their speeds are lower. It is possible therefore to measure the time it takes to travel a given distance, and electronically discriminate protons and deuterons from other particles.[5] A timing signal can be generated by placing a very thin (500 Å) carbon foil in the flight path; electrons produced when the particles pass though the carbon foil are detected by a channel plate detector. These electrons provide the start signal. A stop signal is obtained when the particle arrives at the solid state detector. The resolution is not strongly affected by the carbon foil since it is very thin. The spatial resolution obtained by this method is limited essentially by the energy resolution of the solid state detector ($\sim$ 15 keV or 250 Å in polystyrene).

1.2 SECONDARY ION MASS SPECTROMETRY (SIMS)

For many years, SIMS depth profiling has been widely applied in the research areas of semiconductors, metallurgy, and geology. It started gaining popularity in polymer research when high resolution profiling of polymer composition was desired. It was first used by Whitlow *et al.* in studies of polymer mutual-diffusion,[6] Russell *et al.* in studies of ordering of diblock copolymer,[7] and Jones *et al.* in studies of surface enrichment due to the isotopic effect.[8]

SIMS is not as well characterized as RBS and FRES for quantitative analysis. For the latter techniques, the cross section of the α particle in different materials and the stopping power of both α particle and proton in various materials is extensively studied. The Rutherford scattering cross section and the stopping power on various target atoms are not strongly affected by the neighboring atoms. Furthermore, since the mapping of the concentration profile in RBS and FRES is not a sequential process, the techniques are to a large extent immune to drifting of the beam current and detector efficiency. SIMS, however, measures the depth dependence with a sequential sputtering process. The sputtering rate and the ion yield in SIMS are sensitive to the sample composition. This makes it difficult to obtain precise concentration *vs.* depth profiles from samples which consist of very different components. In particular, when these components are immiscible, calibration samples (uniform films with differing composition) are difficult to make. However, isotopic labeling does not affect the sputtering rate significantly and thus is ideal for SIMS study.

The accurate control of the beam condition over a long running time is essential.

Due to slight variations of the sputtering conditions between runs, it is desirable to know extra information of the sample in order to effectively reduce the raw spectra. In this section, the characterization of SIMS is discussed in detail.

1.2.1 Description of the Technique

A schematic sketch of SIMS is shown in Figure 1.1. A low energy (1-keV to 10-keV) intermediate mass ion (such as Ar^+ or O_2^+), impinges upon a sample, losing its energy primarily through elastic collisions with the atomic cores of the target material (nuclear energy loss). The recoiled particle receives a portion of energy from the primary ion and collides with another particle, which in turn may recoil and collide with more particles. As a result of such a series of collisions some atoms can gain momentum toward the surface of the sample and enough energy to escape from the sample. The majority of sputtered atoms originate in the top monolayer of the sample. The ejected species can be single atoms (ions), as well as clusters of atoms (neutral or charged). The vast majority of ejected species are neutral, with a small amount being positively or negatively charged. The ratio of yields of ionized and neutral species is very sensitive to the conditions of the surface. In SIMS, the charged species — the secondary ions — are analyzed. If one wants to focus on the composition of the surface layer of the sample, static SIMS uses only a small dose of ions to sputter particles from the surface layer. To measure the depth concentration profile, the primary ion beam is focused and rastered across a small area of the sample repeatedly. As the surface of the sample is gradually eroded due to the ion sputtering, the change of the yield of various species in the secondary ions reveals the composition *vs.* depth profile of the sample. This process is

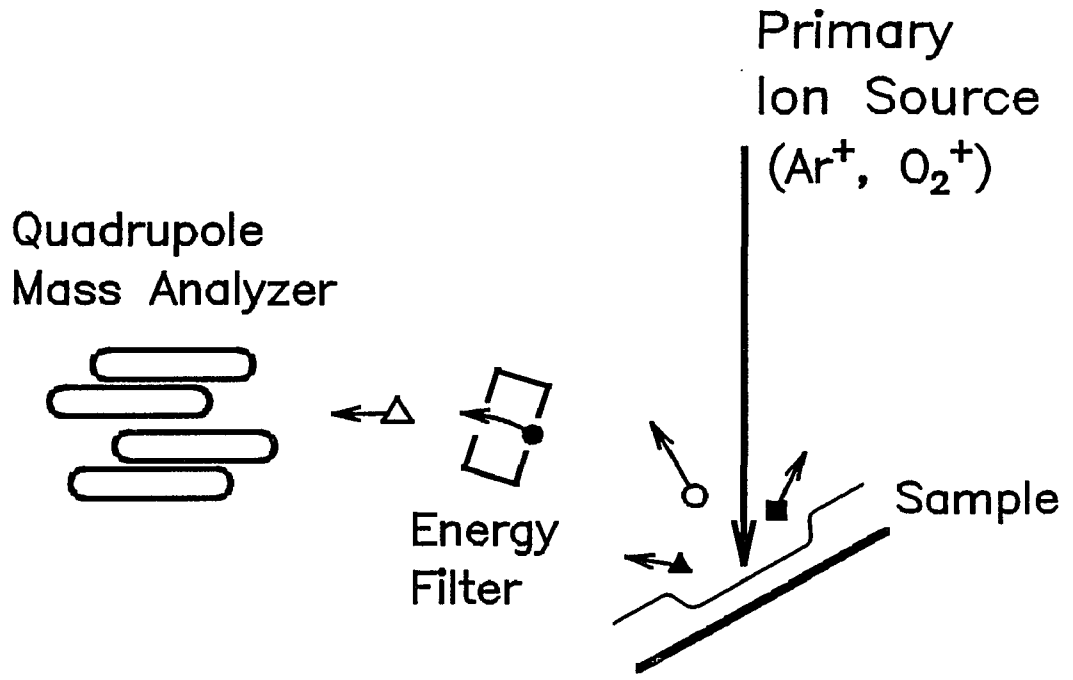

Figure 1.1 A schematic of SIMS. The rastered primary ion beam erodes the sample surface. The secondary ions ejected from the center of the sputtered crater are analyzed to obtain the composition information of the sample.

referred to as dynamic SIMS.

Samples consisting of mixtures of hydrogenated polymer and its deuterated counterpart are ideal for SIMS study. Deuterium and hydrogen have excellent mass contrast. The interference of H_2^- with the D^- signal (in contrast to a strong H_2^+ vs. D^+ interference) is extremely low (see Figure 1.2). This allows SIMS to profile, at reasonable signal to noise ratios, samples with very low deuterium concentration.

In the early stage of the sputtering, the surface of the sample is modified. Due to preferential sputtering effects, the composition of the surface is changed, which may change the sputtering rate as well.[10,15] The bombardment by the primary ion beam also

causes extensive recoiling (mixing) of the atoms in the target and broadens the depth profile. A steady state is typically achieved after the sample is sputtered for approximately 100 Å. In order to achieve the steady state sputtering before the region of interest is reached, it is desirable to cover the sample by a thin layer of polystyrene. This is especially important if the features close to the surface are being studied.

1.2.2 Characterizing SIMS

In order to characterize the SIMS technique, a test profile was taken on a bilayer sample of deuterated polystyrene (d-PS) and protonated polystyrene (h-PS). The polymer films were made by the spin casting technique from chlorobenzene solution. The silicon substrate was dipped briefly in dilute ($\sim 10\%$) HF solution to remove the oxide and then the d-PS bottom film was spun cast directly onto the substrate. The h-PS top film was spun cast on a microscope slide and then floated off in distilled water, from which it was picked up on top of the bottom film. This was accomplished by moving the bottom sample towards the floating film from the air side to avoid contamination of the interface from any impurities in the water. The bilayer was allowed to dry in air and then was annealed for 10 minutes at 180 °C, mostly to remove any strain produced by the spinning process. For the molecular weight of the polymers used, $M_w = 1\,950\,000$ for d-PS and $M_w = 2\,650\,000$ for h-PS, the broadening of the interface due to diffusion is expected to be less than 100 Å during the annealing time,[9] smaller than the ≈ 100 Å resolution of SIMS. The thicknesses of the top and bottom films, as measured by ellipsometry, were 1152 ± 6 Å and 910 ± 5 Å respectively, while the total thickness of the bilayer was

measured to be 2067 ± 10 Å.[‡] No change of the thickness was observed after annealing. The sample was covered by a thin ($\sim$ 80 Å) sacrificial layer of d-PS before the SIMS spectrum was taken.

The measurement was performed with a focused 2-keV, 20-nA Ar^+ beam at 30° off-normal incidence, rastering across a 0.5×0.5-mm^2 area. To eliminate interference from ions scattered from the edge of the sputtered crater, an electronic gate was set so that only secondary ions scattered from a square in the center 30% (0.15×0.15-mm^2) of the rastered area were counted. The raw spectra of selected species are plotted in Figure 1.2. Data points for each element were taken at 2 minute intervals. One should notice that the mass 2 signal (deuterium) is very low in the h-PS region. A large part of this signal can be attributed to the natural abundance (0.15%) of deuterium in the h-PS sample. This imposes a lower limit on the volume fraction of approximately 0.5% that SIMS can profile.

1.2.3 Sputtering Rate

It has been observed that for organic samples the sputtered crater depth as a function of sputtering time (the sputtering rate) of SIMS is controlled mainly by the effective content of carbon atoms in the sample.[10] The presence of certain elements, or the molecular structure, in the sample may change the sputtering rate unpredictably. For isotopically

---

[‡]The thicknesses of individual films were chosen such that the ellipsometry result is most accurate, i. e. both thickness and index of refraction can be accurately obtained. In calculating the total thickness of the sample from the ellipsometry result, the index of refraction is fixed to the average value (1.575) obtained from the measurement on the individual films.

labeled samples, such as samples made of hydrogenated polymer and its deuterated counterpart, (as most of samples in this thesis are), the isotopic labeling should not significantly alter the sputtering rate. This is well demonstrated by the smooth carbon yield in Figure 1.2. The cover layer/h-PS, h-PS/d-PS, and d-PS/Si interfaces are positioned at $6.1 \pm .1$, $103.5 \pm .1$, and $181.5 \pm .1$ datapoints respectively. This gives a sputtering rate of $11.9 \pm .1$ Å per data point (6.0 Å/min) in the h-PS layer and $11.7 \pm .1$ Å per data point (5.9 Å/min) in the d-PS layer, which are equal within the experimental error.

The sputtering rate is usually stable during the process of a single sample run because of the ability to accurately control the beam energy and current. The sputtering rate may, however, be sensitive to many different factors which can not always reproduce exactly. Keeping the sputtering rate constant between samples is difficult, especially after a long period of time, or after the machine settings have been altered. It is experienced that the sputtering rate can vary by as much as 15%. Although frequent checks of the sputtering rate, using samples with known thickness, can limit the uncertainty in sputtering rate within a few percent, far more accurate sputtering rates can be obtained for samples that are not too thick (less than 1 micron), if the thickness of each sample is predetermined and the sample is run all the way to the substrate. Accurate measurement of the sample thickness can readily be obtained using techniques like ellipsometry. Alternatively, if the amount of one component in the sample is known well, the integral of that component can also be used for sputtering rate determination. The thickness method and integral method, in many cases can both be used to cross check with each other; especially when the run is unstable (as may occur in highly

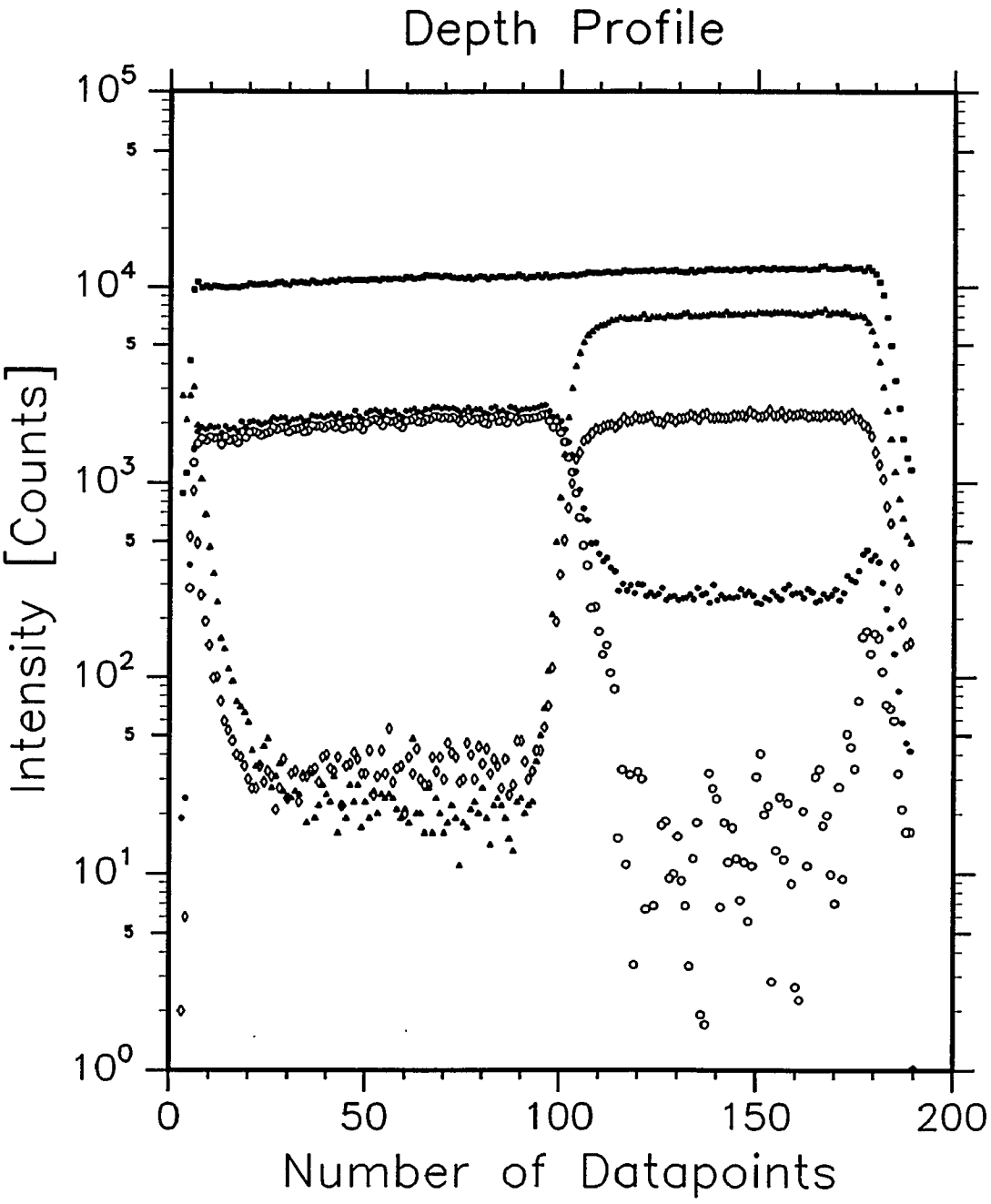

Figure 1.2 SIMS profile of C^- (■), D^- (▲), CD^- (◇), raw CH^- (●), and net CH^- (○) of a h-PS/d-PS (1152±6 Å/910±5 Å) bilayer sample.

insulating thick samples) so that drifting of the sputtering rate is suspected. For thicker samples where sputtering through is not practical, complementary methods, RBS or FRES for example, are desirable.

1.2.4 Ion Yield and Volume Fraction

The measured yield of different species may vary between runs, and thus gives only an approximate volume fraction of the components in the sample. To determine the volume fraction more precisely, we usually calibrate to part of the sample where the volume fraction has reason to be considered known well, such as in the bulk of the sample, or to the integral of the component over the sample. However, it is known that the ion yield is not strongly affected (within 5-6%) by the isotopic difference in the sputtered species when their mass differences are within 10%.[11,12,13] For example in Figure 1.2, the raw CH^- (mass 13 a. m. u.) signal, $S_{(13)}$, also includes the signal from $^{13}C^-$, which is expected to have the same ionization probability as $^{12}C^-$. So the net CH^- intensity, S_{CH^-}, is given by

$$S_{CH^-} = S_{(13)} - f_1 f_2 S_{(12)} \ . \qquad \textbf{(1.4)}$$

with f_1 the abundance of ^{13}C in the sample and f_2 incorporating the difference in time spent in counting. Such correction is significant since C^- yield is one order of magnitude higher than the CH^- yield. S_{CH^-} so calculated (using $f_1 = 0.0111$, the natural abundance of ^{13}C, and $f_2 = 2$) is plotted in Figure 1.2 as open circles (○) and indeed achieves approximately the same maximum level as S_{CD^-} (◇). (The raw CD^- (mass 14 a. m. u.) signal should also be corrected for the $^{13}CH^-$ signal by taking $S_{(14)} - f_1 S_{CH^-}$,

but such correction is important only for low deuterium concentration samples). Obviously, the ratio between the net CH^- (S_{CH^-}) and CD^- (S_{CD^-}) intensities is a good indication of the deuterium volume fraction. Volume fraction determined in this way is usually accurate within 5%. However, since the carbon yield is much higher than that of CH, the signal to noise ratio of CH spectrum is severely limited.

1.2.5 Spatial Resolution

The penetration of the primary ions and the recoil of the target atoms broadens the

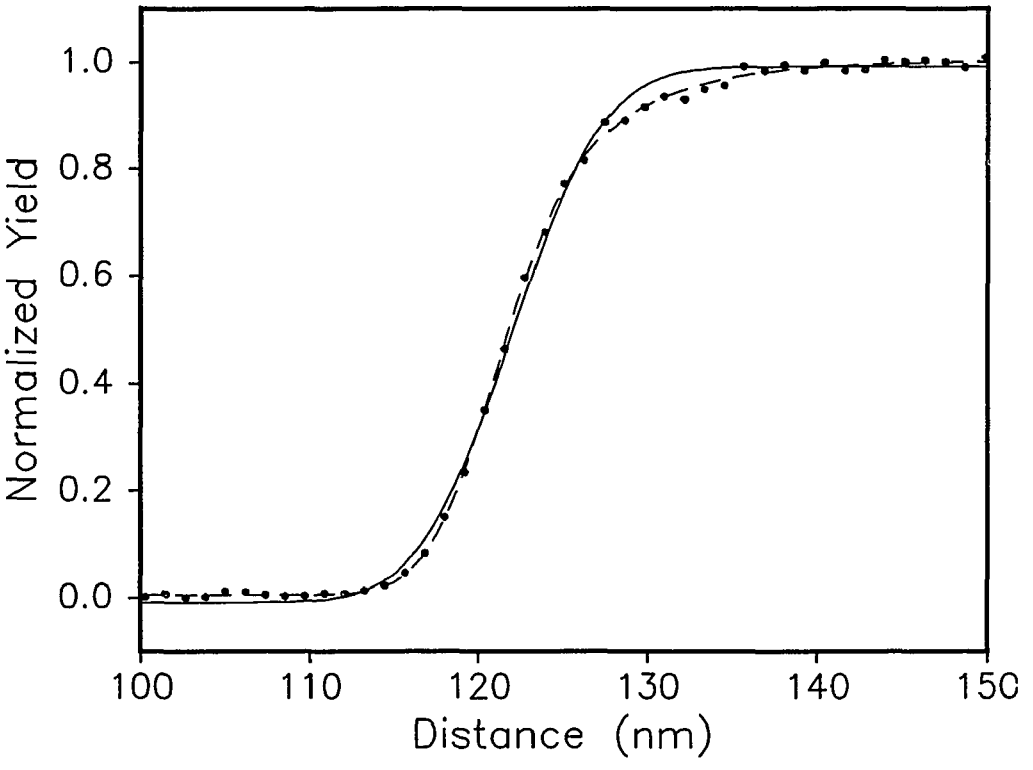

Figure 1.3 The interface of an h-PS/d-PS bilayer sample as measured by SIMS. The solid line is the fit by error function with $\sigma = 42$ Å. The dashed line is the fit by eq (1.5).

interface. The variation of the film thickness will also reduce the sharpness of the measured interface. The spatial resolution of SIMS can be estimated by fitting the width of the rising edge of the spectrum taken from the test sample (Figure 1.3). The solid line represents the best fit by an error function which gives the standard deviation, σ, of 42 ± 1 Å, corresponding to a FWHM of 100 ± 3 Å. (This interfacial width includes the real interface roughness and the broadening resulting from the preanneal of the sample which is estimated to be within 10 - 50 Å range.)

Several samples similar to the test sample with different top layer thickness were measured. Table I is a summary of the resolution as a function of the interface depth. From the table we can conclude that the depth resolution does not degrade significantly for the depth range studied. The constant resolution over a depth of a few thousand angströms is vividly demonstrated[14] by the profile taken on a diblock copolymer sample. The diblock copolymer forms a lamella structure with a period of 400 Å with sharp interfaces. The shape of each lamella layer profiled by SIMS repeats exactly, indicating that the broadening of interface by SIMS is steady over the distance profiled.

Table I SIMS Resolution at Different Depths.
Data is Obtained from Different Samples.

Depth (Å)	Resolution, σ (Å)	σ' (Å)	ξ (Å)
443	46	41	52
896	54	51	52
1150	42	33	52
2245	43	–	–

A close look at Figure 1.3 reveals that the Gaussian function does not represent SIMS resolution very well. The broadening of the profile to the forward direction is larger than that to the backward direction. The broadening to the forward direction is also more robust than a Gaussian function. An empirical function representing SIMS resolution well is given by,

$$\int_{-\infty}^{x} p(x')dx' = \frac{1}{\pi}\cdot\left[1+\mathrm{erf}(x/\sqrt{2}\sigma')\right]\cdot\tan^{-1}(e^{x/\xi}) \quad . \tag{1.5}$$

Note that $p(x)$ approaches to zero asymptotically as $e^{-x/\xi}$ for $x\rightarrow+\infty$ (Laplace probability distribution) and $e^{-x^2/2\sigma'^2}$ for $x\rightarrow-\infty$ (Normal distribution). It can be seen from Figure 1.3 that (1.5) fits the interface profile much better. Fitting results of other measured profiles of originally sharp interfaces using (1.5) are listed in Table I.

1.2.6 Effects of the Substrate

When the feature of interest is next to the Si substrate, it might be necessary to precisely determine the position of the interface relative to the D^- or CD^- signals. Figure 1.4 is an expansion of the profile of Figure 1.2 near the silicon substrate. The profiles are normalized for the purpose of comparison and the lines are fit by error functions (for carbon and CH + CD profiles) or Gaussian function (for oxygen profile). It is observed that the (50% point) falling edge of the C signal (183.07 ± 0.05) agrees with the oxygen peak (182.9 ± 0.1) but lags the falling edge of CH + CD signal (181.9 ± 0.1) by an effective distance of 12 ± 2 Å. This suggests that a layer of carbon is accumulated at the substrate in the course of the sputtering. This is consistent with the observation that (a)

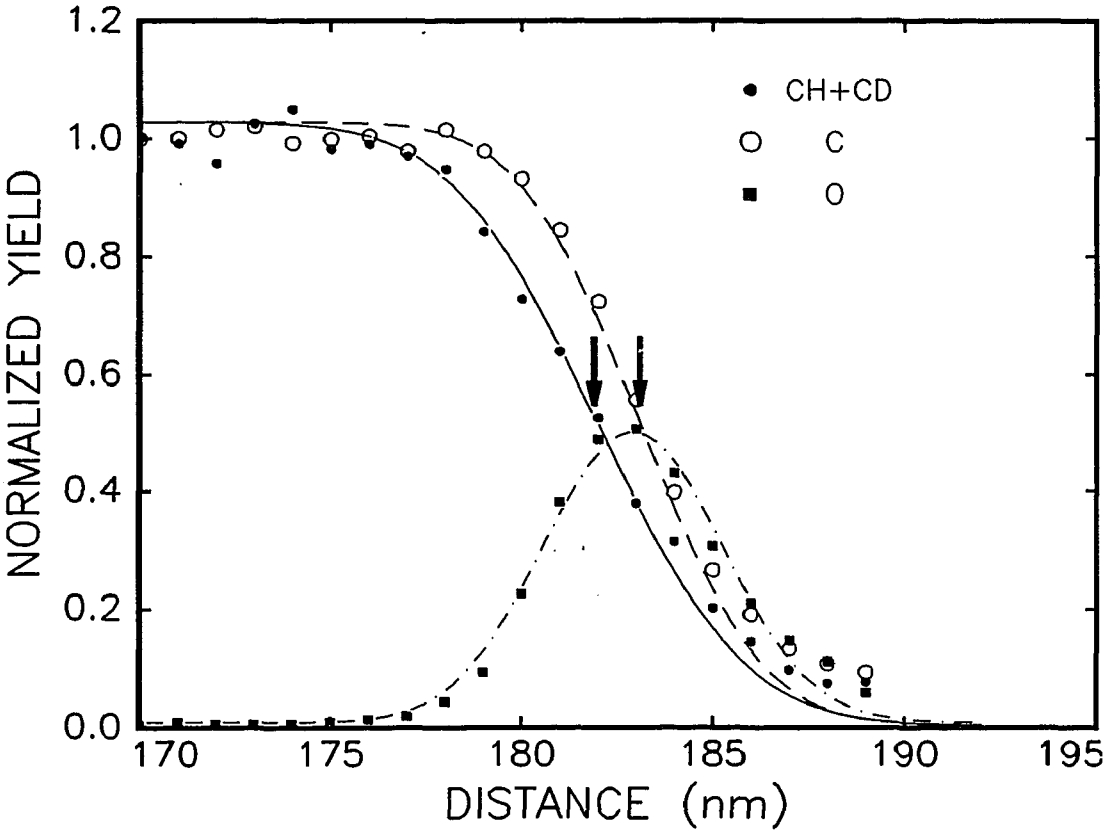

Figure 1.4 The expanded portion of the falling edge next to the silicon substrate of (●) CH + CD signal, (○) C signal, and the oxygen peak resulting from oxidation on silicon surface (■).

carbon has high sputtering resistance and thus is the controlling factor for the sputtering rate for most organic samples,[10] and (b) after treatment by high energy (MeV) Ar^+ beam, most polymers are ultimately transformed into a very carbon rich substance.[15,16] Further more, it can also been seen from Figure 1.2, the CH signal possess a small peak at the back edge where no hydrogenated polymer should present. This peak is equivalent to a thin polystyrene layer of 6 ± 1 Å thick. From the experience of many samples when the back is excepted to be covered mainly by deuterated polymer, the appearing of such a peak is more a rule than an exception. The effective thickness

of these CH peaks ranges around 10 ± 5 Å. Obviously, the possibility of existence of contamination at the silicon surface can not be completely ruled out, but given the care taken during the sample preparation, such contamination is very unlikely. Since both the effects are relatively small and less consistent between samples, they are not well characterized at this moment. In practice, the position of the substrate is determined from the falling edge (50% point) of the combined spectra of CH and CD.

1.3 MUTUAL-DIFFUSION PROFILE MEASURED BY SIMS

A bilayer sample of dPS ($M_w = 713\,000$, $M_w/M_n = 1.05$) and hPS ($M_w = 770\,000$, $M_w/M_n = 1.04$) with initially sharp interface was annealed at 170 °C for 2 hours. The profile obtained by SIMS is plotted in Figure 1.5. The dashed curve is the least square fit to the data by an error function. The good statistics of the data enables the detection of a small discrepancy between the profile and the error function. This discrepancy indicates that the mutual-diffusion coefficient is a function of dPS volume fraction. Such a volume fraction dependence can be obtained from the profile using equation (6.1). The result is plotted in Figure 1.6 as open circles. The mutual-diffusion coefficient is smaller at the region near equal mixture of dPS and hPS. This is in agreement with the "*fast model*" prediction, equation (6.1).[17] The least square fit to the data gives a value of $\chi = 0.00016 \pm 0.00001$.

The volume fraction dependence of the mutual-diffusion coefficient was measured previously by Green *et al.* using FRES on a series of bilayer samples with small volume fraction difference.[18] The value of χ resulted from fitting of their data (at 174 °C) is

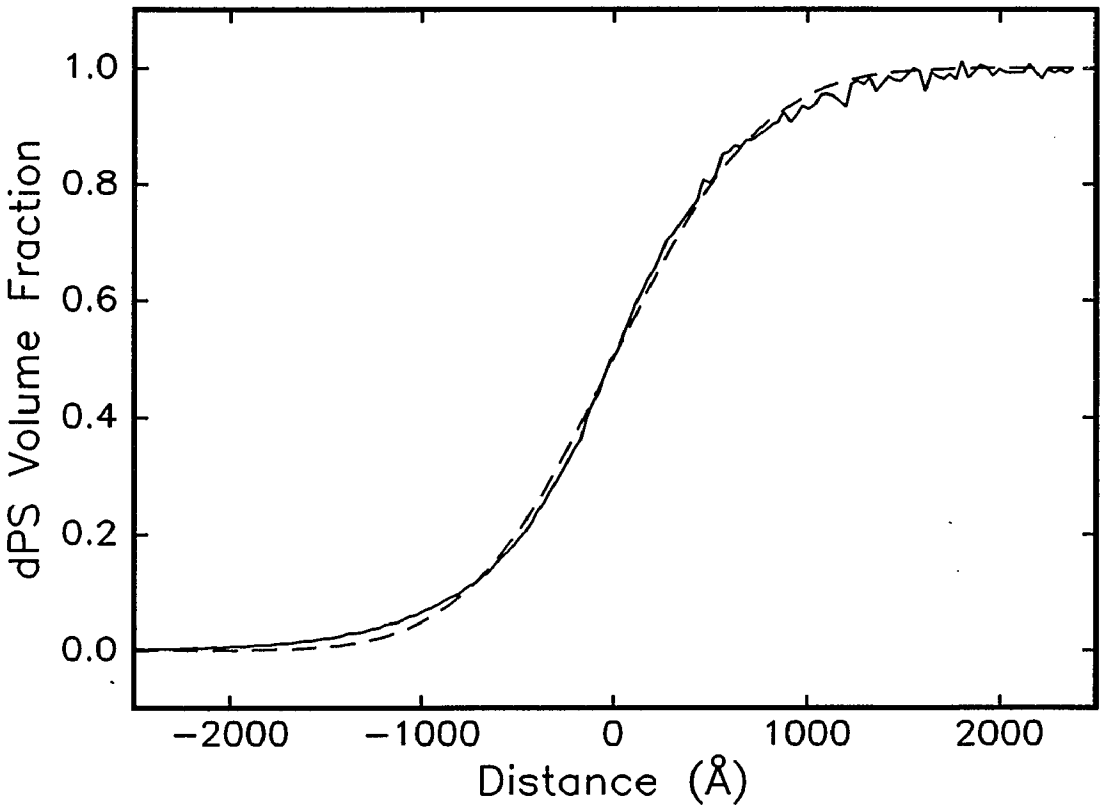

Figure 1.5 The interfacial profile (solid curve) as measured by SIMS of a dPS and hPS bilayer with initially sharp interface, and the error function fit (broken curve) to the profile.

0.00018. The calculated curve using this χ value is draw on Figure 1.6 as the dashed curve, which appeared fitting the data at the left half side better. On the other hand, χ measured by small angle neutron scattering by Bates *et al.* is 0.00016 ± 0.00004.[19]

The above example demonstrated the advantage of good statistics SIMS can provide. Within the range of volume fraction between 0.4 to 0.6, however, both the slope and the integral of the profile can be determined from the data with good confidence. Yet the diffusion coefficient within this range does not fit the theoretical curve very well. A slight change of the sputtering rate and ion yield during the run may explain this error.

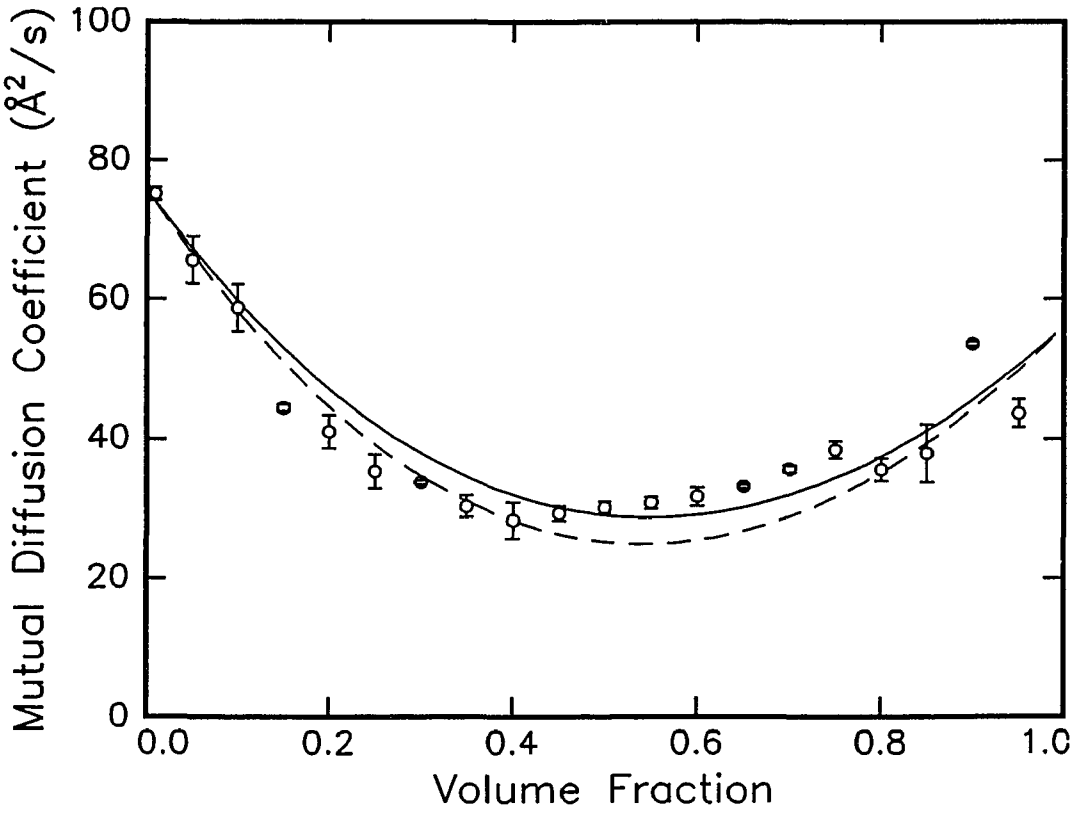

Figure 1.6 The diffusion coefficient as a function of volume fraction obtained from Figure 1.5. The "fast model" fit (solid curve) gives χ=.00016. The dashed curve is the calculation using χ=.00018.

1.4 SUMMARY

For many features in polymer physics — such as the surface enrichment of the d-PS component in a d-PS/h-PS blend discussed in the previous chapter, and the configuration of the polymer chain near a surface that will be discussed later in this thesis — the characteristic length scale is on the order of R_g, the polymer radius of gyration, which typically ranges from a few tens of angströms to several hundred angströms. The abilities of the ion scattering techniques discussed above in measuring concentration

Table II Comparison of Techniques: SIMS, RBS, FRES, XR, NR

	SIMS (2-keV, 20-nA)[a]	SIMS (6-keV, 100-nA)[a]	RBS, TOF-FRES
Resolution (FWHM)	100 Å	300 Å	250 Å
Probing depth	$< 1\,\mu m$	$< 3\,\mu m$	$< 1\,\mu m$
Typical sampling area	$0.5 \times 0.5\,mm^2$		$1 \times 1\,mm^2$, $1 \times 4\,mm^2$
Contrast provided by	Nuclear mass differences or/and preferential cluster formation		Nuclear mass differences
H and D contrast	excellent		none, good
Data type	Real space profile convolved by the resolution		Real space profile convolved by the Resolution
Facilities	Ion source, high vacuum systems, mass spectrometer (in house)		Van de Graff accelerator, vacuum systems, solid state detector (in house)
Acquisition time	600 Å/hr	3000 Å/hr	~ 1 hour

[a] $0.5 \times 0.5\,mm^2$ rastering area, 30° off-normal incidence.

Table II continued

	FRES	X-ray Reflectivity	Neutron Reflectivity
Resolution (FWHM)	800 Å	~ 10 Å	10 - 20 Å
Probing depth	< 1 μm	< 5000 Å	< 1 μm
Typical probing area	1 × 4 mm	0.5 × 5.0 mm	Large sample (> 50 × 50 mm) is desired to reduce the data acquisition time
Contrast provide by	Nuclear mass difference	Electron density	Nuclear scattering length
H and D contrast	good	none	excellect
Data type	Real space profile convolved by the resolution	*k*-space profile convolved by *k*-space resolution	*k*-space profile convolved by *k*-space resolution
Facilities	Ion accelarator, vacuum systems, solid state detector (in house)	synchrotron is desired for measurement of low reflectivity at large *k*	Reactor or spallation neutron source is required
Acquisition time	~ 1 hour	2 - 3 hours	> 12 hours

profiles on such a length scale are illustrated in Figure 1.7. The solid line is the profile calculated from equation (2.2) for $\phi_\infty = 0.18$ and $\phi_1 = 0.90$. The dotted line corresponds to the same curve convolved with a Gaussian function of full width half-maximum, FWHM = 800 Å, typical of the FRES resolution. From the figure it can be seen that, with this resolution, the shape of the profile is not resolved and only the total surface excess, z^*, is obtainable. The shape of the profile becomes apparent after an improvement of the resolution by a factor of 3, corresponding to that of TOF-FRES. Finally, with a resolution of 100 Å, which is achievable by SIMS by careful optimization of sputtering conditions, the decay length is well resolved. Further improvement of the

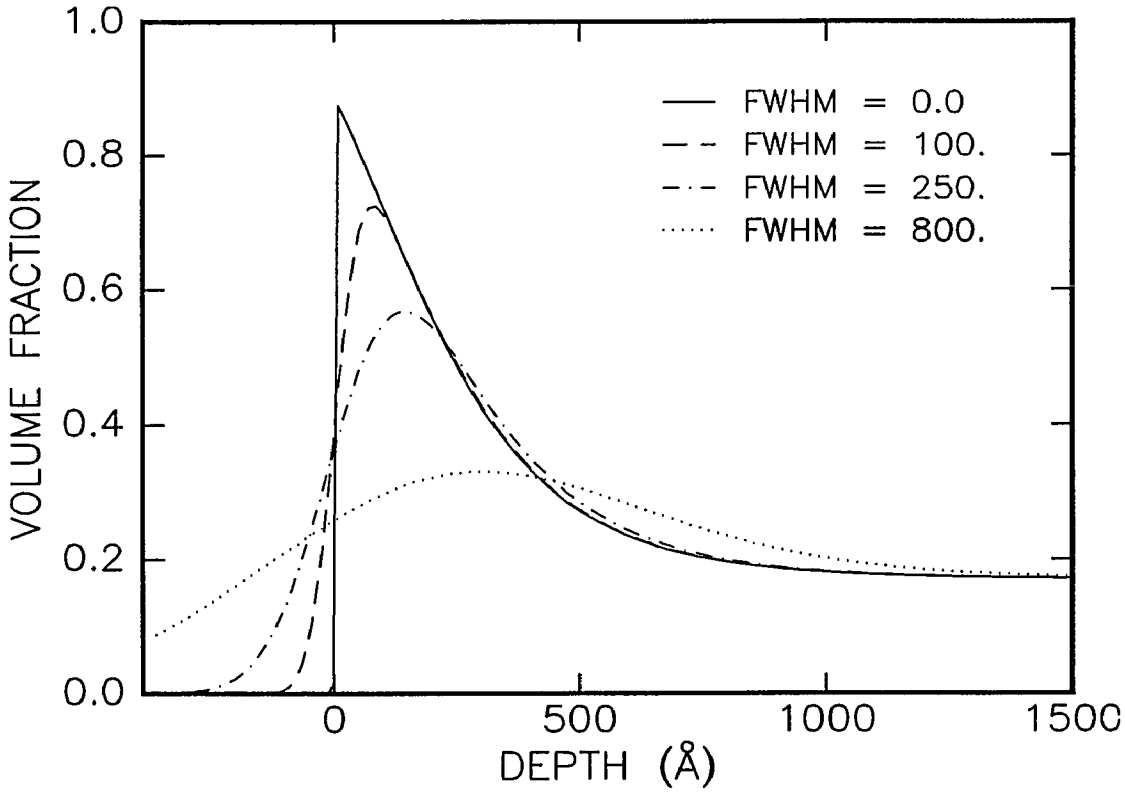

Figure 1.7 Effects of instrumental resolution (FWHM) on the determination of the shape of the concentration profile calculated from equation (2.2).

resolution, which would enable one to probe the very near surface region in the first 50 Å, is not currently possible with ion scattering techniques. In order to probe this region, neutron reflection is more appropriate.[8]

A comparison of advantages and disadvantages of ion scattering techniques as well as neutron and x-ray reflectivity is summarized in Table II. Comparing to other ion scattering techniques, SIMS provides the best resolution. There is no intrinsic restriction in SIMS for how deep it can profile. However, due to the slow sputtering rate, running SIMS at high resolution condition for samples thicker than 1 μm is unrealistic. Using a 100-nA beam at 6-keV (with the same area and incident angle) increases the sputtering rate by approximately a factor of five, with a spatial resolution around $\sigma = 120$ Å (FWHM = 300 Å).

Even though the systems for which SIMS can be applied for quantitative analysis are limited, and obtaining good data and reducing the raw data properly requires skill, the good depth resolution (100 Å), the ability to profile small concentration differences, and the straightforward interpretation of the profile makes SIMS a tool with unsurpassed advantages.

REFERENCES

1. P. J. Mills, P. F. Green, C. J. Palmstrøm, J. W. Mayer, and E. J. Kramer, *Appl. Phys. Lett.* **45,** 957 (1984).

2. L. R. Doolittle, *Nucl. Intr. and Meth.* **B9,** 344 (1985).

3. A reference in surface analysis techniques, including ion scattering techniques can be found in: L. C. Feldman and J. W. Mayer, *Fundamentals of Surface and Thin*

Film Analysis (North-Holland, New York, 1986).

4. J. F. Ziegler, *Helium stopping powers and ranges in all Elements* (Pergamon Press, New York, 1977); H. H. Anderson and J. F. Ziegler, *Hydrogen Stopping Power and Ranges in all Elements* (Pergamon Press, New York, 1977).

5. J. Sokolov, M. H. Rafailovich, R. A. L. Jones, and E. J. Kramer, *Appl. Phys. Lett.* **54,** 590 (1989).

6. S. J. Whitlow and R. P. Wool, *Macromolecules* **22,** 2648 (1989).

7. T. P. Russell, V. R. Deline, V. S. Wakharkar, and G. Goulon, *Bulletin Mater. Res. Soc.* October, 33 (1989).

8. R. A. L. Jones, L. J. Norton, E. J. Kramer, R. J. composto, R. S. Stein, T. P. Russel, A. Mansour, A. Karim, G. P. Felcher, M. H. Rafailovich, J. Sokolov, X. Zhao, and S. A. Schwarz, *Europhys. Lett.* **12,** 41 (1991).

9. P. F. Green and E. J. Kramer, *Macromolecules* **19,** 1108 (1986); *J. Mater. Res.* **1,** 202 (1986).

10. H. Gokan, S. Esho, and Y. Ohnishi, *J. Electrochem. Soc.* **130,** 143 (1983).

11. S. A. Schwarz, *J. Vac. Sci. Tech. A* **5,** 308 (1987).

12. U. Soedervall, H. Odelius, A. Lodding, and E. U. Engstroem, *Scanning Mirosc.* **1,** 471 (1987).

13. H. Gnaser, I. D. Hutcheon, *Phys. Rev. B* **35,** 877 (1987).

14. S. Zheng, (Private Communication).

15. D. Briggs and M. J. Hearn, *Vacuum* **36,** 1005 (1986).

16. D. E. Williams and L. E. Davis, *Characterization of Metal and Polymer Surfaces* (Edited by L. H. Lee), vol 2, P53, (Academic Press, New York, 1977).

17. E. J. Kramer, P. F. Green, and C. J. Palmstrøm, *polymer* **25,** 473 (1984).

18. P. F. Green and B. L. Doyle, *Phys. Rev. Lett.* **57,** 2407 (1986).

19. F. S. Bates and G. D. Wignall, *Phys. Rev. Lett.* **57,** 1429 (1986).

CHAPTER 2

Concentration Profiles at the Surfaces of d-PS/h-PS Blends

A miscible blend in contact with a surface is intrinsically an inhomogeneous system. The two components of the blend interact differently with the surface, therefore the surface composition is usually not the same as the bulk. The equilibrium surface profile is determined by the balance between the placement at the surface of the lower surface energy component and the cost of producing a composition gradient in the bulk. In the bulk (the region far away from the surface) where the effect of the surface vanishes, the blend approaches a homogeneous limit characteristic of the infinite system. Phenomena such as surface wetting (covering of the surface by a macroscopic layer of the lower surface energy component) have been observed in various binary mixtures of small molecules[1]. While the complete wetting is easily observable, the observation of

prewetting and the study of the wetting transition is difficult due to the short decay length in the small molecule fluids. The surface profile in a macromolecular system is much wider due to its small entropy of mixing. The surface profile may also depend on the molecular weight of the macromolecule, thus reveals the unique properties associated with the long chain nature of the macromolecule. The most complete studies thus far on surface segregation have been done on the deuterated polystyrene/hydrogenated polystyrene (d-PS/h-PS) system. This system is an ideal model system where a small difference in the monomer size and in the polarizability of the C−H and C−D bonds lowers the surface energy of the d-PS component and produces a small unfavorable bulk Flory interaction parameter, χ.[2] The surface excess of the d-PS component was first observed by Jones *et al.*[3] using the technique of forward recoil elastic scattering (FRES), and the decay for low bulk concentration was later probed by neutron reflectivity.[4]

Although the surface excess and long-range diffusion profiles that control the kinetics of segregation at long times can be readily studied by FRES, its poor depth resolution ($\sim$800 Å) precludes detailed measurements of the shape of either the non-equilibrium or equilibrium profile. Neutron (or x-ray) reflectivity is very sensitive to the scattering length density (or electron density) profile and thus to the shape of the depth concentration profile. However, the model profiles that can be fit to a particular reflectivity data are often not unique. And since the scattering length density (electron density) is a characteristic of the average of all components present at the same depth, the reflectivity data is also very sensitive to the features that are not of primary interest but are difficult to control during the sample preparation. Most, if not all, uncertainties

could probably be unraveled by either improved instrumental resolution or a larger range of reflectivity data, if the technology were able to deliver the capability. At the present time, the reflectivity technique is an excellent means of measuring the depth profile in greater detail only if sufficient information of the sample is already obtained which often means obtaining the result from a direct profiling method such as ion scattering.[5]

In order to accurately determine the shape of the concentration profile at the surface of the d-PS/h-PS blend and the dynamical factors involved in attaining equilibrium, we measured the composition at the surface of d-PS/h-PS blends using the techniques of secondary ion mass spectrometry (SIMS) and time of flight forward recoil elastic spectroscopy (TOF-FRES).[6] Under the conditions described later, these techniques have resolutions of 115 and 250 Å, respectively, and the data are straightforward to interpret in a model independent way. The results can then be used to test the predictions of the mean-field theory.

2.1 PREDICTIONS OF THE MEAN-FIELD THEORY

Several authors[7,8,9] have applied the mean-field formalism to investigate the phenomena of surface segregation in binary polymer blends. Most studies assumed a δ-function (nearest neighbor) interactions between the monomers and the surface. The theory can easily be extended to include long range interactions between the monomers and the surface providing that such interactions are known. The following discussion will be limited in the case of δ-function interactions.

Consider that a binary blend occupies the upper half space $z \geq 0$ of the coordinate

system, with use of the notation of Schmidt and Binder,[7] the total free energy per unit area of the polymer blend, of concentration, $\phi(z)$, is given by

$$\frac{F[\phi(z)]}{k_B T} = \int_0^\infty dz \left[G(\phi) - \Delta\mu\,\phi + \frac{a^2}{36\phi(1-\phi)} \left(\frac{d\phi}{dz} \right)^2 \right] + F_s \,, \qquad \textbf{(2.1a)}$$

where $G(\phi)$ is the Flory-Huggins free energy

$$G(\phi) = \frac{\phi}{N_A} \ln\phi + \frac{1-\phi}{N_B} \ln(1-\phi) + \chi\phi(1-\phi), \qquad \textbf{(2.1b)}$$

$\Delta\mu = \partial G(\phi)/\partial\phi\big|_{z=\infty}$ is the bulk chemical potential difference between the two components A and B, with polymerization indices N_A and N_B, respectively, a is the statistical segment length, and F_s is the "bare" surface free energy (the free energy contributed from the enthalpic interaction between the monomers and the surface only). In order to solve equation (2.1a) analytically, we assume that F_s is a function only of the surface concentration, ϕ_1, or equivalently that the interaction potential at the surface is a δ-function. The validity of this approximation will be discussed later. This approximation has the advantage that the solution to the integral equation becomes insensitive to the exact functional form assumed for $F_s(\phi_1)$. It simply provides a boundary condition for the segregation profile whose shape away from the surface is determined entirely by the bulk thermodynamic quantities, $G(\phi)$ and $\Delta\mu$.

The integral part of equation (2.1a) represents the increase of the free energy due to the concentration gradient. Minimizing the functional of equation (2.1a) yields a differential equation,

$$\frac{d\phi(z)}{dz} = \frac{6}{a}\left\{\phi(1-\phi)\left[G(\phi) - G(\phi_\infty) - \Delta\mu(\phi-\phi_\infty)\right]\right\}^{1/2}, \tag{2.2}$$

that determines the concentration profile, $\phi(z)$, for minimal increase of the free energy yet achieves a given concentration difference in the melt. This surface profile approaches to the asymptotic bulk volume fraction value exponentially as,

$$\phi(z) - \phi_\infty \propto e^{-z/\xi}. \tag{2.3}$$

Indeed when ϕ is close to ϕ_∞, $G(\phi)$ can be expanded in a power series,

$$G(\phi) = G(\phi_\infty) + \Delta\mu(\phi-\phi_\infty) + \frac{1}{2}\frac{\partial^2 G}{\partial\phi^2}\bigg|_{\phi_\infty}(\phi-\phi_\infty)^2, \tag{2.4}$$

then equation (2.2) is linearized to be

$$\frac{d(\phi-\phi_\infty)}{dz} = \frac{\phi-\phi_\infty}{\xi}, \tag{2.5}$$

where ξ is given by

$$\xi = \frac{a}{6}\left[\frac{1-\phi_\infty}{2N_A} + \frac{\phi_\infty}{2N_B} + \chi\phi_\infty(1-\phi_\infty)\right]^{-1/2}. \tag{2.6}$$

The total surface excess is determined by how strong the surface energy difference between the components is. With $d\phi/dz$ substituted by equation (2.2), minimizing equation (2.1a) with respect to ϕ_1 obtains the condition for the equilibrium surface enrichment:

$$-\frac{dF_s(\phi_1)}{d\phi_1} = \frac{a}{3}\left[\frac{G(\phi_1) - G(\phi_\infty) - \Delta\mu(\phi_1 - \phi_\infty)}{\phi_1(1-\phi_1)}\right]^{1/2}. \qquad (2.7)$$

The left-hand side of this equation yields the incremental bare surface energy saved by covering the surface with an extra low surface tension component, while the right-hand side is the incremental energy spent in establishing the segregation profile below the surface.

2.2 EXPERIMENT

The polymers used in this study were h-PS (Pressure Chemical Company) and d-PS (Polymer Laboratories Ltd) of molecular weight 1 800 000 ($M_w/M_n < 1.3$) and 1 030 000 ($M_w/M_n < 1.15$), respectively. The small-angle neutron scattering (SANS) experiments of Bates and Wignall[10] measured $\chi = -(2.9\pm0.4) \times 10^{-4} + (0.20\pm0.01)/T$, for a 50/50 blend of d-PS and h-PS. Assuming negligible concentration dependence of χ, the blend of the molecular weights used in this experiment has an upper critical solution temperature of 176 °C at a critical d-PS concentration $\phi_c = 0.57$. A series of blends with d-PS volume fraction, ϕ_∞, ranging from 0.005 to 0.33 were prepared, and films of 2-3 μm thick were spun cast onto thin silicon wafers from toluene solutions. The samples were then sealed in glass ampules in a vacuum of 10^{-6} Torr and heated in a vacuum oven at 184 °C for times ranging from 3 to 45 days. This temperature was chosen so as to be near the coexistence curve, but still in the one-phase region.

After annealing, the samples were examined by the technique of time of flight

forward recoil elastic scattering (TOF-FRES). TOF-FRES is similar to the standard FRES technique[6] except that the spatial resolution is improved by replacing the thick absorber foil used to stop the scattered α particles with a time of flight detector assembly (TOF) requiring only a thin foil to generate timing signals from passing ions. By simultaneously measuring the energy and transit time across a fixed gap for each particle, the device can discriminate electronically between the lighter and faster H and D ions and the slower α particles. For the typical FRES geometry, the energy resolution is about 15 keV, which translates into a depth resolution of approximately 250 Å for amorphous solid polystyrene,[5,11,12] as compared to 800 Å for FRES that uses a mylar foil ($\sim$ 10 μm) placed in front of the detector to physically stop the α particle.[5]

After TOF-FRES spectra are obtained, the samples were prepared for SIMS analysis, by floating onto their surface an additional $\sim$400-Å-thick PS film and evaporating a $\sim$60-Å-thick layer of gold on the whole assembly. No interfacial mixing between the components can occur in this process since both sample and coating films are in their glassy state. The purpose of the PS overlayer was to allow steady-state sputtering conditions to be established before the polymer blend surface region was exposed. The Au layer on the outermost surface provided a conducting path to ground in order to prevent charging of the nonconducting polymer film.

The sputtering was performed by using an Atomika 3000-30 ion microprobe and a 2-keV, 30-nA beam of Ar^+ ions at 30° off-normal incidence rastered over a 0.5×0.5-mm^2 region. Negative ions were monitored in order to avoid interference in the deuterium profile from H_2 radicals. This region was carefully chosen not to overlap with the previous beam spot from the TOF-FRES analysis. Occasionally an additional 1-keV de-

focused electron beam incident at 45° was directed onto the sample to eliminate beam-induced charging. The sputtering rate for the above chosen condition was approximately 800 Å/hour.

Figure 2.1 shows the raw SIMS data for a typical sample of d-PS volume fraction $\phi_\infty = 0.18$, annealed for 29 days. The ion masses analyzed correspond to carbon, CH, deuterium, and CD. From the data one first sees the narrow rise in the CH signal mirrored by a dip in D and CD signals, which corresponds to the thickness of the PS overlayer and defines the beginning of the sample surface. The large rise in the D and CD concentration, mirrored by the corresponding dip in the CH signal, is then apparent at the blend surface/overlayer interface. The carbon concentration is of course constant in all layers of the sample and was used as a monitor of the beam current. In this case, the flat carbon trace illustrates the stability of the sputtering beam over a 10-hour period, the acquisition time of this spectrum.

In standard SIMS experiments the sputtering time is directly converted to a depth scale by mechanically sensing the depth of the sputtered crater. This technique cannot be used with polymer films that are soft and therefore easily deformed. As a result the depth scale was calibrated by sputtering through a thin d-PS film, whose thickness of 560 Å was independently measured with ellipsometry. On the basis of this calibration, sputtering with the beam conditions described above yield resolutions for the 14% to 86% rise and fall widths of 110 and 120 Å, respectively. The worsening of the resolution (by 10 Å) between the front and back edge of the d-PS layer may come from the thickness variation of the d-PS layer within the crater. The characteristics of SIMS is discussed in detail in chapter 1. As shown in Figure 1.7, the resolution of SIMS

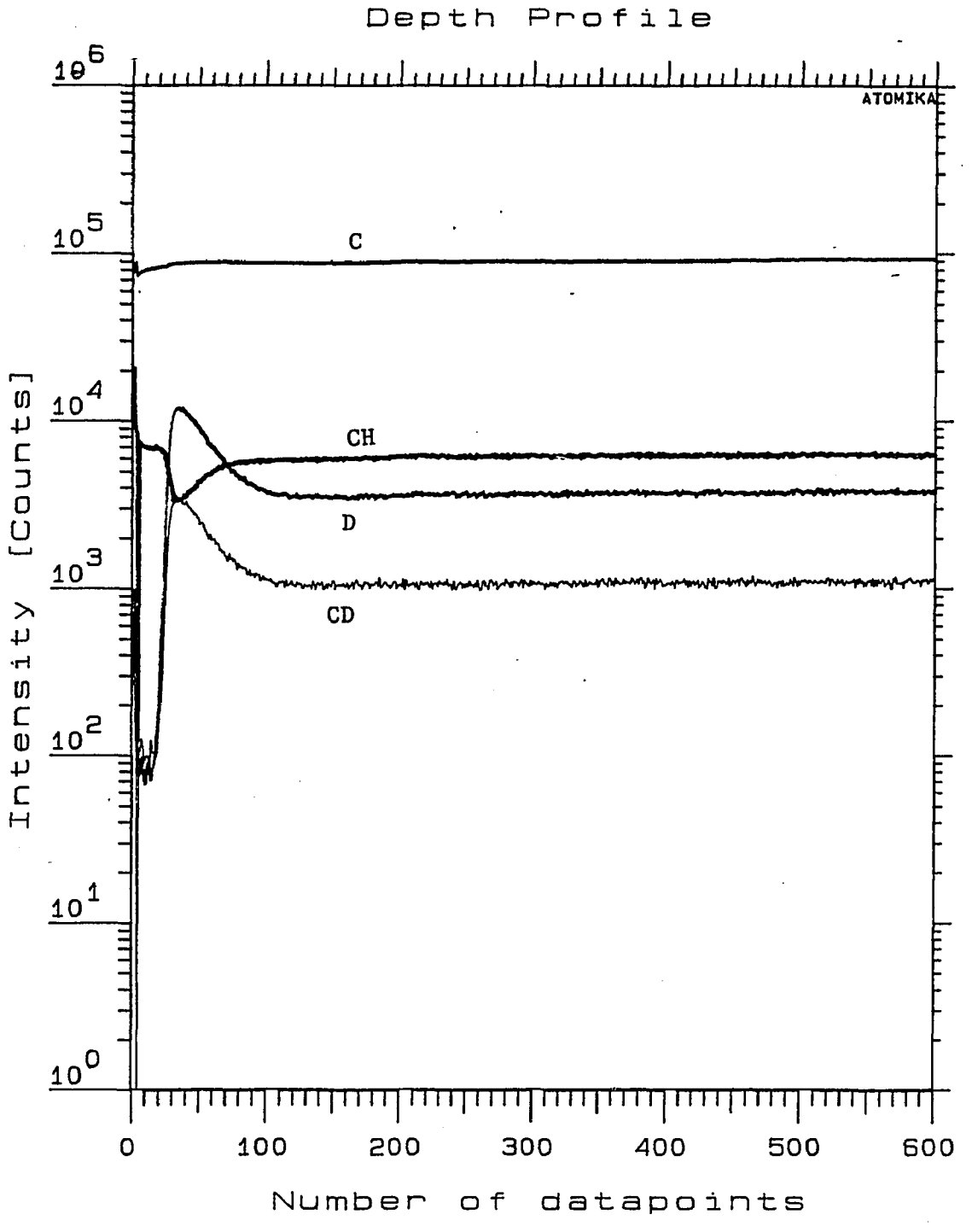

Figure 2.1 Raw SIMS data of a $\phi_\infty = 0.21$ d-PS sample annealed for 29 days. The data show scans for D^-, C^-, CH^-, and CD^- ions.

allows the form of the concentration profile derived from mean-field theory in equation (2.2) to be probed.

The sputtering rate of SIMS is difficult to be maintained constant, however, z^*, the total surface excess defined as

$$z^* = \int_0^\infty (\phi(z) - \phi_\infty) dz, \tag{2.8}$$

can be quickly and efficiently measured by FRES. Consequently, the assumed calibration for all SIMS samples discussed in this work was checked by measuring z^* independently with FRES.

2.3 RESULTS AND DISCUSSION

Table III Summary of Results of SIMS and TOF-FRES Measurements: Concentration Profile of d-PS/PS Blends

ϕ_∞	$\phi_\infty{}'$ [a,b]	ϕ_1 [b]	ϕ_1 [c]	z^* (Å) [b]	z^* (Å) [c]
.005	.0047	0.035 ± 0.004	—	3.3 ± .4	—
.025	.024	0.15 ± 0.01	—	15.4 ± 3.	—
.125	.120	0.68 ± 0.01	0.69 ± .03	110. ± 5.	112. ± 10.
.184	.171	0.88 ± 0.01	0.87 ± .03	192. ± 8.	187. ± 14.
.210	.200	0.90 ± 0.02	0.90 ± .03	215. ± 10.	215. ± 15.
.265	.242	—	0.95 ± .03	—	271. ± 19.

[a]Volume fraction of d-PS at the depleted region next to the surface.
[b]Results from SIMS experiments.
[c]Results from TOF-FRES experiments.

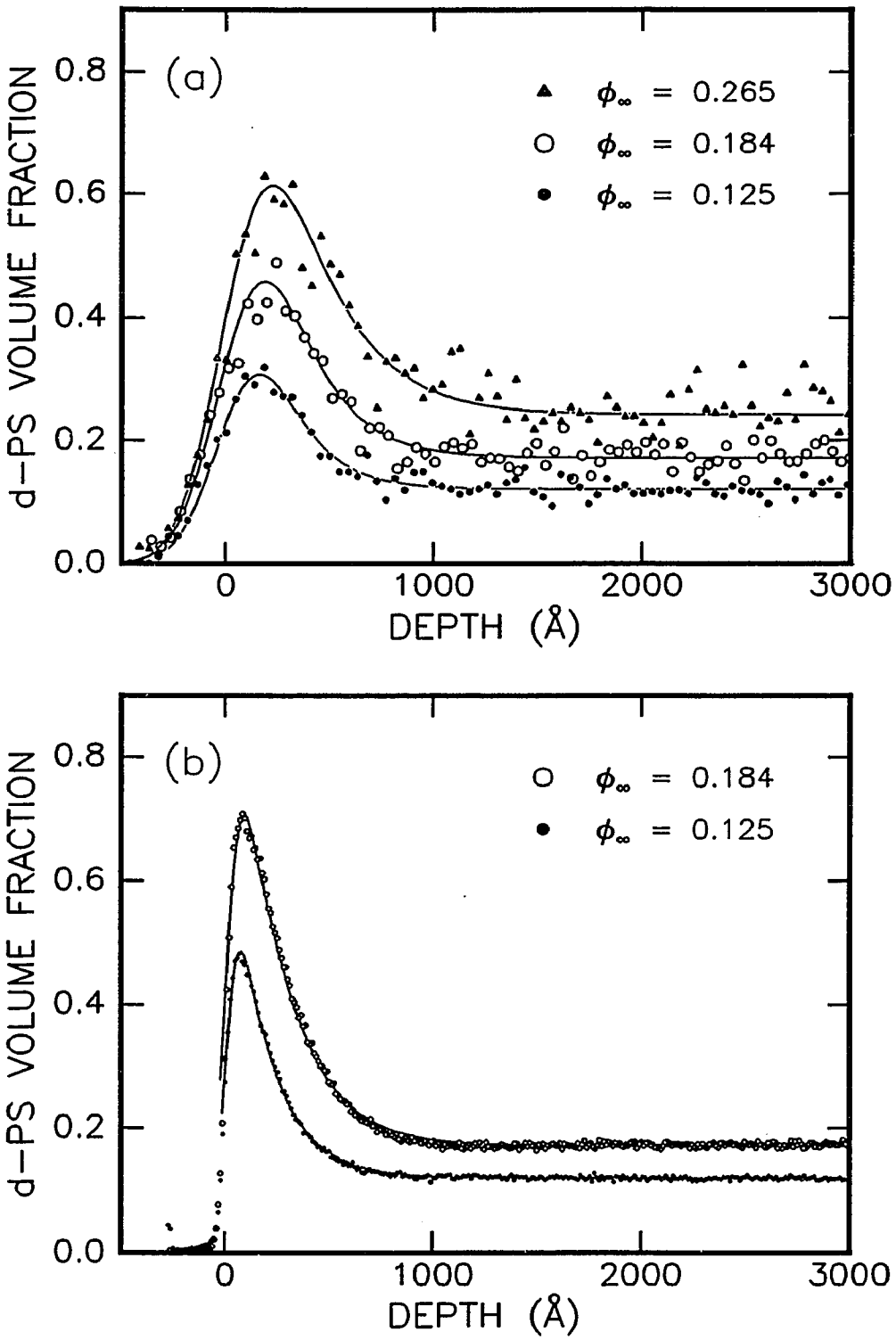

Figure 2.2 (a) TOF-FRES and (b) SIMS data from samples annealed at 184°C for 29 days with initial volume fractions ϕ_∞, of (▲) 0.265, (○) 0.184, (●) 0.125.

Figure 2.2(a) shows TOF-FRES data from three samples annealed at 184 °C for 29 days with bulk volume fractions $\phi_\infty = 0.125$, 0.184, and 0.265. Figure 2.2(b) shows the SIMS data from the two lower concentration samples. The solid lines in both figures correspond to fits of equation (2.2) with three free parameters, ϕ_1, ϕ_∞',[§] and χ. The profile is in good agreement with that predicted by the mean-field outlined in section 2.1 and in all cases, best fits were obtained for $\chi = 1.5 \pm 0.1 \times 10^{-4}$, in good agreement with the value extrapolated from the results of Bates and Wignall,[2,10] $\chi = 1.5 \pm 0.2 \times 10^{-4}$. The fit parameters as well as z^* are tabulated in Table III and plotted in Figure 2.3. From Table III as well as Figure 2.3 it can be seen that SIMS yields the same (to within experimental error) results as the TOF-FRES technique, confirming that heavy ion sputtering from polymer films maintains a depth-independent rate over the region studied and reliable, quantitative, and reproducible results can be obtained. Furthermore, comparison of parts (a) and (b) of Figure 2.2 indicates an additional important aspect of SIMS, namely, the improved signal-to-noise ratio, which allows the study of low-composition blends and detection of minor composition fluctuations.

2.3.1 Bulk Volume Fraction Dependence

Plotted in Figure 2.3(a) is z^* *vs.* ϕ_∞. We find the surface excess is nearly proportional to ϕ_∞, with the proportionality constant of $K = 1075 \pm 23$ Å. From Figure 2.3(b) it can be seen that ϕ_∞ increases rapidly, with nearly full surface coverage by the d-PS component already occurring at $\phi_\infty \sim 0.10$. Hence, the linear increase in z^* is due

---

[§] ϕ_∞' denotes the effective bulk concentration in the near surface region.

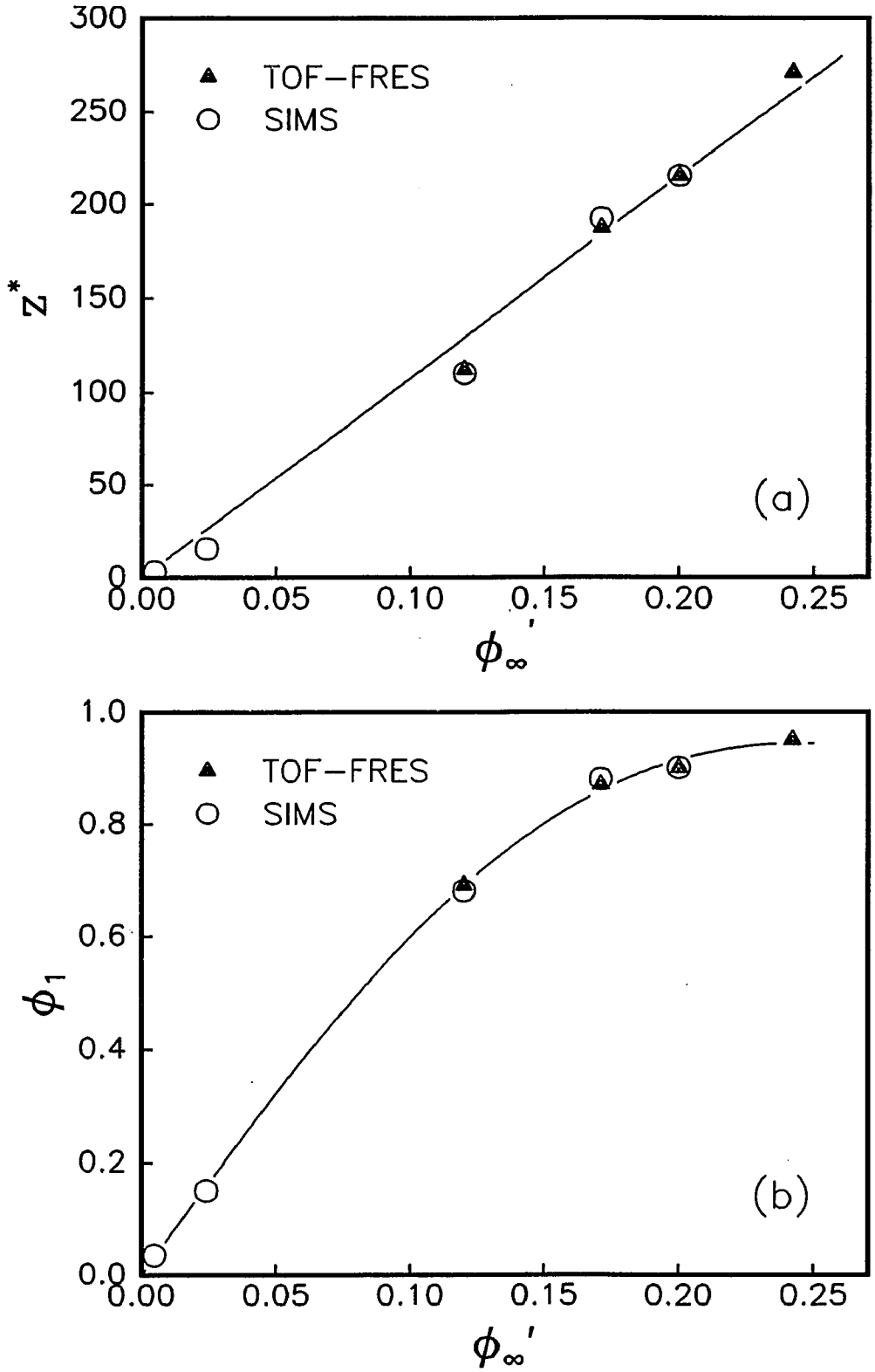

Figure 2.3 (a) Surface excess z^* and (b) surface concentration as measured by TOF-FRES (▲) and SIMS (○) as functions of ϕ_∞'.

mainly to the broadening of the decay profile with increasing ϕ_∞. The increase in the decay length ξ, as ϕ_∞ approaches ϕ_c is predicted by equation (2.2) and was shown previously[4,12] to coincide with the correlation length for density fluctuations in the bulk for $\phi_\infty < 0.10$. In Figure 2.3(b) we plot the projected surface concentration ϕ_1 as a function of ϕ_∞. The solid line is drawn to guide the eye. In order to actually predict the dependence of ϕ_1 on ϕ_∞, the solution to equation (2.7), $F_s(\phi_1)$ must be determined. In Figure 2.4 we plot the right-hand side of equation (2.7), for the experimentally measured values of ϕ_1, and equate it to $dF_s(\phi_1)/d\phi_1$. From the dashed line in Figure 2.4 it can be seen that the empirical form assumed by Schmidt and Binder,[7] namely

$$F_s(\phi_1) = -\mu_1\phi_1 - \frac{1}{2}g\phi_1^2, \qquad \textbf{(2.9)}$$

where μ_1 and g are related to the interactions between the monomers with the surface and the missing interactions between the neighboring monomers, is only a good approximation to the data for small ϕ_1. Including terms of order ϕ_1^3 did not significantly improve the fit.

The functional form that gives a better fit to the data is drawn as a solid line in Figure 2.4 and is given by

$$F_s(\phi_1) = -\mu_1\phi_1 + \alpha\phi_1\ln\phi_1 + \beta(1-\phi_1)\ln(1-\phi_1), \qquad \textbf{(2.10)}$$

with $\mu_1 = 0.027\pm0.005$ Å, $\alpha = 0.0030\pm0.0007$ Å, and $\beta = -0.0095\pm0.0007$ Å. This result is intuitively reasonable. The first term of this equation represents the chemical potential difference between the surface and bulk, which also appears phenomenologically in the formulations of Schmidt and Binder[7] and Cohen and Muthukumar.[9] The latter two terms are surface entropic factors, by analogy to the Flory-Huggins terms in

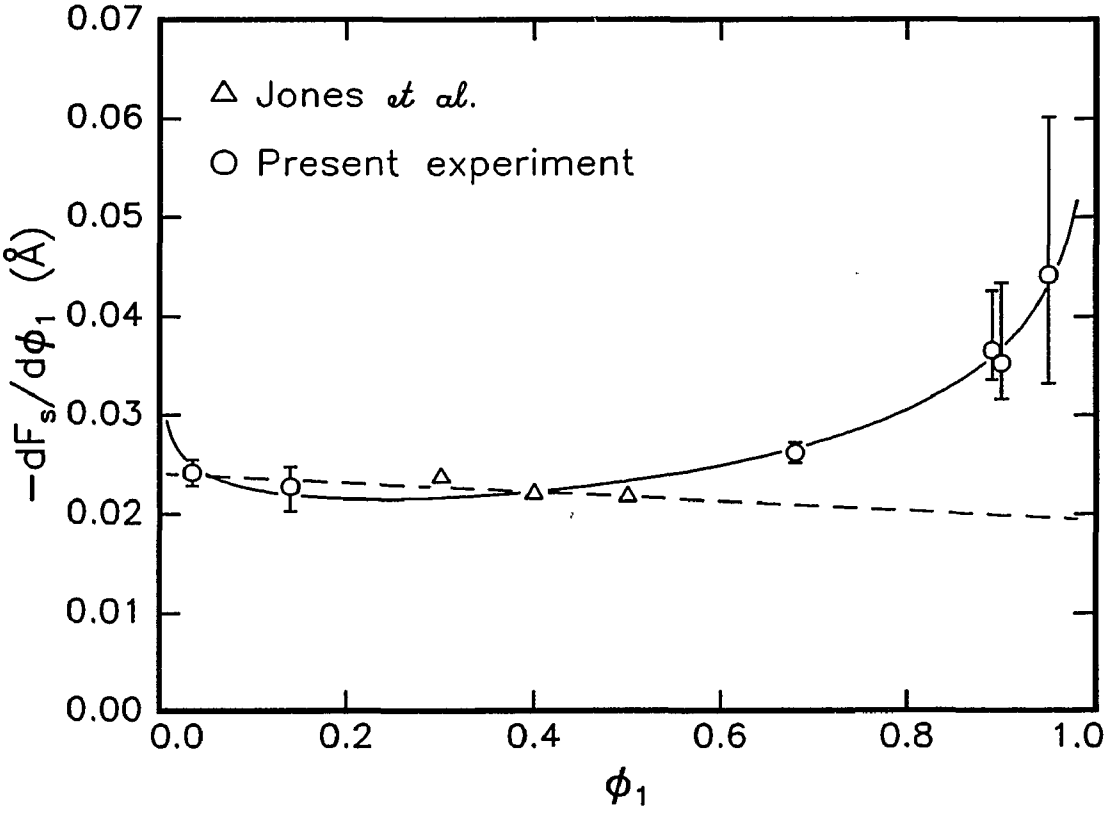

Figure 2.4 Derivative of the surface free energy vs the surface concentration. The dashed line is a linear function fit to Jones *et al.* The solid line corresponds to a fit with equation (2.10).

equation (2.1b).

The analogy to the Flory-Huggins entropy of mixing is probably superficial. The replacement of one composition by the other next to the surface itself is not expected to change the entropy of the system. The entropic effect due to the difference in the chain length between d-PS and h-PS used in our system is expected to be included in the linear relationship as it is observed that the surface tension is a slowly varying function of the molecular weight. However, the polymers next to the surface may be distorted differently in the presence of other polymers that have different surface interaction energy, in different concentrations. Such an effect is not included in equation (2.1a).

Cohen and Muthukumar[9] have recently derived a more realistic expression for $F_s(\phi_1)$, which includes a local surface interaction and surface entropy terms, as well as odd and even gradient terms to account for the intrinsic spatial asymmetry at the surface,

$$F_s(\phi_1) = -\mu_1\phi_1 + \alpha_1\phi_1\ln\phi_1 + \beta_1(1-\phi_1)\ln(1-\phi_1) + \left[\alpha_2\ln\phi_1 + \beta_2\ln(1-\phi_1)\right]\frac{d\phi_1}{dz} + \ldots \quad (2.11)$$

and terms proportional to $(d\phi_1/dz)^2|_{z=0}$ and $(d^2\phi_1/d^2z)|_{z=0}$.

This expression has only three free parameters, μ_1, C_A, and C_B, where $C_A - C_B$ is a term proportional to a surface χ. The α_i and β_i terms are complicated functions of C_A, C_B, N_A, and N_B. The first three terms of equation (2.11) coincide with the functional form that best fits our data. Even though the application of the Doi-Edwards formulation to the region near a surface is not fully warranted, thus limiting the utility of equation (2.11), equation (2.11) at least lends some justification for a surface entropy term similar to the Flory-Huggins expression.

Another important limitation of the theory, of both Cohen and Muthukumar[9] and Schmidt and Binder[7], is the assumption of a short-ranged (δ-function) surface interaction. The effect of taking the surface interaction to be strictly localized at the surface is to make the concentration profile, $\phi(z)$, simply "cut off" the bulk profile at some value ϕ_1 determined by the surface interaction parameters. In the case of Cohen and Muthukumar, this yields unrealistically large values for the gradient terms in equation (2.11). Therefore, deviations of the shape of $\phi(z)$ from bulk behavior would provide clear evidence of the breakdown of the local interaction picture. This is indeed the case of large ϕ_1, as is discussed further in section 2.3.3.

2.3.2 Time Dependence of the Concentration Profile

Figure 2.5 shows the concentration profiles for a series of samples having $\phi_\infty = 0.33$ and annealed for times varying from 3 to 45 days. The solid lines are least square fits to equation (2.2), and the results are summarized in Table IV. ϕ_∞' corresponds to the concentration in a depleted zone adjacent to the surface, as explained in reference 13, which from Figure 2.5 can be seen to be approximately 1000 Å wide. This region is more clearly seen in Figure 2.6, where we plot the depth profile up to 4000 Å from the surface of a $\phi_\infty = 0.21$ sample annealed for 29 days. Figure 2.7 is a plot of z^* and ϕ_1

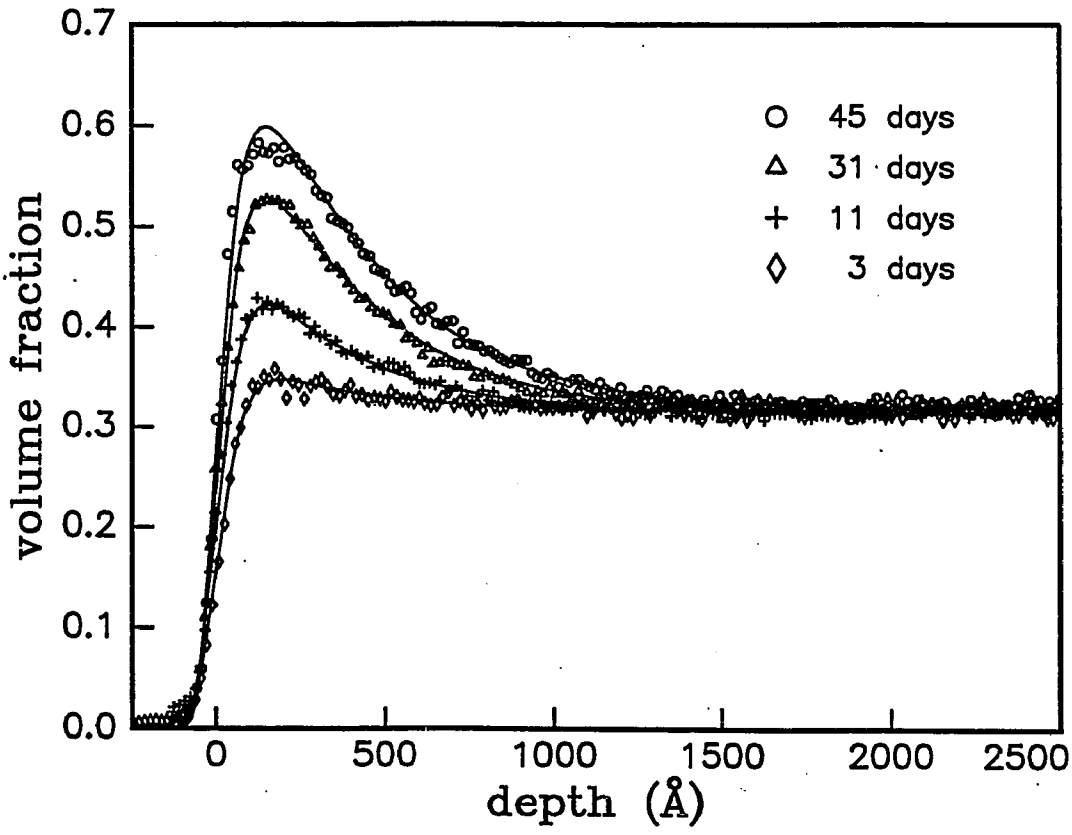

Figure 2.5 Surface concentration profiles for a $\phi_\infty = 0.33$ blend annealed for various times at 184 °C.

Table IV Summary of Results for the Concentration Profiles for a $\phi_\infty = 0.33$ Blend Annealed for Different Times at 184° C.

t (hour)	ϕ_1	z^* (Å)	ϕ_∞'
75.5	0.375	19.2	0.317
268.8	0.490	60.4	0.315
744.0	0.635	119.6	0.312
1080.0	0.700	163.0	0.320
∞^a	0.970	340.	0.330

[a]Predicted values for the equilibrium profile.

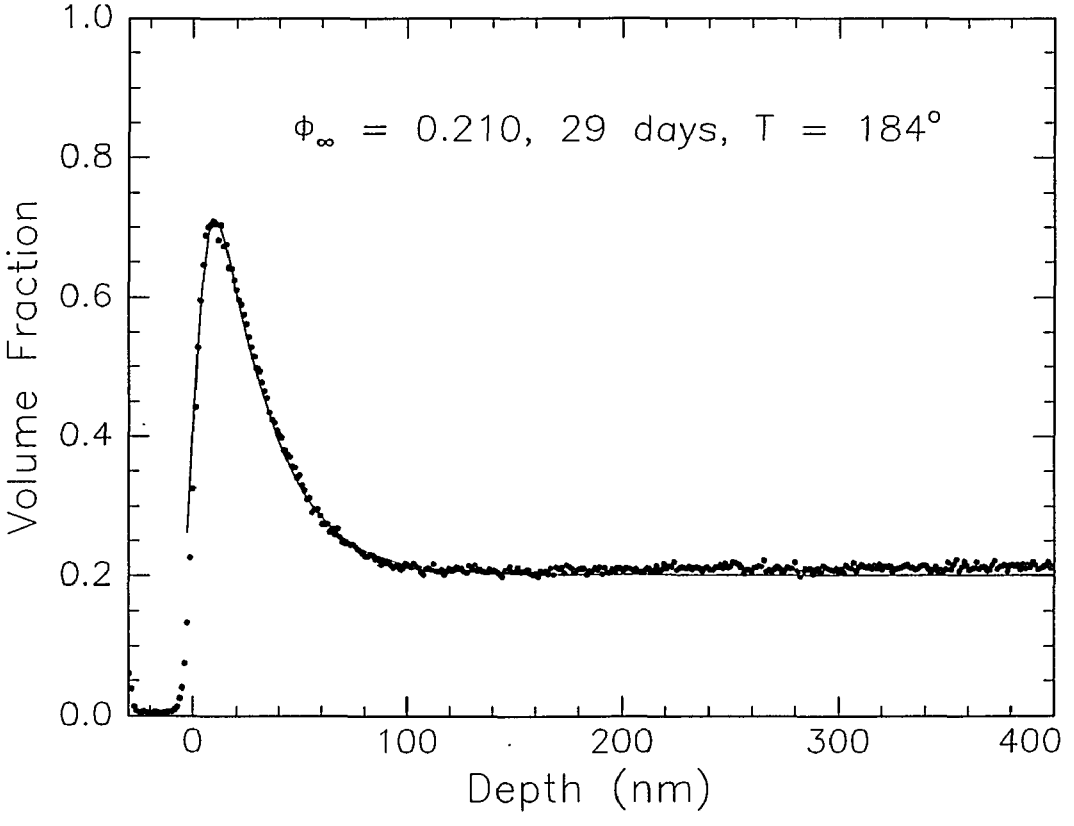

Figure 2.6 Surface concentration profile for a $\phi_\infty = 0.210$ blend annealed for 29 days at 184 °C.

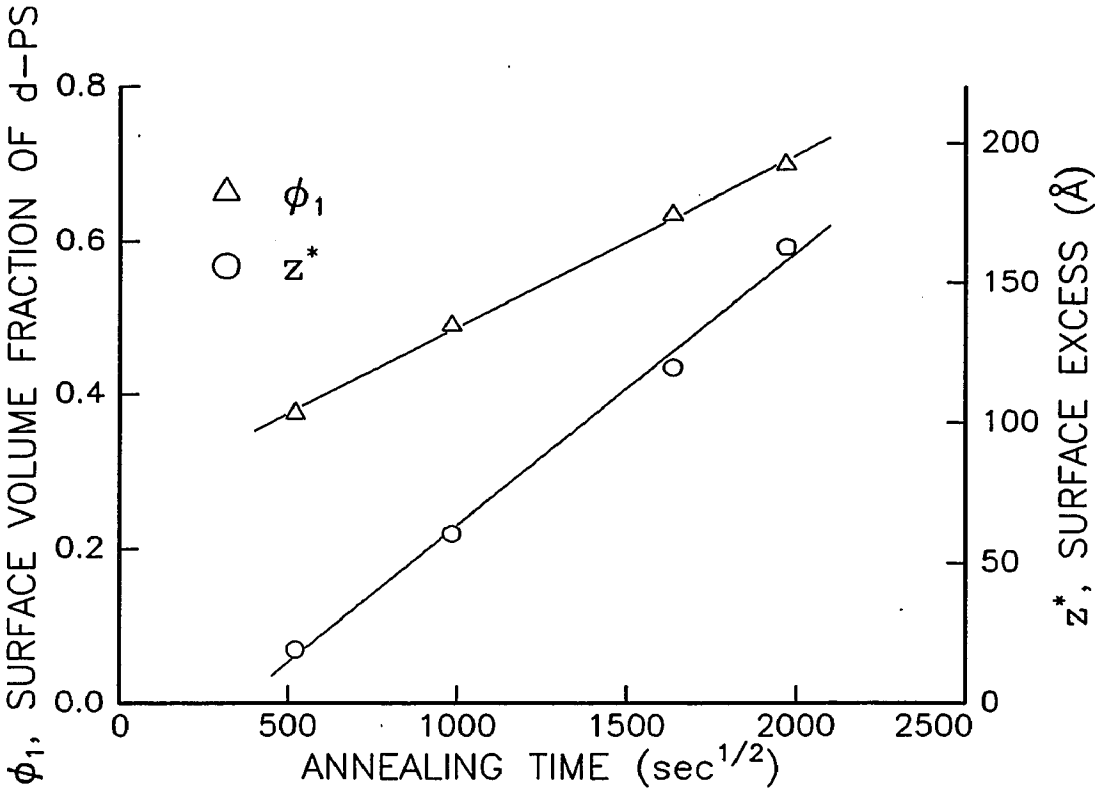

Figure 2.7 Measured surface concentration, ϕ_1, and surface excess, z^*, plotted as a function of the square root of the annealing time.

vs. the square root of the annealing time for the profiles shown in Figure 2.5. As pointed out by Jones and Kramer,[13] conservation of mass requires that the excess material at the surface equal the amount missing from the near surface depleted region. It is reasonable to assume that sufficiently far from the surface the size of the depleted region should scale at $\sqrt{Dt}$, where D is the bulk diffusion coefficient. The surface excess can then be approximated by

$$z^* = (\phi_\infty - \phi_\infty')\sqrt{Dt}\,. \tag{2.12}$$

Contrary to the assumption made in reference 13 of local equilibrium between the surface profile and the depleted region, from Table III and Table IV it can be seen that ϕ_∞' does

not vary much from ϕ_∞ for the measured annealing times. Taking an average value of $\phi_\infty' = 0.316$ from Table IV together with the best fit value for the slope, $0.097 \pm 0.005\ \text{Å} \cdot \text{s}^{-1/2}$, of the z^* curve, yields a mutual diffusion coefficient of $D = 4.8 \times 10^{-15}\ \text{cm}^2/\text{s}$. This result is in good agreement with the mutual diffusion coefficient for a $\phi_\infty \sim 0.3$ blend at 184 °C, $D = 3.0 \times 10^{-15}\ \text{cm}^2/\text{s}$ calculated from the expressions given in the literature[14] and using the measured value of $\chi = 1.50 \pm 0.03 \times 10^{-4}$. From Figure 2.5 and Figure 2.7 one can see that all the profiles for the samples annealed less than 45 days are well fit by equation (2.2) and that ϕ_1 also scales as $t^{1/2}$ in the observed range of annealing times. This scaling indicates that the increase in the surface concentration, *i.e.*, the adsorption to the surface, is not significantly faster than the bulk diffusion rate. Moreover, for each annealing time the profile of minimum energy is consistent with the mean-field prediction, with z^* limited mainly by the bulk diffusion dynamics, indicating that the surface profile maintains a constant dynamic equilibrium with the depleted area, ϕ_∞', which does not vary much from the bulk.

It must be stressed that no evidence exists as yet that these conclusions are generally true at short times. From the fact that the lines in Figure 2.7 do not go through the origin, we can infer that at short time z^* builds up somewhat slower than predicted by equation (2.12).

2.3.3 Form of the Concentration Profile

It has been shown previously that, for low d-PS volume fractions ($\phi_\infty \sim 0.10$), the surface profile can be approximated by a simple exponential function with a decay length

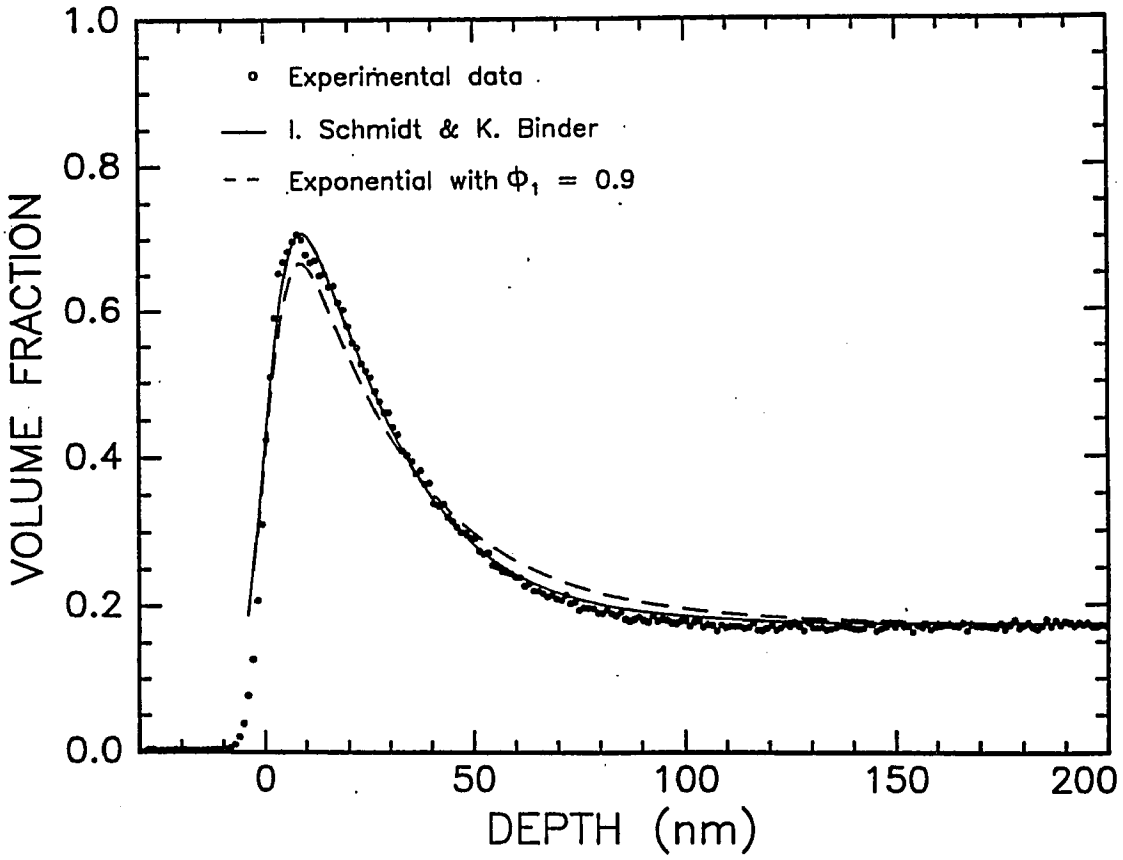

Figure 2.8 Concentration profile for a $\phi_\infty = 0.18$ d-PS/h-PS blend annealed for 29 days at 184 °C. The solid line is a fit to eq (2.2), while the dotted line is a fit to an exponential decay.

equal to the correlation length for concentration fluctuations in the bulk.[4,12] It can be shown from equation (2.2) that in the framework of mean-field theory, the profiles begin to differ significantly from a simple universal exponential decay at higher concentrations. This is illustrated in Figure 2.8, which shows the concentration profile for a $\phi_\infty = 0.18$ blend annealed for 29 days. From Figure 2.8 it can be seen that the spatial resolution of SIMS is sufficient to differentiate between an exponential decay and the mean-field functional form given by equation (2.2). On the other hand, the spatial resolution of SIMS is insufficient to determine the initial slope of the function, $d\phi/dz$, in the near

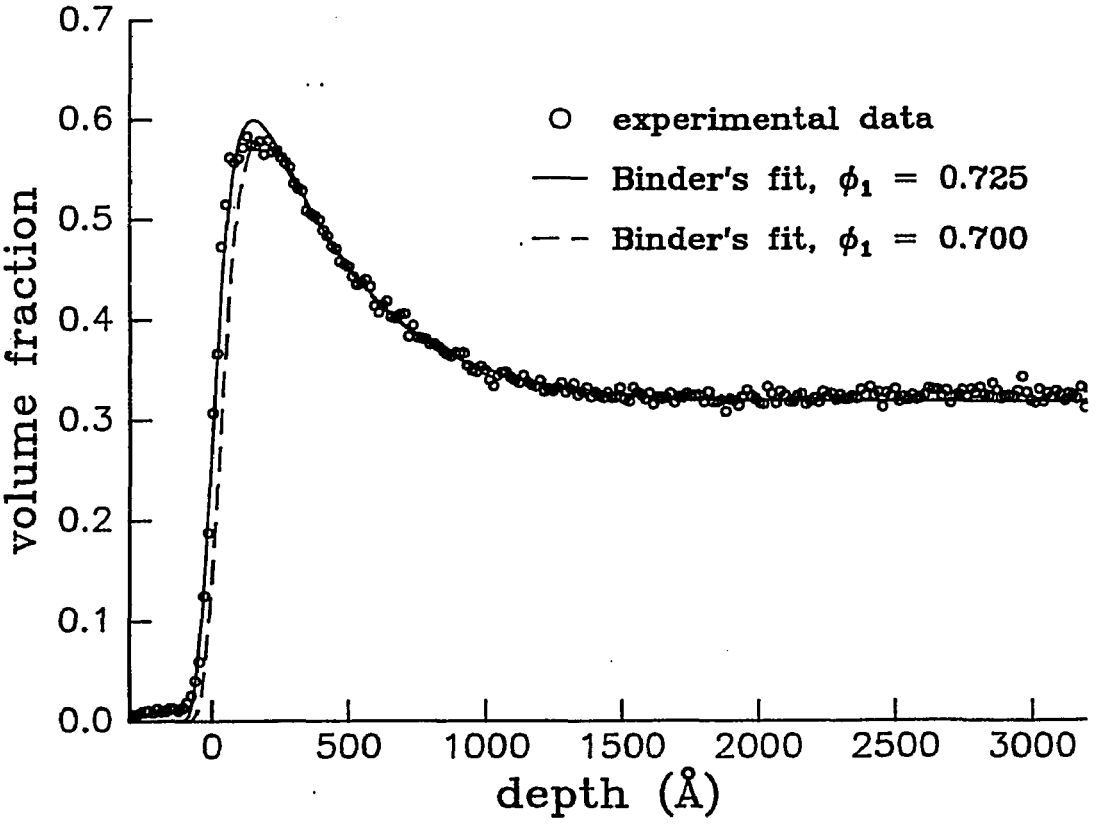

Figure 2.9 Expanded section of the near surface region for the $\phi_\infty = 0.33$ blend annealed for 45 days.

surface region. Neutron reflectivity measurement[4] on samples with $\phi_\infty < 0.15$ indicates that there may be a flattening of the concentration profile in the first 20 Å near the surface. A distinct flat region, approximately 100 Å wide, is clearly seen in Figure 2.9, which shows an expanded portion of the near surface region of the $\phi_\infty = 0.33$ sample annealed for 45 days. As can be seen from Table IV, the z^* for this profile is still far from equilibrium, and hence the width of the flat portion is just a lower limit on the final equilibrium value. The form of the profile in Figure 2.9 is not predicted by equation (2.2) but may still be consistent within the framework of the mean-field model, if one assumes a surface interaction of finite extent rather than the δ-function approximation

used to solve equation (2.2) in closed form. Furthermore, equation (2.7) is a direct result of the δ-function surface boundary conditions,[7,9] and therefore the form of the surface free energy obtained from equation (2.7) and shown in Figure 2.4 may not be correct for large ϕ_∞ and ϕ_1. It should be noted though that, as can be seen from Figure 2.9, the form of the decay of the surface concentration away from the surface layer is still consistent with equation (2.7) and, as mentioned previously, independent of the assumed form of the surface interaction.

From the time dependence data in Figure 2.5, it can be seen that the flat portion does not develop gradually or appear at large ϕ_1, which would be expected if the surface potential were only a function of ϕ_1. In fact, ϕ_1 for the profile in Figure 2.9 is smaller than that for other profiles where this feature is not as obvious. As ϕ_∞ approaches the critical concentration, precise determination of the coexistence curve becomes more important. The experimental error on the value of χ for d-PS/PS blend[2] translates into a 10 °C uncertainty in the determination of the critical temperature for the blend. Hence, we cannot rule out the possibility that in the near surface region we are approaching a coexistence concentration and we are observing the growth of a surface macroscopic layer as predicted in reference 7 and by equation (2.2).

2.4 CONCLUSIONS

In conclusion, it has been demonstrated that the spatial resolution obtained by a combination of ion scattering techniques is sufficient to determine the form of the concentration profile at the surface of a polymer blend. To the resolution of SIMS, the

shape of the profile is consistent with mean-field theory when the bulk volume fraction is small. For samples with high bulk volume fraction, the gradient at the near surface region appeared to be much smaller than predicted. The "bare" surface energy appeared to be a complicated function of the surface volume fraction. We believe the possible reasons for such difficulty are either the lack of a statistical model for polymer chains near a surface or the surface interaction is longer ranged than assumed in the strictly local interaction models. The growth of the decay profile, as well as the surface concentration, seems to be a diffusion-limited process, with a diffusion constant equal to the bulk mutual diffusion coefficient.

REFERENCES

1. M. R. Moldover and J. W. Cahn, *Science* **207,** 1073 (1980); O 'D. Kwon, D. Beaglehole, W. W. Webb, B. Widom, J. W. Schmidt, J. W. Cahn, M. R. Moldover, and B. stephenson, *Phys. Rev. Lett.* **48,** 185 (1982); D. W. Pohl and W. I. Goldburge, *Phys. Rev. Lett.* **48,** 1111 (1982).

2. F. S. Bates and G. D. Wignall, *Phys. Rev. Lett.* **57**, 1429 (1986).

3. R. A. L. Jones, E. J. Kramer, M. H. Rafailovich, J. Sokolov, and S. A. Schwarz, *Phys. Rev. Lett.* **62**, 280 (1989).

4. R. A. L. Jones, L. J. Norton, E. J. Kramer, R. J. Composto, R. S. Stein, T. P. Russell, A. Mansour, A. Karim, G. P. Felcher, M. H. Rafailovich, J. Sokolov, X. Zhao, and S. A. Schwarz, *Europhys. Lett.* **12**, 41 (1991).

5. E. J. Kramer, *Physica B* **173,** 189 (1991).

6. J. Sokolov, M. H. Rafailovich, R. A. L. Jones, and E. J. Kramer, *Appl. Phys. Lett.* **54**, 590 (1989).

7. I. Schmidt and K. Binder, *J. Phys.* **46**, 1631 (1985).

8. H. Nakanishi and P. Pincus, *J. Chem. Phys.* **79**, 977 (1983).

9. M. S. Cohen and J. M. Muthukumar, *J. Chem. Phys.* **90**, 10 (1989).

10. F. S. Bates and G. D. Wignall, *Macromolecules* **19**, 932 (1986).

11. P. J. Mills, P. F. Green, C. J. Palmstrom, J. W. Mayer, and E. J. Kramer, *Appl. Phy. Lett.* **45**, 957 (1984).

12. M. H. Rafailovich, J. Sokolov, X. Zhao, R. A. L. Jones, and E. J. Kramer, *Hyperfine Interact.* **62**, 45 (1990).

13. R. A. L. Jones and E. J. Kramer, *J. Philos. Mag.* in press.

14. P. F. Green and B. L. Doyle, *Phys. Rev. Lett.* **57**, 2407 (1986); P. F. Green and E. J. Kramer, *J. Mater. Res.* **1**, 202 (1986).

CHAPTER 3

Thermodynamics of Grafted Chains in the Melt

Grafted polymer chains can play an important role in modifying the surface properties of solids. In particular, polymers where a polar or reactive end adsorbs to a solid surface while the rest of the chain is chemically inert and miscible within the polymer melt are often used in the manufacturing of adhesives and composite materials. Because of their many practical applications, grafted polymer chains have been the subject of intensive theoretical[1,2,3,4,5,6] and experimental[2,7,8,9,10,11,12] research. The different theoretical models, reviewed by Milner[13], for the grafting dynamics of adsorbed polymers are mainly applicable to stretched chains in dilute solutions. This limit is not appropriate for anchored chains in a melt where, due to screening of the excluded volume interaction and the constraint of constant polymer density, the stretching of the chains is greatly reduced. Numerical calculations for melts, based on self-

consistent lattice models, have recently appeared and are reported to work well in the dense brush regime such as that obtained with block co-polymers at interfaces.[6,14] In order to test these and other models, it is essential to identify the mechanism of the chain attachment, and measure the resulting chain conformations and kinetics. This is achieved most conveniently using the technique of secondary ion mass spectrometry (SIMS), which directly measures the concentration as a function of depth in a model-independent manner for various molecular species with a depth resolution of approximately 100 Å.

3.1 GRAFTING OF CARBOXY TERMINATED POLYSTYRENE TO SI-OXIDE SURFACE

We studied the system of carboxy terminated deutero-polystyrene chains, dPS-COOH ($M_w = 86\,000$, $M_w/M_n < 1.1$), grafted onto Si-oxide-covered substrates in blends with polystyrene (PS, $M_w = 670\,000$, $M_w/M_n \leq 1.06$, Pressure Chemical Company). This system was chosen since polymers capped with carboxylic acid were shown to be far less prone to associate into clusters than those with zwitterion or amine ends.[15] Furthermore, for the molecular weights used in this study, the chemical interactions between the grafted and matrix chains are minimal[16], simulating as closely as possible ideal conditions in a melt.

dPS-COOH is obtained from L. J. Fetters from Exxon Research and Engineering. The molecular weight of dPS-COOH is 86 000 g/mole, obtained by comparing with dPS standard ($M_w = 104\,000$, Polymer Laboratories, Ltd) using gel permeation chromatography (GPC). Samples of dPS-COOH and PS blends approximately 2000 Å

thick were made by spin coating from chlorobenzene solution directly onto oxide-covered Si substrates or by floating a layer of PS on top of another layer of dPS-COOH previously spun directly onto the Si substrate. In both cases the total initial volume fraction, $\phi_{initial}$, of dPS-COOH ranged from 0.01 to 0.33. The samples were annealed in a vacuum of 10^{-5} Torr at 135 °C for 10 days, 160 °C for 48 hours, 200 °C for 13 hours, and 240 °C for 24 hours. The fact that the SIMS profiles of samples with the same total $\phi_{initial}$ are similar in grafting density and distribution regardless of the method of preparation indicates that the equilibrium condition is reached. The arrival of equilibrium condition (at 160 °C for 48 hours) was also confirmed by subsequent time dependent measurement of brush growth (see Chapter 4).

The volume fraction profile of dPS-COOH of a typical sample is plotted in Figure 3.1. The peak next to the substrate surface ($x = 0$) represents the attached chains. The grafting density can be represented by the volume of grafted chains per unit area, z^*, defined in this chapter as

$$z^* = \frac{1}{1-\phi_\infty} \int_0^\infty [\phi(z)-\phi_\infty \vartheta(x)]\,dz \ , \qquad (3.1)$$

where $\vartheta(x)$ is the step function. The factor $1/(1-\phi_\infty)$ in equation (3.1) comes from the assumption that everywhere through out the sample the composition of the un-grafted chains, ϕ_f, and the matrix chains, ϕ_m, has the same ratio, *i. e.*,

$$\frac{\phi_m(x)}{\phi_f(x)} = \text{Const.} = \frac{\phi_\infty}{1-\phi_\infty} \ . \qquad (3.2)$$

The number of grafted chains per unit area, σ, is related to z^* in the following way,

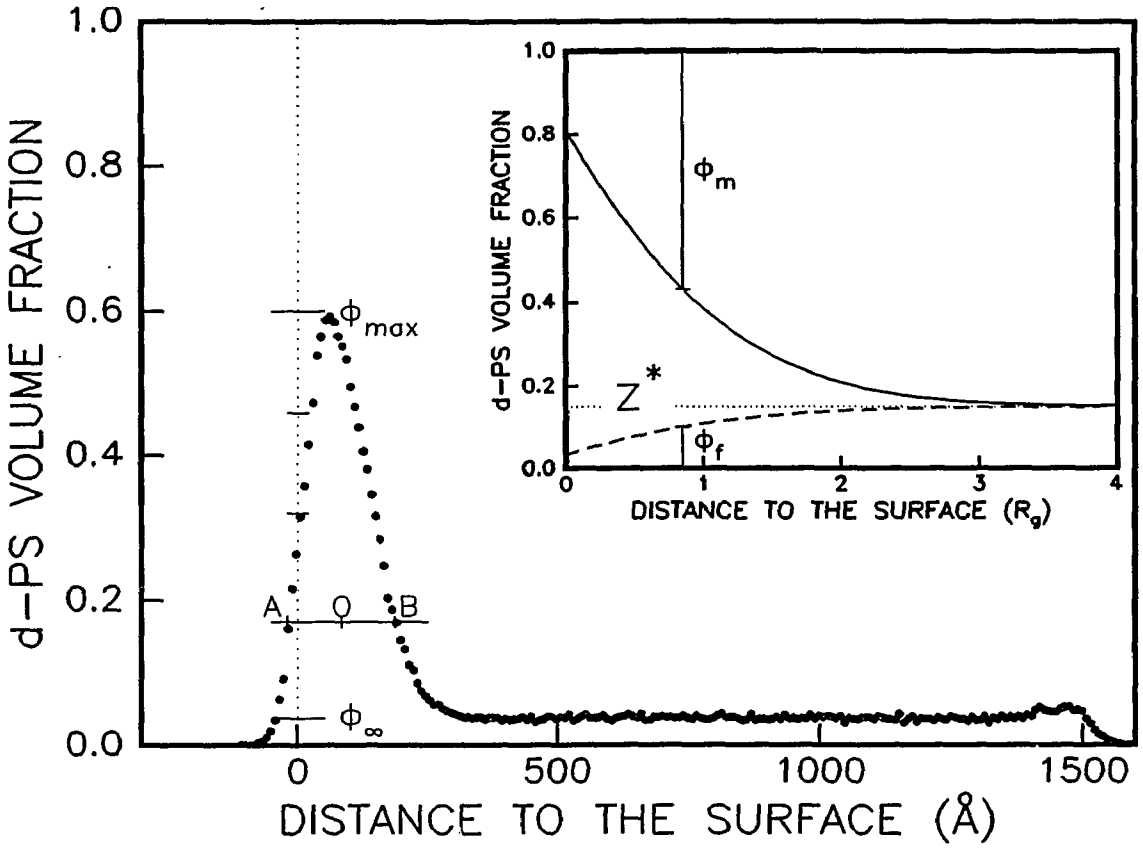

Figure 3.1 The dPS-COOH volume fraction as measured by SIMS of a sample with $\phi_{initial} = 0.094$ annealed at 135 °C for 10 days. The inset shows the definition of z^*.

$$\sigma = \frac{z^*}{Nv} = \frac{z^*\rho}{M}, \tag{3.3}$$

where $v = 173$ Å^3 is the volume of the polymer monomer, $\rho = 1.02 \times 10^{-24}$ g/Å^3 is the density of polymer,[17] and M is the molecular weight of the polymer.

Another quantity that characterizes the grafted chains is the width of the grafted chain profile, w, which is determined in a way demonstrated in Figure 3.1. A line corresponding to volume fraction $\phi_\infty + (\phi_{max} - \phi_\infty)/4$, where ϕ_{max} is the maximum volume fraction from the measured profile, is drawn across the peak. The line intersects

the peak at points *A* and *B*. The distance from the point that bisects *A-B*, *O*, to the surface is defined as *w*. One would consider using such quantities as the average distance of the profile to the surface,

$$\langle x \rangle = \int_0^\infty x[\phi(x)-\phi_\infty \vartheta(x)]dx ,$$

as a better quantity to characterize the profile width. However, it turns out that such an average is too sensitive to the tail of the profile and small variation in selecting ϕ_∞.

3.2 BULK CONCENTRATION DEPENDENCE

The profiles of dPS-COOH ($M_w = 86\,000$) and PS ($M_w = 670\,000$) samples of various initial volume fraction prepared from either blends or bilayers annealed at $T = 160$ °C for 48 hours are shown in Figure 3.2. The quantities σ, ϕ_∞, and w are tabulated in Table V and plotted in the inset of Figure 3.2 (the solid line is to guide the eye). It can be seen that for the lower two concentrations ($\phi_{initial} = 0.0083$ and 0.05, $z^* = 16$ and 66), the profiles have the same width. When the brush density increases to $z^* = 107$, the profile clearly becomes wider. We consider such an increase in profile width to be the result of the stretching of the end-grafted chain due to the limited available space to accommodate relaxed chains at this grafting density. Assuming a monomer density[17] of $\rho = 5.9 \times 10^{-3}$ Å^{-3}, one can approach a packing density for a polystyrene melt of $M_w = 86\,000$ of approximately 22 chains in a cylinder of radius, R_g and length $2R_g$ (the thickness of the unstretched layer). Consequently, one can see from both Figure 3.2 and Table V that when the number of chains grafted in an area πR_g^2 approaches this estimate,

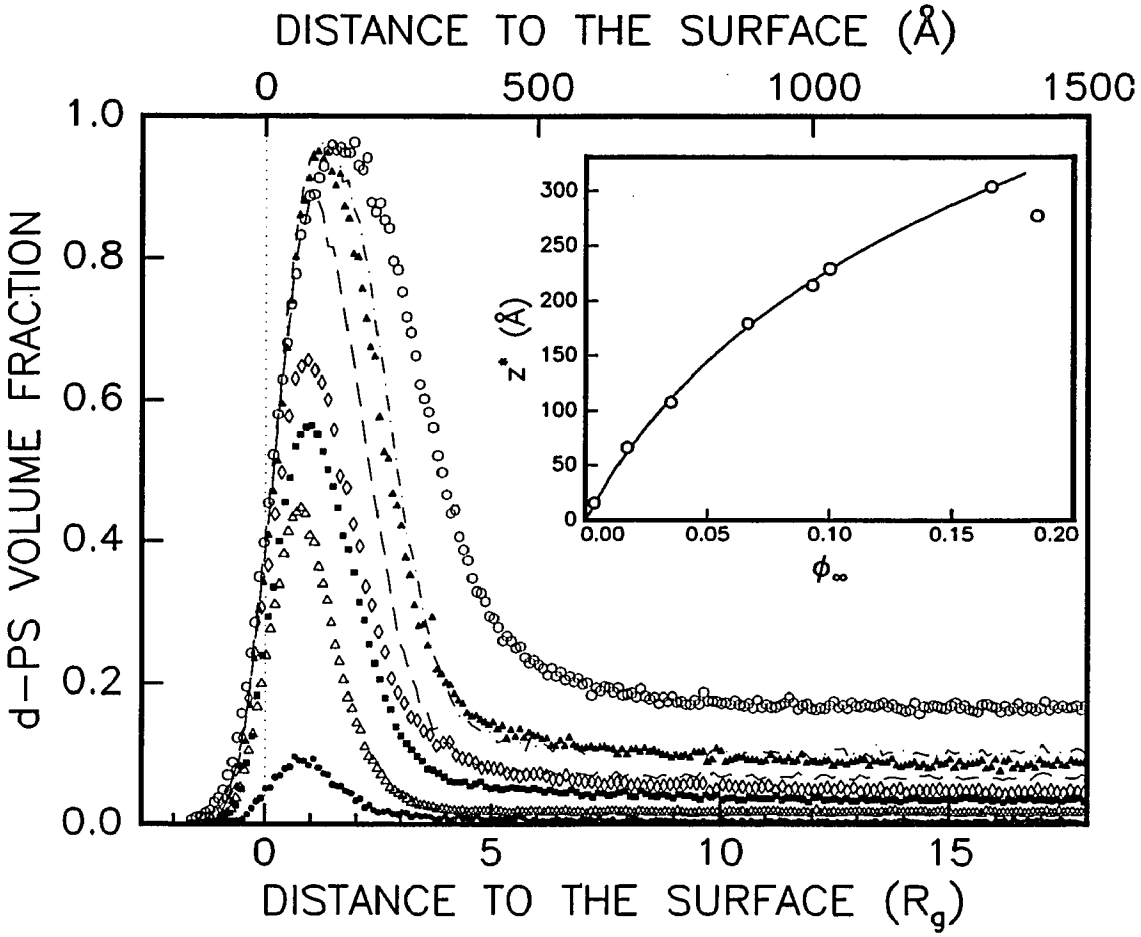

Figure 3.2 Volume fraction of dPS(COOH) from its blend with PS (M_w = 670 000) annealed at T = 160 °C for 48 hours.

the chains are forced to stretch as a result of the melt incompressibility.

The stretching of the grafted chains is the main fact responsible for the deviation of the grafting density from the linear relation with the bulk volume fraction. Because the brush is in contact with the bulk, the chemical potentials, μ_σ and μ_∞, of the grafted and ungrafted chains respectively, should be equal. For a solution, given the molar Gibbs function as a function of the molar fractions of each components x_i, $g = g(x_1, x_2, \ldots, x_i, \ldots, x_k)$, the chemical potential of the ith component is

Table V Summary of Data For dPS-COOH/PS[a] Samples Annealed at 160 °C

$\phi_{initial}$	ϕ_∞	z^* (Å)	w (Å)	σ (10^{-3} Å^{-2})	σ (πR_g^2)
0.0083	0.0034	16.	71. ± 10.	-0.093	2.05
0.05	0.017	66.	71. ± 4.	0.38	8.5
0.094	0.035	107.	110. ± 5.	0.62	14.
0.154	0.066	179.	126. ± 5.	1.04	23.
0.19	0.093	214.	145. ± 5.	1.24	27.
0.22	0.10	229.	142. ± 6.	1.33	29.
0.29	0.166	303.	181. ± 7.	1.75	39.
0.34	0.185	277.	268. ± 6.	1.61	35.
0.196[b]	0.136	179.	182. ± 5.	1.04	23.

[a]PS $M_w = 670\,000$ unless otherwise stated.
[b]Matrix consists of 50% PS of $M_w = 670\,000$ and 50% PS of $M_w = 1700$.

$$\mu_i = g + \frac{\partial g}{\partial x_i} - \sum_j x_j \frac{\partial g}{\partial x_j} \,. \tag{3.4}$$

Ignoring the interaction of the end-group with other monomers, and using Flory-Huggins free energy, the chemical potential of the un-grafted dPS-COOH chain (of degree of polymerization N) is

$$\frac{\mu_\infty}{k_B T} = \ln(\phi_\infty) + (1-\phi_\infty)\left[1-\frac{N}{N'}\right] + (1-\phi_\infty)^2 N\chi \,, \tag{3.5}$$

where $\chi = (1.7 \pm 0.4) \times 10^{-4}$ is the Flory interaction parameter[16] at 160 °C and N' is the degree of polymerization of the matrix polymer.

The chemical potential of the attached chains can be approximated by;

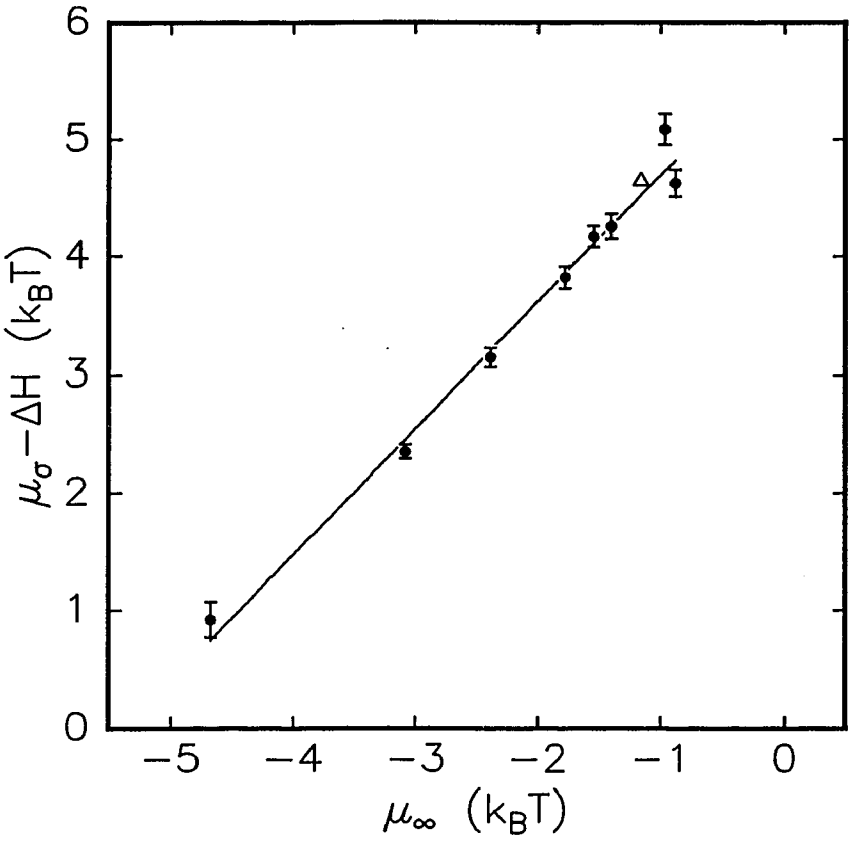

Figure 3.3 μ_σ *vs.* μ_∞ for dPS(COOH) in a melt of PS (M_w=670,000) matrix (●) and PS (M_w=670,000) plus PS (M_w=1700) matrix (△) at 160 °C.

$$\frac{\mu_\sigma}{k_BT} = \ln(\sigma\pi) + \frac{3}{2}\frac{r^2}{a^2N} + \frac{\Delta H}{k_BT} + C_\sigma \,, \tag{3.6}$$

where π is the cross-sectional area of the polymer chain. Taking the specific volume of 1.0 ml/mg for polystyrene[17] (at 160 °C) and the fact that the deuterium substitution in organic molecule reduces the size only slightly,[18] we get $\pi = 31$ Å^2. The first term in equation (3.6) represents the occupational entropy of the attached end, in analog to the $\ln(\phi_\infty)$ term in equation (3.5). The second term is the stretching entropy of the grafted chains. Other unknown factors associated with the occupational and stretching entropy

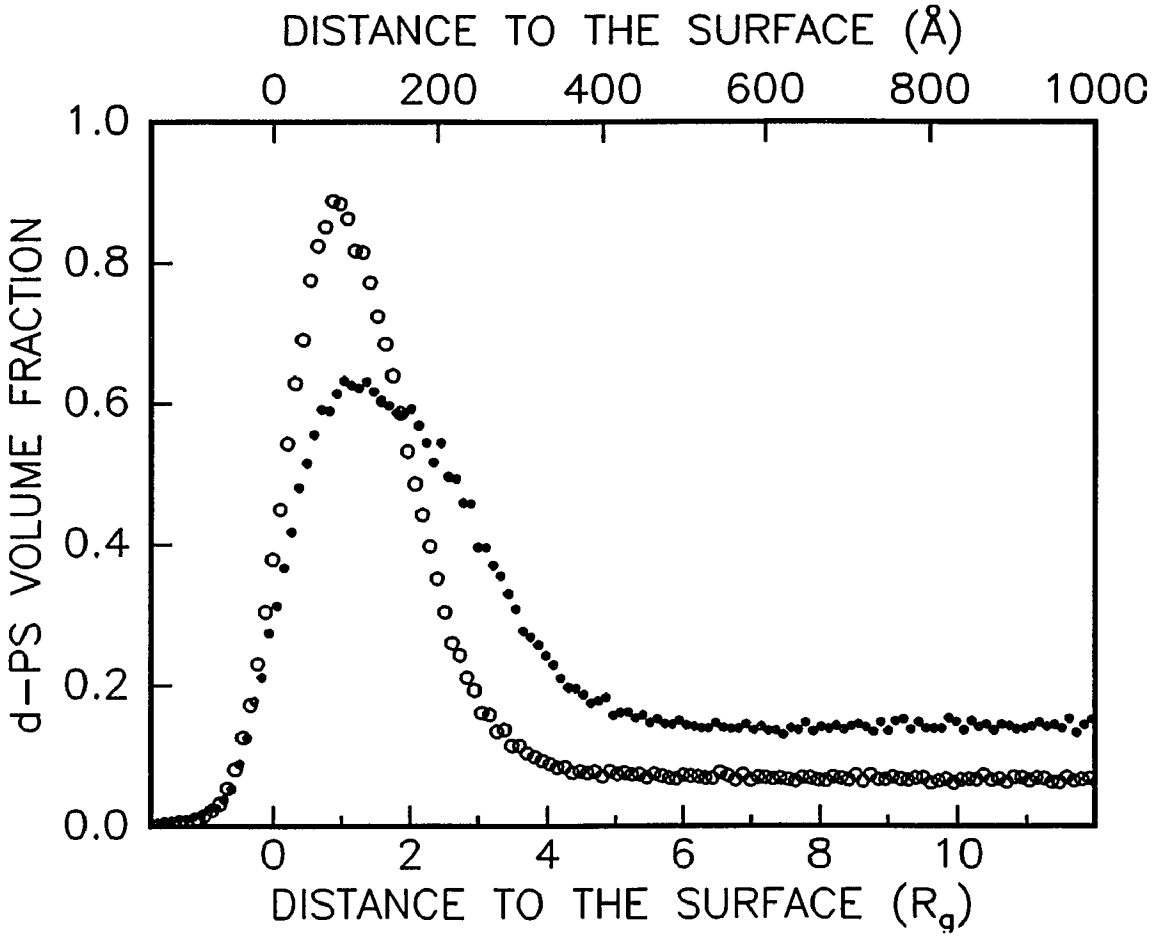

Figure 3.4 Concentration profiles of dPS(COOH) in PS (M_w=670000) matrix (○) and 50% PS (M_w=670000) 50% PS (M_w=1700) matrix (●).

is represented in the temperature independent constant C_σ, which can be determined in the following way: Considering the case of $\Delta H = 0$, the possibility of finding a site on the surface occupied by the chain end will be $\sigma\pi = \phi_\infty/N$. With use of $\mu_\sigma = \mu_\infty$ at the limit of $\phi_\infty \to 1$, we get

$$C_\sigma = \ln N - \frac{3}{2}\frac{r_0^2}{a^2 N} . \tag{3.7}$$

where r_0 is the mean end-to-end distance of unstretched chain.

r in equation (3.6) is defined as the average distance to the surface of the free end of the grafted chain. Since we do not have an exact solution for the conformation profile, we take **r** to be approximately equal to w. Figure 3.3 is a plot of $\mu_\sigma - \Delta H$ *vs.* μ_∞, calculated from the data in Table V. The fitted slope is 1.07 ± 0.06, and the intercept of the fitted line with the vertical axis should give the value of ΔH ($-5.8 \pm 0.1\, k_B T$ with $T = 160$ °C, or -5.0 kcal/mol).

In order to further test the validity of this formulation, we prepared a bilayer sample corresponding to $\phi_{\text{initial}} = 0.20$, but where the matrix layer was composed of 50% PS of $M_w = 670\,000$ and 50% PS of $M_w = 1\,700$. From Figure 3.4, we see that as expected by mean field theory[19], the shorter chains swell the grafted layer. The resulting entropy loss increases the energy of the grafted chains. To obtain the same grafting density, the end-labeled chain concentration in the bulk needs to be higher. Substituting the measured values of σ and ϕ_∞ into equations (3.6) and (3.5) we see from Figure 3.3 that the experimental point (triangle) agrees well with the predicted value.

3.3 TEMPERATURE DEPENDENCE

The enthalpy of attachment of -5.0 kcal/mole obtained from the equilibrium grafting density as a function of bulk volume fraction can also be verified by temperature dependence measurement. Figure 3.5 plots μ_σ *vs.* μ_∞ for the same samples of dPS-COOH/PS mixture annealed at 135 °C (▲), 160 °C (●), 200 °C (○), and 240 °C (△), where $\Delta H = -5.0$ kcal/mole is used. The solid line is the fit to the 160 °C data (which is the solid line in Figure 3.3 translated by $\Delta H/k_B T$ units). With the slope fixed at 1.07,

the dashed line is the fit to the data obtained at 200 °C. Its intersection with the vertical axis is 0.05. The data obtained at other temperatures fall closely to 160 °C data as well.

The mechanism of attachment is not very clear at this time. Given the fact that the energy of interaction is small, the attachment is likely due to intermolecular interaction. In this case, the probability of chains being grafted and the probability of chains being free are determined by the Boltzmann distribution, that is,

$$\frac{z^*}{\phi_\infty} \propto e^{-\beta\Delta E} . \tag{3.8}$$

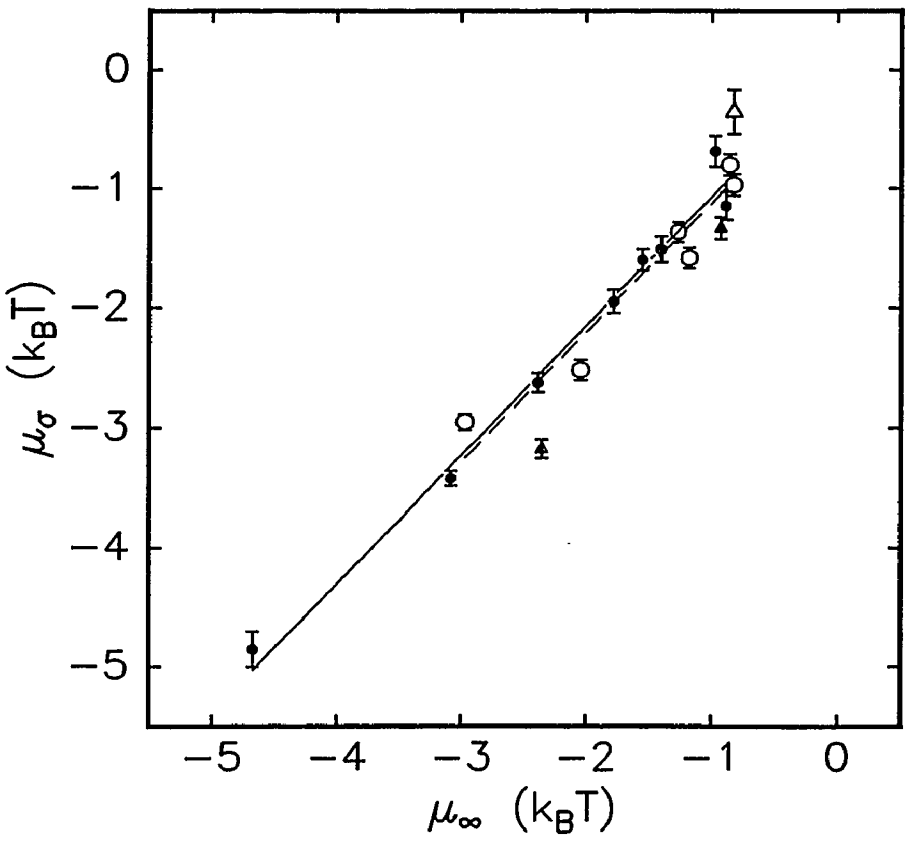

Figure 3.5 μ_σ *vs.* μ_∞ for the dPS-COOH/PS mixture annealed at 135 °C (▲), 160 °C (●), 200 °C (○), and 240 °C (△).

where ΔE is the sum of the enthalpy of attachment, ΔH, and the configuration entropy, $T\Delta S$, $\Delta E = \Delta H + T\Delta S$.

If the attachment is of chemical origin, for example,[20,21]

$$\text{PS-COOH} + \text{SiOH} \rightharpoonup \text{PS-COOSi} + \text{H}_2\text{O} \ , \tag{3.9}$$

where the carboxyl end group and the silanol are respectively the acid and alcohol groups which react to liberate water and form the PS-COOSi ester, the equilibrium constant, K, for this reaction[22] is

$$K \equiv \frac{[\text{H}_2\text{O}] \cdot [\text{PS-COOSi}]}{[\text{SiOH}] \cdot [\text{PS-COOH}]} = C_0 e^{-\frac{\Delta H - T\Delta S}{k_B T}} \ , \tag{3.10}$$

where C_0 is a temperature independent constant, and ΔH is the enthalpy change of the reaction. The concentration of the ester, [PS-COOSi], is simply the grafted chain density, which is proportional to z^*, and the concentration of unreacted PS-COOH is proportional to the volume fraction of unattached chains in the bulk, ϕ_∞. If we assume that the density of OH groups on the silicon oxide surface is similar to that previously measured on silica and glass particles[16], approximately 3 to 5 groups per 10^2 Å^{-2}, then the concentration on the surface is to first order unaffected by the attachment of the polymer chains whose grafting density, $\sigma = z^*\rho/N$ (where ρ is the density of polystyrene and N is the polymerization index of the grafted chain), is on the order of 10^{-3} Å^{-2}. Similarly, the H_2O concentration is unaffected since it is primarily determined by the base pressure of the vacuum system. The equilibrium constant, K, becomes proportional to the ratio of the experimentally measured quantities z^* and ϕ_∞ and one arrives at a same equation as (3.8) which can be rewritten as,

$$\ln\left[\frac{z^*}{\phi_\infty}\right] = -\frac{\Delta H}{k_B T} + \ln C_0 + \frac{\Delta S}{k_B} . \qquad (3.11)$$

Equations (3.8) and (3.11) are equivalent to $\mu_\sigma = \mu_\infty$, when the molecular weight of matrix chain and the molecular weight of end-labeled chain are equal, *ie.*, $N = N'$.

3.4 DISCUSSION

Despite the success in describing the grafting of end-functionalized chains in the melt to a surface by the thermodynamic equilibrium between grafted chains and chains in the bulk, some questions remain unsolved.

The segregation of deterated polystyrene monomer to the surface is ignored, thus the grafting density is overestimated. Samples of dPS ($M_w = 104\,000$) and hPS ($M_w = 670\,000$) blend shows that the segregation is a factor of 10 lower. We believe the grafting is mainly a result of end attachment for end-functionalized chains.

The reference state of the chemical potential of COOH-dPS chains in bulk, μ_∞ is in a melt of pure COOH-dPS chains. The interpenetration between the grafted chains and the matrix chains is ignored. The error in entropy might have been taken cared of by the correct determination of constant C_σ. The monomer-monomer interaction between dPS and hPS, on order of $N\chi$, is small and the interpenetration is probably weak, so the error resulting from the monomer-monomer interaction should not be significant.

Estimation of the stretching energy is quite primitive. This is indeed a two folded problem. First, since a statistical model for chains in contact with a surface is not

available, the average position of the other end is approximated by the width of the profile which itself is some what subjective. Since the instrumental resolution folds the peaks of different width to a different degree, the 1/4 rule used for determining w is not too reliable. Second, the entropy expression, $S = 3\mathbf{r}^2/2R_0^2$, can be derived either assuming the ends are fixed at a displacement of $\mathbf{r}$, or assuming each segment has equal preferred orientation of $\mathbf{r}/N$. It is not clear, however, whether the expression is valid for chain distortion caused by the presence of a surface.

It should also be pointed out that the correct expression representing chemical potential risen from stretching entropy of the grafted chains should be

$$\mu_{\Delta S} = \frac{d}{dn}\left(n\frac{3}{2}\frac{\mathbf{r}^2}{R_0^2}\right) = \frac{3}{2}\frac{\mathbf{r}^2}{R_0^2} + \frac{3}{R_0^2}\mathbf{r}\cdot\frac{d\mathbf{r}}{dn} . \qquad (3.12)$$

The second term in the above equation, the effect on the stretching of other grafted chains by adding or removing one chain, is neglected, resulting the underestimation of the chemical potential of the grafted chains.

REFERENCES

1. T. Cosgrove, T. Heath, B. van Lent, F. Leermakers, and J. Scheutjens, *Macromolecules* **20**, 1692 (1987).
2. M. Muthukumar and J. S. Ho, *Macromolecules* **22**, 965 (1989).
3. S. T. Milner, T. A. Witten, and M. E. Cates, *Macromolecules* **21**, 2610 (1988).
4. T. Cosgrove, *J. Chem. Soc. Faraday Trans.* **86(9)**, 1323 (1990).
5. C. Ligoure and L. Leibler, *J. Phys.* France **51**, 1313 (1990).

6. K. Shull, *J. Chem. Phys.* **94,** 5723 (1991).

7. G. Hadziioznnou, S. Patel, S. Granick, and M. Tirrell, *J. Am. Chem. Soc.* **108,** 2869 (1986).

8. J. H. Tauton, C. Toprakcioglu, L. J. Fetters, and J. Klein, *Nature* **333,** 712 (1988).

9. S. S. Patel and M. Tirrell, *Ann. Rev. Phys. Chem.* **40,** 579 (1989).

10. P. Auroy, L. Auvray, and L. Leger, *Phys. Rev. Lett.* **66,** 719 (1991).

11. S. K. Satija, *et al.*, preprint.

12. R. A. L. Jones *et al.*, preprint.

13. S. T. Milner, *Science* **22,** 905 (1991).

14. K. H. Dai, E. J. Kramer, and K. R. Shull, preprint.

15. L. J. Fetters, W. W. Græssley, N. Hadjichristidis, A. D. Kiss, D. S. Pearson, and L. B. Younghouse, *Macromolecules* **21,** 1644 (1988).

16. F. S. Bates and G. D. Wignall, *Macromolecules* **19,** 932 (1986).

17. T. G. Fox, Jr. and P. J. Flory, *J. Appl. Phys.* **21,** 581 (1950).

18. L. S. Bartell and R. R. Roskos, *J. Chem. Phys.* **44,** 457 (1966).

19. P. G. de Gennes, *Scaling Concepts in Polymer Physics,* (Cornell University Press, Ithaca, N.Y. 1979).

20. Independent infra-red spectroscopy experiments are in progress to determine k in the absence of PS. D. Allara, (private communication).

21. E. A. Moelwyn-Hughes, *Physical Chemistry,* (Pergamon Press, 1964) p.1022.

CHAPTER 4

Kinetics of Brush Construction

Equilibrium brush density as a function of the concentration of the free chain adjunct to the surface in melt has been studied in the previous chapter. The equilibrium condition is reached when the energy associated with the end-adsorption is equal to the energy required for the chain to be stretched. The dynamical aspect of the brush formation is expected to be controlled by the same adsorption-stretching mechanism. Ligoure and Leibler[1] described the formation of the brush from separated adsorption and desorption parts, where the adsorption is controlled by diffusion for low brush density, but is significantly slowed down when the brush density becomes high and the chain started being stretched.

4.1 SAMPLE PREPARATION

We measured the brush density as a function of time with the carboxy terminated deuterated polystyrene (dPS-COOH) in a matrix of polystyrene (PS), binding to native silicon-oxide on a silicon substrate. The molecular weight of dPS-COOH is 86 000 g/mole, measured by GPC on the dPS component prior to attachment of the COOH end. The samples were prepared by first spin casting, out of chlorobenzene solution, a layer of polystyrene ($M_w = 670\,000$, $M_w/M_n \leq 1.06$) on the silicon substrate, then placing on the top a layer of dPS-COOH. Samples were made on each of the following two types of substrates: Native oxide-covered silicon substrate as received from the supplier, and silicon substrates covered by a self-assembled octadecyltrichloro-silane (OTS) monolayer. The oxide-covered substrate was washed in a solution of $H_2O_2 : NH_4OH : H_2O = 1 : 1 : 3$ mixture at 80 °C for 5 minutes before use. After the wash, water wets the substrate completely, indicating the existence of a clean oxide layer. The purpose of the OTS monolayer is to prevent the PS-COOH from adsorbing, so that the diffusion coefficient of PS-COOH in the PS matrix can be measured. The thicknesses of the samples were measured using ellipsometry. On the oxide-covered substrate, the thickness of the bottom PS layer and the top dPS-COOH layer are 2450 ± 20 Å and 430 ± 8 Å respectively. On the OTS covered substrate, the thickness of the PS and dPS-COOH layers are 3000 Å and 2500 Å respectively. Two samples otherwise identical to the above samples except with inert dPS (Polymer Laboratories Ltd, $M_w = 104\,000$, $M_w/M_n \leq 1.05$) in the place of dPS-COOH were also made as control samples. The above samples were then cut into small pieces and annealed at

160 °C for varies times up to 6 days. The concentration profiles after the annealing were measured by the dynamic secondary ion mass spectrometry (SIMS) technique.

4.2 BULK DIFFUSION OF THE END-LABELED CHAINS

Figure 4.1 is a plot of the concentration profiles of the dPS-COOH/PS and dPS/PS bilayer samples made on the OTS covered substrate annealed at 160 °C for 40.5 minutes. While the chemical difference of the end-group itself is not expected to affect the diffusion of a long polymer chain, the diffusion rate can be strongly affected if the polar end-group has the tendency to aggregate. Such an effect was not found in our system as seen in Figure 4.1 where mutual-diffusion profiles of dPS-COOH/PS and dPS/PS (the distance is scaled by $N_{dPS}/N_{dPS\text{-}COOH}$) are shown to be identical. Furthermore we can compare the mutual-diffusion profile with that calculated from the diffusion equation,

$$\frac{\partial \phi}{\partial t} = \frac{\partial}{\partial x}\left[D(\phi)\frac{\partial \phi}{\partial x}\right], \tag{4.1}$$

where $D(\phi)$ is the composition dependent mutual-diffusion coefficient,[2,3]

$$D(\phi) = \phi_A{}^2 \phi_B{}^2 \left(\frac{N_A}{\phi_A} D^*{}_A + \frac{N_B}{\phi_B} D^*{}_B\right)\left(\frac{1}{N_A \phi_A} + \frac{1}{N_B \phi_B} - 2\chi\right), \tag{4.2}$$

where D^*_A and D^*_B are the tracer diffusion coefficient of polymer A and B respectively. Since dPS and PS are chemically identical polymers we assume their self-diffusion coefficients scale as the inverse square of the molecular weight only, *i. e.*, $D^*_A = D^*_B N_B{}^2/N_A{}^2 \equiv D^*$. Since the OTS monolayer prevents the adsorption of dPS-COOH to the surface, the closed boundary condition, $\partial\phi/\partial x|_{x=0} = 0$, applies.

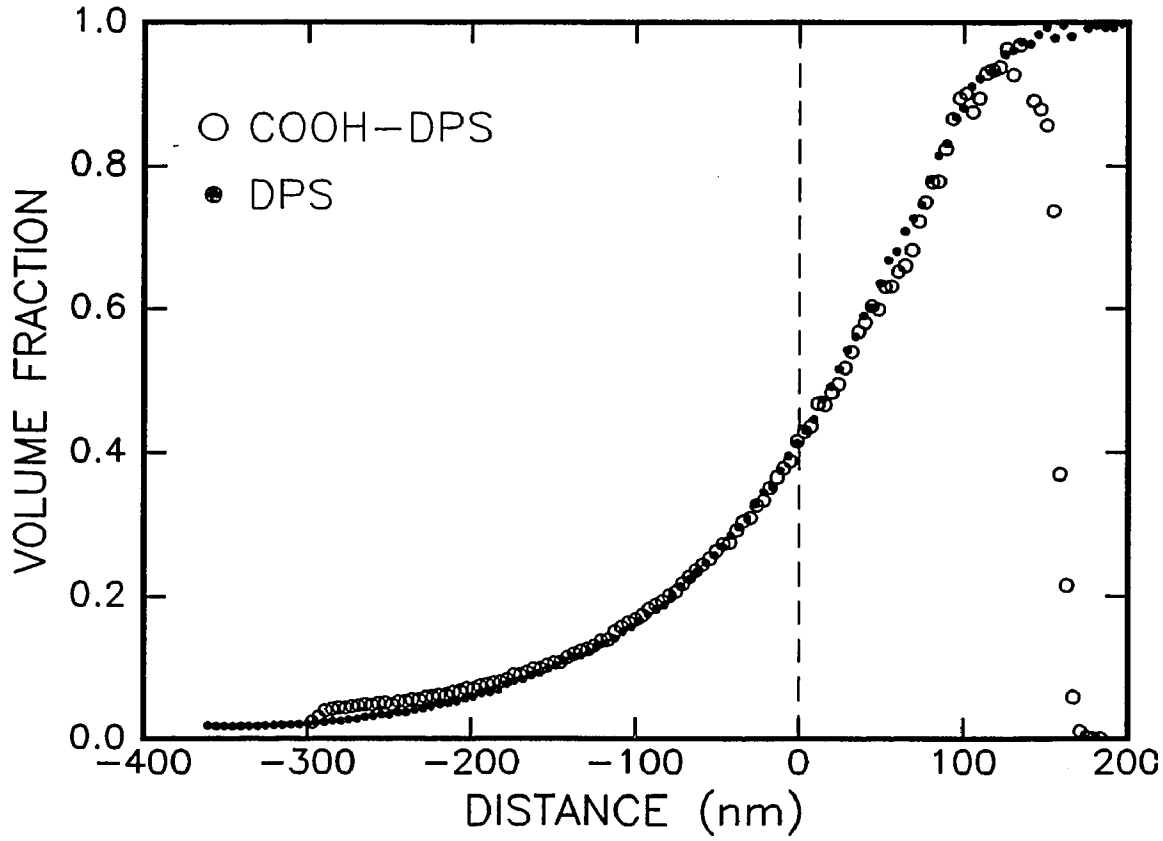

Figure 4.1 Comparison of diffusion profile of COOH-dPS (○) and dPS (●) into hPS ($M_w = 670\,000$) matrix.

Consequently, the self-diffusion coefficient can be obtained by fitting the diffusion profiles and the results agree reasonably well† with those in the literature.[4]

4.3 TIME DEPENDENCE OF THE BRUSH GROWTH

†It is found within the time scale of this experiment, that the diffusion coefficient obtained from fitting the data by equation (4.1) decreases as a function of annealing time. Such anomalous mutual-diffusion behavior will be discussed later. Meanwhile a diffusion coefficient proportional to $t^{-1/2}$ is used in the subsequent discussions in this chapter.

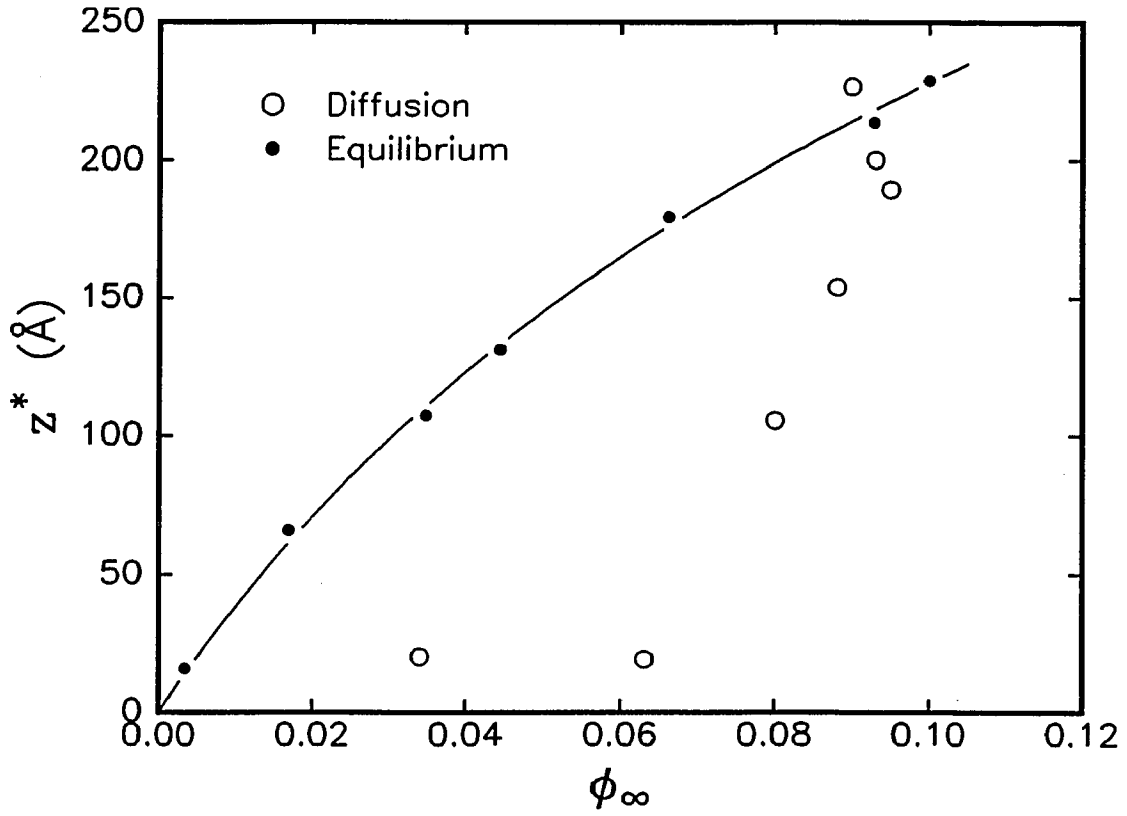

Figure 4.2(a) The brush density as a function of the unattached chain concentration next to the brush for the growing brush (○) and the equilibrized system (●).

For the samples made on native oxide covered silicon substrate, when the dPS-COOH diffuses through the PS layer and reaches the substrate, it can be attached to the substrate. Figure 4.3 is the plot of the dPS-COOH profiles at different annealing time as measured by SIMS. The brush density (the volume of chains adsorbed per unit area) z^*, the width of the profile w, and the concentration of dPS-COOH in the region next to the brush ϕ_0, of samples with different annealing time are summarized in Table VI. Comparing the data with the equilibrium result, it can be seen from Figure 4.2(a) that z^* as a function of dPS-COOH concentration next to the brush is significantly lower than

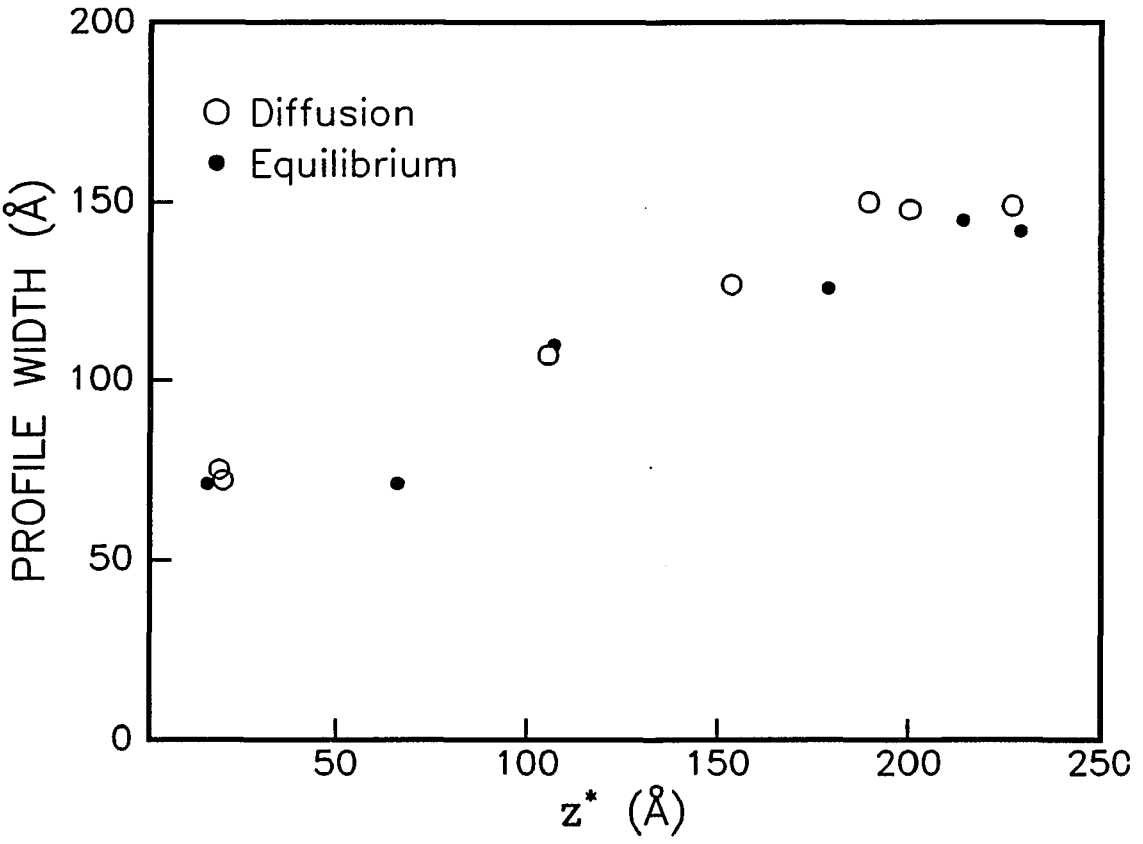

Figure 4.2(b) The brush width as a function of the brush density for the growing brush (○) and the equilibrized brush (●).

Table VI Summary of Time Evolution of Brush Construction

Time (min)	ϕ_∞	z^* (Å)	w (Å)
20.	0.034	20.1	72.
40.	0.063	19.2	75.
120.	0.080	105.	107.
260.	0.088	154.	127.
780.	0.093	200.	148.
1260.	0.095	189.	150.
8460.	0.090	227.	227.

the equilibrium value, indicating that the brush construction is controlled by the ability of the end-functionalized chain to penetrate through the existing brush at the surface. This is also indicated by the fact that after a long time annealing, when the bulk concentration is nearly uniform in the sample, the brush density continues to increase for a much longer time (Figure 4.3). On the other hand, the width of the brush as a function of the brush density is the same as that of the brush in equilibrium (Figure 4.2(b)), indicating that the time it takes for the adsorbed chains to reach minimum energy configuration is shorter than the time needed for the chains to be adsorbed.

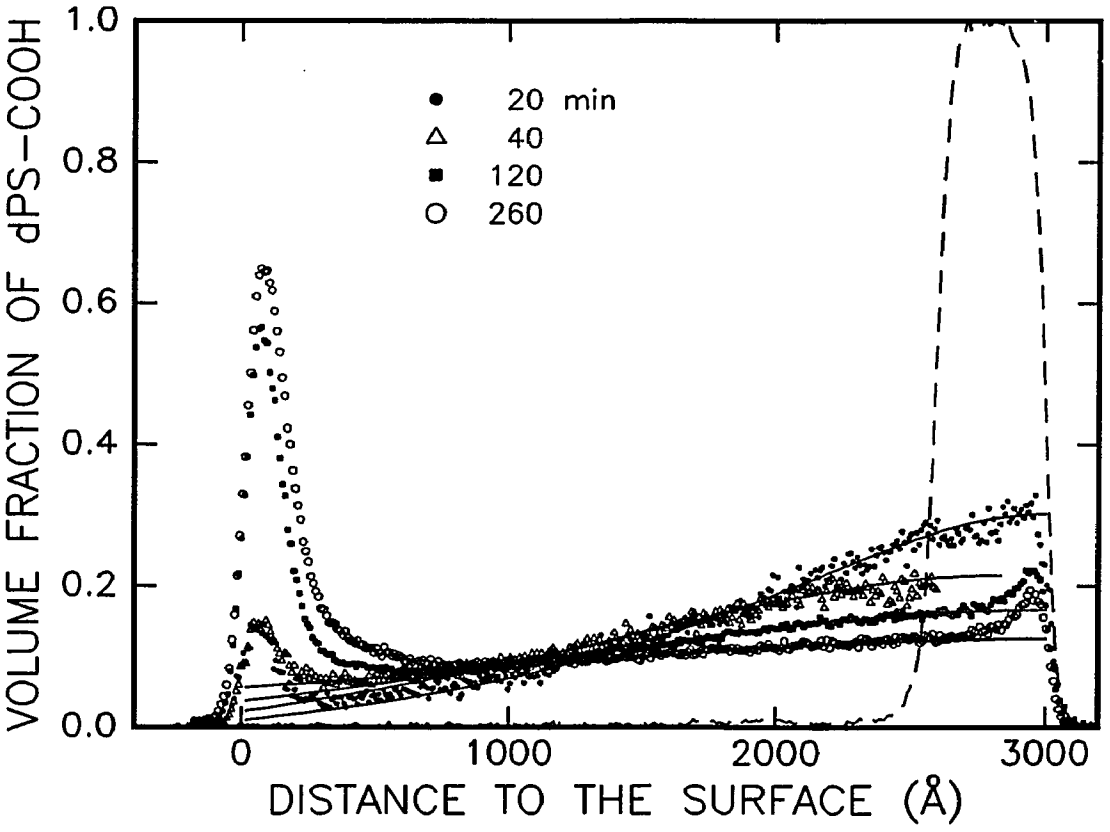

Figure 4.3 The dPS-COOH concentration profile after annealed at 160 °C for (●) 20 minute, (△) 40 minute, (■) 120 minute, and (○) 260 minute. The dPS-COOH is initially deposited on the top of a PS layer.

Knowing that the equilibrium between the adsorbed dPS-COOH chains and the free dPS-COOH chains is dynamic, there should be constant exchange between the adsorbed and the free chains. For a system approaching equilibrium, the rate of increase of the adsorbed chain density is governed by the net flux near the surface. Thus the boundary condition should be written as:

$$\frac{dz^*}{dt} = D\frac{\partial \phi}{\partial x}\bigg|_{x=0} = S\phi(0) - Rz^* , \tag{4.3}$$

where S describes the rate of adsorption and R describes the rate of the desorption. The ratio between R and S, $T = R/S$, determines z^* as a function of dPS-COOH concentration in the bulk. The adsorption and desorption rates, R and S, are expected to be functions of z^* as well as the structure of the brush, and thus will vary during the course of the brush construction.

Ligoure and Leibler[1] and Milner[5] calculated the process of brush construction in solution. Their calculation can be used to determine R and S as functions of z^*, ϕ_∞, and w. In order for a chain to be grafted, the COOH labeled end has to penetrate through the existing brush. At the moment when the labeled end is at a distance x from the surface, the chain will be, on average, stretched by $w - x$, with w the stretching of the chains in the existing brush. Thus for a chain to be grafted, It has to overcome a potential barrier of the form

$$\frac{f(x)}{k_B T} = \frac{3}{2}\frac{(w-x)^2}{R_0^2} + \hbar\sqrt{-\Delta H/2\mu}\ \delta(x) . \tag{4.4}$$

The second term represents the interaction between the monomer with the surface, which

has one bound state of ΔH, the energy of the interaction. If the concentration of the end-labeled chain is low and the interaction between the end-labeled chain and the matrix chain is negligible, the evaluation of the probability distribution of the labeled end, $P(x, t)$, is described by the Fokker-Plank equation:[5,6]

$$\frac{\mathrm{d}}{\mathrm{d}t}P(x,t) = -\frac{\mathrm{d}}{\mathrm{d}x}J(x,t) = \frac{\mathrm{d}}{\mathrm{d}x}\left[D^*\left(\frac{\mathrm{d}}{\mathrm{d}x}P(x,t) + P(x)\frac{\mathrm{d}}{\mathrm{d}x}f(x,t)\right)\right] . \qquad (4.5)$$

Since the brush growth is controlled by the adsorption and desorption at the surface, the change of $P(x, t)$ is slow everywhere except at the surface and the current, $J(x)$, will be nearly constant. Setting the left side of equation (4.5) to zero, the flux of the chain end distribution can be written as:

$$\frac{\pi}{N\upsilon}\frac{\mathrm{d}z^*}{\mathrm{d}t} = \left[\int_0^\infty \mathrm{d}x\; e^{f(x,t)}/D^*\right]^{-1} \left[P(x,t)\,e^{f(x,t)}\right]_0^\infty = J_{\text{in}} - J_{\text{out}} , \qquad (4.6)$$

where $\upsilon = 173\ \text{Å}^3$ is the volume of the polymer monomer, $\pi \sim 31\ \text{Å}^2$ is the inverse of the number of available adsorbing sites per unit area, and $\pi z^*/N\upsilon$ is the fraction of adsorbing sites being occupied, that is, $P(0, t) = \pi z^*/N\upsilon$.

For a very asymmetric function $f(x)$, The integration in equation (4.6) can be evaluated using the approximation introduced by Halperin:[5,7]

$$\int_0^\infty \mathrm{d}x\, e^{f(x,t)} = l e^{f_m(t)} , \qquad (4.7)$$

where l is the width for the barrier at k_BT below the maximum and $f_m(t)$ is the maximum of the energy barrier at time t, which is the stretching energy of the chain when the chain end just reaches the surface but before being attached:

$$\frac{f_m(t)}{k_BT} \equiv \frac{f(0+,t)}{k_BT} = \frac{3}{2}\frac{w(t)^2}{R_0^2} \quad . \tag{4.8}$$

We can then write

$$\begin{aligned} J_{\text{in}} &= \frac{D^*}{l}\frac{\phi}{N}e^{-\frac{f_m}{k_BT}} \\ J_{\text{out}} &= \frac{D^*}{l}\frac{z^*\pi}{Nv}e^{-\frac{\Delta H}{k_BT}} \quad . \end{aligned} \tag{4.9}$$

Note in equation (4.9), $P(\infty, t)$ is substituted by ϕ/N. The equilibrium condition is reached when J_{in} equals to J_{out}. Comparing this with the equilibrium condition of $\mu_\infty = \mu_\sigma$ in section 3.3, it can be seen that the molecular weight difference between the grafting and the matrix chains is ignored.

l can be determined from $w^2 - (w-l)^2 = 2R_0^2/3$. With $R_0 = 210$ Å, and w ranging from 72 - 227 Å, l ranges from 70 - 150 Å. Since l does not significantly affect the result,[‡] we take it to be a constant of 100 Å. With this approximation, J_{out} is, as expected, proportional to z^*. The J_{out}/z^* ratio can be determined by substituting the equilibrium z^*, w, and ϕ_∞ data obtained in section 3.2 into the condition for equilibrium, $J_{\text{out}} = J_{\text{in}}$. We obtain $J_{\text{out}}/z^* = 2.3\times10^{-7}$ Å (D^*/l) at 160 °C.

The diffusion equation can now be solved numerically (Appendix A) using equation (4.9) as the boundary condition. The calculated brush density as a function of time is plotted in Figure 4.4 (solid curve). The agreement between the calculation and experimental data (open circles) is very good. The calculated diffusion profile of

---

[‡]Different l values were checked in the subsequent calculations and the effect was found to be insignificant.

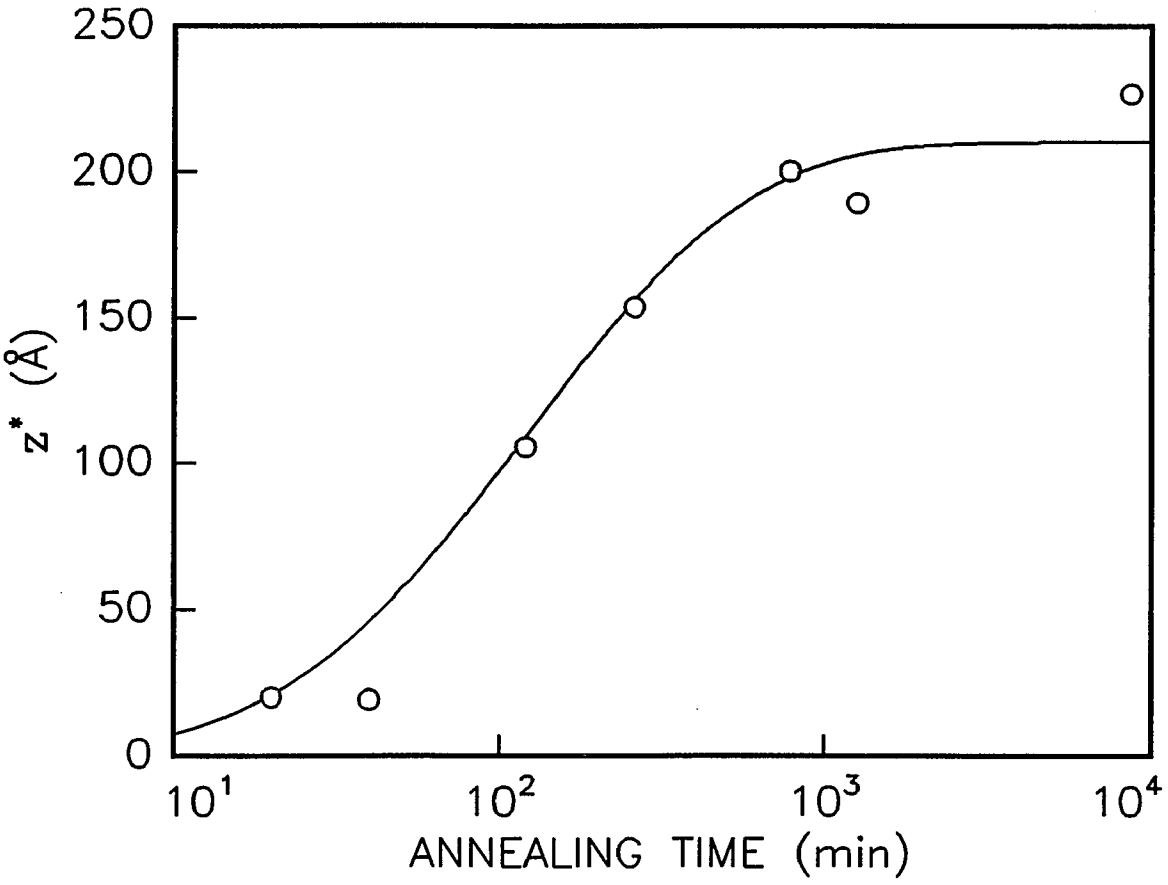

Figure 4.4 The growth of brush density as a function of annealing time. The solid line corresponding to the calculation.

dPS-COOH is also in good agreement with the experimental profile obtained by SIMS (Figure 4.3).

Before the brush density becomes very high, the final equilibrium value, as well as the value at intermediate time, of z^* is sensitive to the interaction energy ΔH. The time dependent increase of brush density may provide a method of measuring interaction energy between a functional group and a surface, when the energy is so large that at equilibrium, almost all chains are adsorbed.

4.4 CONCLUSIONS

The diffusion of COOH labeled polystyrene in polystyrene matrix is not affected by the functional end group. The construction of the brush is controlled initially by the diffusion. When the brush density is significantly high, so the adsorbed chains are stretched, the stretching energy becomes the controlling factor of the brush construction. The time dependence of the brush construction can thus be calculated assuming a constant flux near the surface. The measurement provides an excellent means of obtaining the interaction energy between an end-group and a surface.

REFERENCES

1. C. Ligoure and L. Leibler, *J. Phys.* France **51,** 1313 (1990).
2. H. Sillescu, *Makromol. Chem., Rapid Commun.* **5,** 519 (1984).
3. E. J. Kramer, P. F. Green, and C. J. Palmstrom, *Polymer* **25,** 473 (1984).
4. P. F. Green and E. J. Kramer, *J. Mater. Res.* **1,** 202 (1986).
5. S. T. Milner, *Macromolecules* **25,** 5487 (1992).
6. N. G. van Kampen, *Stochastic Processes in Physics and Chemistry,* (North-Holland, Amsterdam, The Netherlands, 1987).
7. A. Halperin, *Europhys. Lett.* **8,** 351 (1989); A. Halperin, *Macromolecules* **22,** 2403 (1989).

CHAPTER 5

Statistics of Polymer Chains in a Heterogeneous Environment

It has been recognized many decades ago that the polymers adsorbed at the surfaces of dispersive particles keep the particles from aggregating.[1,2] Since then, the problem of the polymer chain adsorbed to a surface in a dilute solution has been attracting constant attention. In comparison, the configuration of the polymer chains next to a surface in the melt is less extensively studied, although interest has been growing recently. Obtaining an exact solution is far more complicated for concentrated solutions or melts than for dilute solutions. The adsorption of chain to a surface out of a dilute solution can usually be effectively treated using a mean-field approximation, as long as the concentration of the polymer is not very high. For a chain near a surface in a melt, the mean-field approach is not valid. However, this fact is easily overlooked. Assumption

of either a reflecting wall or single chain statistics is made without justification in many theoretical studies.

This part of the thesis is an attempt to address this problem. The discussion at the moment is restricted to configuration of linear polymer chains next to a surface in a melt of identical chains.

5.1 POLYMER CHAINS IN A HOMOGENOUS ENVIRONMENT

Let's first review the configuration of linear polymer chains in a homogenous environment. One unique property of the macromolecule is that its molecular weight, or the length of the chain, can vary over orders of magnitudes and its physical properties can usually be expressed in power laws of the molecular weight. Such scaling law is the manifestation of the long chain nature of the polymer. One quantity requiring attention is the size of the chain which can be characterized by its root-mean-square of end-to-end distance,

$$R_0 \equiv \left\langle (r_0 - r_N)^2 \right\rangle^{1/2} , \tag{5.1}$$

or its radius of gyration,

$$R_g \equiv \frac{1}{N} \left\langle \sum_{i=0}^{N} (r_i - r_c)^2 \right\rangle^{1/2} , \tag{5.2}$$

where N is the number of segments in the chain, $\mathbf{r}_i$ is the position of the ith segment alone the chain, and $\mathbf{r}_c$ is the center of mass of each chain. The scaling of the size as a function of N can be written as

$$R_0 \propto R_g \propto N^{\nu} . \tag{5.3}$$

A significant amount of work has been done and a quite clear picture has been obtained for chains in homogenous solution or melt. In a dilute solution of a good solvent, when inter-penetration between polymer chains is weak, the polymer chains can be in any possible configuration satisfying the physical constraint of not crossing itself, with equal probability.[3] With a mean-field approach, Flory first derived the scaling exponent, ν, of the molecular weight dependence of the chain size, is $3/(d+2)$, where d is the space dimensionality.[4] In a space of dimension less than 4, self-exclusion causes the polymer chain to swell.

Such behavior of chains in a melt is commonly referred to as a *self-avoiding random walk* chain. The use of the expression "random walk" is due to historical reasons and may be misleading. It implies that the probability distribution of the chain in all configurations can be simulated by a procedure that each segment proceeds randomly toward the next unoccupied site from the site of the previous segment. A probability distribution obtained in such a manner is not reversely symmetric. Also, a section of a self avoiding chain has preferential configurations, depending on where the section is located within the chain. A chain in dilute solution is more stretched in the center than in the ends.[5] Consider a 6 segment chain in a 2-dimensional square lattice. Taking different orientations in space as different configurations, there are 142 possible configurations. In 92 cases, the three monomers in the end are in gauche configuration and in 50 cases they are in trans configuration. For the three monomers next to the end, 88 cases of configuration are gauche and 54 cases are trans. Such effects become more

significant as the chain becomes longer. For a 7 segment chain, the trans to gauche ratio of the end three monomers is 0.627 (79/126), while for 2nd, 3rd, and 4th monomer the trans to gauche ratio is 0.553 (73/132). The probability distribution of a section of chain with equal length is also depend on the total length of the chain. A three segment chain in a square lattice has three configurations, trans, L-gauche, and R-gauche with 1/3 of possible of each. For the first three segments in a five segment chain, the probability distribution of trans, L-gauche, and R-gauche is 9/25, 8/25, and 8/25 respectively.

In a concentrated solution or a melt, a polymer chain is expected to behave as an "ideal" chain[6] which can be described as a random walk without self-exclusion. Thus the spatial extension of a chain in melt scales as the square root of the molecular weight:

$$R_0^2 = 6R_g^2 = a^2N \,, \tag{5.4}$$

a, called the Kuhn step length, is a function of factors such as the monomer size, chain stiffness, etc.

Intuitively, such "ideal" behavior of a chain in melt can be understood in a way that, when moving from one segment to the next segment, a chain can not distinguish whether the surrounding monomers belong to the same chain, or belong to other chains, so the chain has no preferred direction for the next step.[7] Formally, this idea is reflected in the mean field theory, that the self-exclusive potential of the chain in question is compensated precisely by the exclusive potential from the other chains.[6]

It must be stressed, however, that the monomers of a polymer chain in a melt nevertheless do exclude each other. The set of possible configurations of each chain in

the melt is the same as that in dilute solution.[§] We will denote this set of possible self-excluding configurations, c_i, as $\mathbb{C} = \{c_i\}$. The configurational state of a system of N chains is determined by the configurations of all chains, $\mathfrak{C} = (c_1, \ldots, c_i, \ldots, c_N)$. The principle of equal weight requires that the probability of finding the system in state $\mathfrak{C}$, $P(\mathfrak{C})$, is the inverse of the number of possible states $\Omega(\mathfrak{C})$ of the system:

$$P(\mathfrak{C}) = \frac{1}{\Omega(\mathfrak{C})} . \tag{5.5}$$

Thus the probability of the ith chain being in configuration c_i is

$$P(c_i) = \frac{\Omega(\mathfrak{C}|c_i)}{\Omega(\mathfrak{C})} , \tag{5.6}$$

where $\Omega(\mathfrak{C}|c_i)$ is the number of possible states of the system given that the configuration of the ith chain is c_i.

The difference between chains in melt and chains in dilute solution is that in dilute solution, a single chain isolated from others by the solvent can be treated as an isolated system, so that the configurations of chains are independent, while in a melt, the polymer chains are strongly entangled to each other, so that the configurations of each individual chains, c_i, are not independent. In a dilute solution, the number of all possible states $\Omega(\mathfrak{C})$ is

---

[§]With the exceptions of a small number of configurations that are allowed in solution but violate the connectivity of the other chains in a densely packed melt. The number of such configuration should not be large enough to explain the swelling of polymer chains in solution, if it does contribute at all. Note that the chains become "ideal" when as much as 20% void exists in a melt.

$$\Omega(\mathfrak{C}) = \omega^N , \tag{5.7}$$

where ω is the number of elements in C, and the number of possible states with given ith chain configuration c_i, $\Omega(\mathfrak{C}|c_i)$ is

$$\Omega(\mathfrak{C}|c_i) = \omega^{N-1} , \tag{5.8}$$

so that the probability of the ith chain in configuration c_i is always $1/\omega$.

For a melt of N chains, since the configuration of one chain restricts the other, not only is the number of states much smaller than that in the dilute solution, but also is $\Omega(\mathfrak{C}|c_i)$ a function of c_i. It can be seen from equation (5.6) that for each individual chain in the melt, all configurations are not necessarily realized with equal probability. Instead the configurations of a chain are weighted by $\Omega(\mathfrak{C}|c_i)$. Given the fact the chains do not swell, one can conclude that the configuration of one chain less expanded in space allows the other chains to take more possible configurations.

To give an "ideal chain" a precise description, we assume that the chains in the melt are *Gaussian chains*, which are defined here as chains obeying the following two propositions:

Proposition 1: *Any segment with the same arbitrary length within a Gaussian chain has the same configurational distribution, regardless of its position along the chain.*

Proposition 2: *Any segment with the same arbitrary length within a Gaussian chain has the same configurational distribution, regardless of the total length of the chain.*

The above propositions are sufficient to derive the scale law in equation (5.4), but it can

be stronger than necessary to describe a chain in melt. Monte Carlo simulation is a good way to further confirm whether the above propositions are satisfied by a chain in the melt.

5.2 POLYMER CHAINS NEXT TO A SURFACE

Polymer chains with one or both ends located at the surface form an ensemble which can be realized experimentally by attaching polar or reactive groups to one end of a small number of chains in the melt, so that the end will be adsorbed to the surface. Theoretical predictions of the segmental distribution can then be verified.

It is generally agreed among theorists that the surface in a polymer melt does not affect the screening of the self-excluding effect. However, the subtler question of how the chain interacts globally with the surface can easily be overlooked. One assumption is that the chains will have equal distribution over all possible configurations satisfying the surface condition. The mathematical problem of the distribution under such an assumption was solved by Hesslink.[8] The probability distribution of the free end is

$$P(x) = xe^{-x^2/4R_g^2}, \tag{5.9}$$

and the segmental density as a function of distance to the surface is

$$\rho(x) = \frac{1}{R_g^2}\int_x^{2x} e^{-t^2/2R_g^2}dt = \frac{1}{R_g}\left[\mathrm{erf}(z/R_g) - \mathrm{erf}(z/2R_g)\right]. \tag{5.10}$$

The segmental density given in equation (5.10) approaches zero at the surface and peaks at a distance approximately $.969R_g$ from the surface. Such a mushroom-like distribution

has a drawback. For a polymer melt in contact with a surface, all chains will of course have their end located to one side of the surface. The chains having no end in contact with the surface will certainly be further way from the surface compared to those with at least one end in contact with the surface. Thus, on average, a polymer melt will have a region near the surface with a depleted density on the order of R_g. This contradicts the experimental evidence. From x-ray reflectivity measurements, thick polymer films (> 1000 Å) were found to have sharp interfaces at both soft (vacuum) and hard (silicon) surfaces,[9] and the density of polymer films as thin as 30 Å (much thinner than R_g) did not change significantly from the bulk.

Recalling that each chain in a melt is affected by the rest of the chains in the system, the response of a chain to a surface should be similarly affected. If a chain extended less in space is favored by the rest of the chains, we can make a similar assumption that a chain not leaving space between itself and the surface is also favored.

A model that does not change the density of the melt near the surface and predicts the segmental density of chains with one end at the surface peaks at the surface is to consider the surface as reflecting. A chain undergoes a random walk under the mean field in the melt; when it reaches to the surface it is reflected by the surface. A system with a uniform distribution of ends and a constant density is self-consistent under this model.

The following example will clarify the term reflecting surface.[¶] Figure 5.1 presents all possible configurations of a two or three segment chain in a square lattice, with the

---

[¶]The example is to demonstrate only the effect on the chain's response to the surface due to the matrix chains. What is not considered here is the screening of self-exclusion between monomers due to the matrix chains.

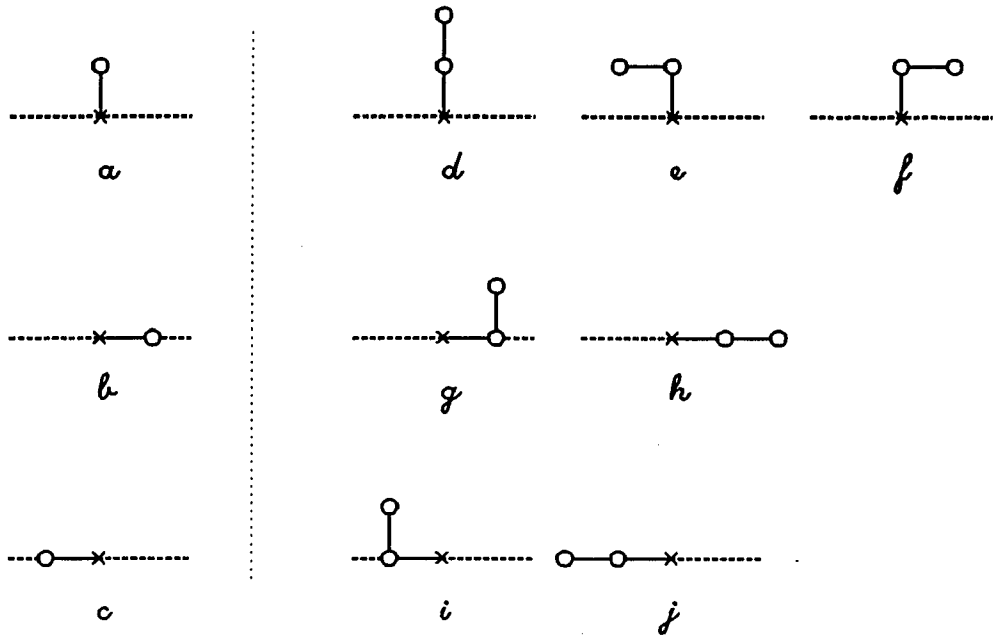

Figure 5.1 Possible configuration of two (*a* - *c*) or three (*d* - *j*) segment chain next to a neutral, impenetrable surface, with the first segment attached to the surface.

first segment (×) fixed at a surface (the dashed line). If each configuration has equal probability, as in the case of a single isolated chain, then the possibility for the two segment chain to be in configuration *a*, *b*, or *c* is 1/3 each, and the possibility for the three segment chain to be in configuration *d* - *j* is 1/7 each. Consider the first two segments in the three segment chain. The probability distribution of its configuration corresponding to configuration *a*, *b*, and *c* is not equal but is 3/7, 2/7, and 2/7 respectively. By reflecting surface, we mean that the probability distribution of the first two segments is not affected by the presence of the second segment. The combined probability of *d*, *e*, *f*, combined probability of *g*, *h*, and combined probability of *i*, *j*, are

each still 1/3. This lead to a probability of 1/9 for the cases in d-f and 1/6 for the cases in g, h. The comparison of probability distributions are summarized in Table VII.

The reflecting surface model becomes very persuasive if we consider it as an immediate result of a *Gaussian chain* with the following proposition added to the definition:

> **Proposition 3:** *Any segment of the same arbitrary length near a surface has the same configurational distribution that depends only on its spatial position relative to the surface, regardless of its position within the whole chain and the length of the whole chain.*

For a Gaussian chain in a d dimension space with one end positioned at a reflecting surface of $d-1$ dimension, the probability distribution of the ith segment in the chain as a function of distance to the surface is:

$$P_i(x) = 2\left[\frac{d}{2\pi i}\right]^{1/2} e^{-\frac{d}{2}\frac{x^2}{i}}, \qquad (5.11)$$

From the above equation, the average distance of the other end to the surface can be obtained as,

Table VII Configuration Distribution of Single Chain and Chains in the Melt

	a-c	d-f	g,h	i,j
Single chain	1/3	1/9	1/6	1/6
Chains in the melt	1/3	1/7	1/7	1/7

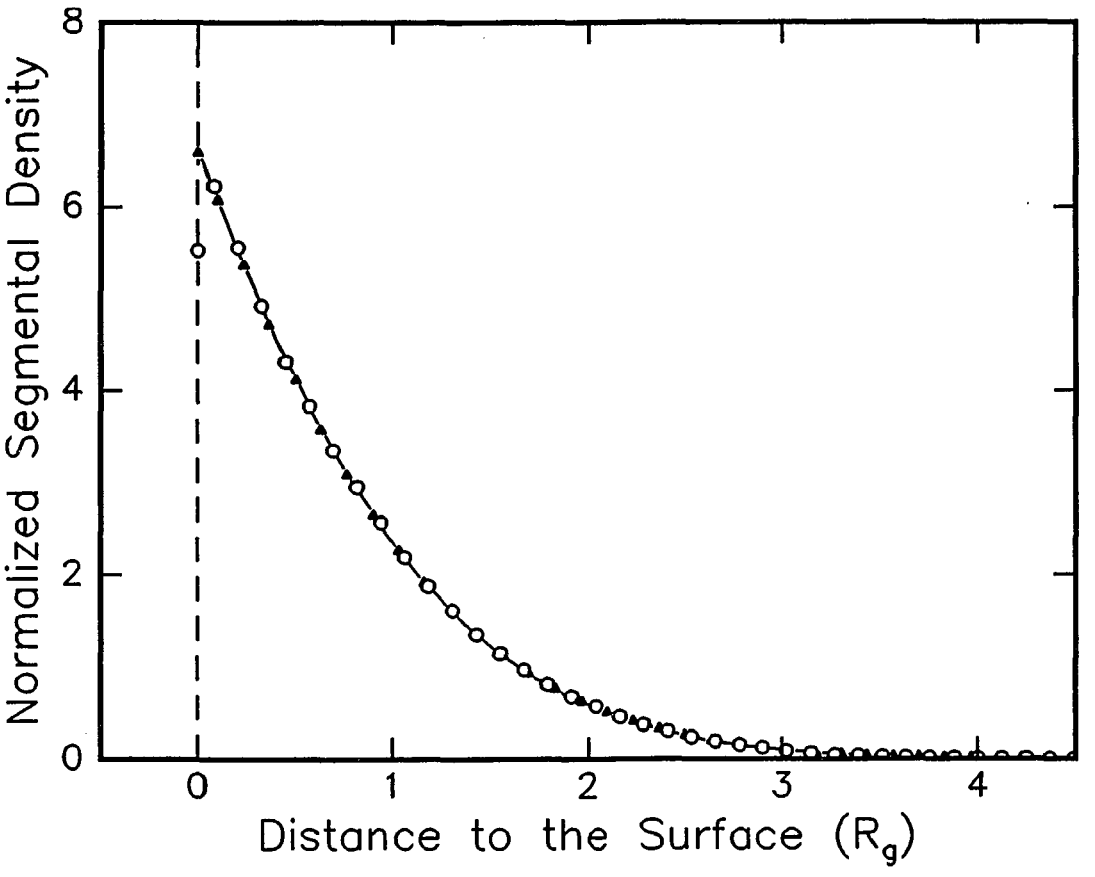

Figure 5.2 The segmental distributions of a Gaussian chain with one end attached to a surface. The probabilities of moving away from the surface are set to be 1/5 (○) and 1/6 (▲).

$$\langle x \rangle = \int_0^\infty x P_N(x) dx = \sqrt{\frac{2}{\pi}\frac{N}{d}} = \frac{2}{\sqrt{\pi}} R_g \,. \tag{5.12}$$

For a dPS of molecular weight 86000, $\langle x \rangle = 85.5$ Å in a three dimension space. If polymer chains in a melt is indeed Gaussian even near the surface, the value of $w = 71$ Å as the estimation of the average end-to-end distance in Chapter 3 is an underestimation.

The segmental distribution is

$$\rho(x) = \sum_{i=1}^{N} P_i(x) \ . \tag{5.13}$$

Figure 5.2 is the segmental distribution obtained from Monte Carlo simulation of a random walk in a cubic lattice: A chain starts from the surface and undergoes random walk in such a manner that it moves to all possible neighboring sites with equal probability from the current position. The segmental distribution is well approximated by an error function (the solid line in Figure 5.2),

$$\rho(x) = \rho_0 e^{-(x+h)^2/2w^2} \qquad (x > 0) \ , \tag{5.14}$$

with $h/R_g = 2.35 \pm 0.03$, $w/R_g = 1.66 \pm 0.01$.

In a solvent, a chain with one end grafted to a planar surface is repelled by the surface and makes very few additional contacts with the surface.[10] For the chain in a melt, the segmental distribution is maximum near the surface and the number of additional contacts is $\langle \nu \rangle \sim N^{1/2}$.

It should also be pointed out that the exact probability distribution of segments near a surface is not crucial. Except at the few layers next to the surface, the profile is not strongly affected by that distribution. Also plotted in Figure 5.2 as filled triangles (▲) is the result of Monte Carlo simulation assuming that the chain has probability of 1/6 to move away from the surface when the current position is at the surface. The difference between the two cases shown in Figure 5.2 is very small.

5.3 SOME FURTHER COMMENTS

Only the two simplest models of how the chains in a melt respond to the presence of a surface are discussed. There is no concrete proof for the reflecting surface model yet although the author is biased toward it. Even for chains in a homogenous melt, between the statistical principle of equal weight and the ideal chain assumption there exists a large theoretical gap which no one at this moment is sure can ever be closed. Experimentally however, much evidence, including neutron scattering experiments[11] and Monte Carlo simulations, confirm the ideal chain assumption. To conclude the chapter, the author would like to quote some recent developments in the area and offer some comments:

1. Shull[12] calculated the segmental distribution of a "dry brush" by solving the diffusion like equation for the chain configuration. In the limit of very low brush density, the result is very similar to the profile in Figure 5.2. The slightly lower volume fraction at the surface is probably due to the repulsive force resulting from the expression of the chemical potential. Despite the similarity in the result, Shull's theory is a hybrid of the reflecting surface and the single chain configuration. A compressibility energy has to be introduced to conserve the density. It is not clear whether the similarity in the results is accidental.

2. Measurement of the profiles of dPS end-grafted to a surface in a hPS matrix is currently underway using the techniques of SIMS and neutron reflection.[13] The preliminary result shows that the volume fraction of dPS reduces near the surface. If this result sustains, it points to the possibility of spontaneous symmetry break down, so the polymer chains near a surface will be in two phases, one consisting of mushroom like chains and the other consisting of pancake like chains to fill the space below the mushroom like chains.

3. Monte Carlo simulation of a polymer melt in contact with a surface has recently been performed by Dickman.[14] In the simulation, a chain was attached permanently to a surface that is in contact with a melt. The behavior of this chain is monitored over time. The segmental density of the chain averaged over time is shown to peak at the surface.

4. Previous Monte Carlo simulations of polymer melts are focused on verifying the scaling exponent of the molecular weight dependence of the chain size. Much less has been done at the more fundamental level of verifying the Gaussian chain propositions proposed above. A particularly interesting system would be a ring macromolecule in a dilute solution. Since there is no preferred position in a ring macromolecule, the segmental distribution should be similar to that of a Gaussian chain. However, since a single ring macromolecule was found to swell, the second proposition for Gaussian chain should be violated.

5. A melt consisting of two types of chains that have different interactions with the surface is an interesting and also rather practical problem. The difference in the interaction affects the composition of the melt globally by attracting the preferred component near the surface. Whether the interaction affects locally the probability of random walk along the surface and away from the surface is not clear yet. A Monte Carlo simulation should also provide insight into this problem.

REFERENCES

1. E. L. Mackor, *J. Colloid Sci.* **6**, 492 (1951); E. L. Mackor and J. H. van der Walls, *ibid.* **7**, 535 (1952).

2. D. J. Meier, *J. Phys. Chem.* **71**, 1861 (1967).

3. P. G. de Gennes, *Scaling Concepts in Polymer Physics* (Cornell University Press, Ithaca, NY, 1979).

4. P. Flory, *Principles of Polymer Chemistry*, Chap. XII, (Cornell University Press, Ithaca, N.Y. 1971).

5. J. des Cloizeaux and G. Jannink, *Polymers in Solution: Their Modelling and Structure,* (Oxford University Press, New York, 1990).

6. P. Flory, *J. Chem. Phys.* **17**, 303 (1949).

7. T. P. Lodge, N. A. Rotstein, and S. Prager, *Advances in Chemical Physics, Vol LXXIX*, Edited by I. Prigogine and S. A. Rice, (John Wiley & Sons, Inc., 1990).

8. F. Th. Hesslink, *J. Phys. Chem.* **73**, 3488 (1969).

9. W. Zhao, X. Zhao, M. H. Rafailovich, J. Sokolov, T. Mansfield, R. S. Stein, R. C. Composto, E. J. Kramer, R. A. L. Jones, M. Sansone, and M. Nelson, *Physica B* **173**, 43 (1991).

10. E. A. DiMarzio and F. L. McCrackin, *J. Chem. Phys.* **43**, 539 (1965).

11. R. G. Kirste, W. A. Kruse, and J. Schelten, *Makromol. Chem.* **162**, 299 (1973); D. G. Ballard, J. Schelten, and G. D. Wignall, *Eur. Polym. J.* **9**, 965 (1973); J. P. Cotton, D. Decker, H. Benoit, B. Farnoux, J. Higgins, G. Jannick, R. Ober, C. Picot, and J. des Cloizeaux, *Macromolecules* **7**, 863 (1974).

12. K. R. Shull, *J. Chem. Phys.* **94**, 5723 (1991).

13. Y. Liu *et al.*, to be published.

14. R. Dickman, (Private Communications).

CHAPTER 6

Mutual-Diffusion between Comparable Polymers in the Intermediate Time Scale

More than twenty years ago, de Gennes introduced the reptation hypothesis to describe at the molecular-level the dynamics of polymer melt.[1] The idea was enhanced by detailed theoretical work of Doi and Edwards.[2,3] As a result, two important predictions concerning the motion of linear polymer chains in an unsheared melt were obtained. The first prediction is that the self-diffusion coefficient of linear polymer chains is inversely proportional to the square of the molecular weight. The second prediction is that at time less than the reptation time (the time for the chain to completely move out of the original tube), the mean square displacement in space as a function of time exhibits several distinct scaling regimes. Experimental verification of these predictions is widely regarded as a touchstone of the reptation model. The large volume

of experimental work in diffusion coefficient measurements prior to 1990 has been reviewed by Lodge *et al.*[4] Studies of diffusion at time less than reptation time are not abundant due to the lack of techniques with high spatial resolution. Another difficulty involved with the latter prediction is that unless the measurement is done with very high precision, it can not distinguish between the reptation prediction and the similar prediction of the Rouse model. Recent developments in neutron reflectivity technique made it possible to measure interfacial width with high spatial resolution; as a result, several measurements of interfacial broadening at early stages have emerged.[5,6] Most evidence obtained so far seems to confirm the reptation model predictions, especially the first one. However, as pointed out by Lodge *et al.*,[4] although in many instances the self-diffusion coefficient is inversely proportional to the molecular weight of the polymer, the absolute value of diffusion coefficient is not consistent with the prediction based on the reptation model[7] and the scattering of the data is substantial. We report here a recent measurement of mutual-diffusion between polystyrene and deuterated polystyrene using dynamic secondary ion mass spectrometry (SIMS). SIMS combines the advantages of being able to profile in direct space with spatial resolution of 100 Å (Chapter 1), less than the size of a typical high molecular weight polymer. Our result reveals that the diffusion of polymer may exhibit anomalous behavior to a distance scale far larger than the size of the polymer chain.

6.1 EXPERIMENTAL PROCEDURES

We measured the mutual-diffusion between polystyrene and deuterated polystyrene of

various molecular weights, as summarized in Table VIII. dPS and hPS films were made by spin casting separately onto a silicon substrate and a glass slide. The film spun on the glass slide was then floated off on water and transferred on the top of the film spun on the silicon substrate to form a bilayer sample. Since the film on water was picked up by approaching the bottom layer covered substrate from the air side, the interface will be free of contamination from the glass or water. Chlorobenzene, instead of toluene, was used as a solvent to obtain (visually) a smoother film. The thickness of both layers were measured by ellipsometry to an precision better than 1%. The samples were kept in vacuum better than 10^{-6} Torr for at least 4 hours at room temperature before being annealed in a vacuum oven with preset temperature of 160 °C for times ranging from 5 minutes to 8 hours. The base pressure of the oven was less than 20 microns. This pressure was achieved in less than 25 minutes (Figure 6.1) by a mechanical pump. The samples were quenched to room temperature in less than 15 seconds by laying them on a large aluminum block after being taken out of the oven. For shortly annealed samples,

Table VIII List of Bilayer Samples

	dPS			hPS		
	Thickness	M_w	M_w/M_n	Thickness	M_w	M_w/M_n
I	2000 Å	188000	1.02	3000 Å	220000	1.03
II	2000 Å	104000	1.02	4000 Å	770000	1.04
III	2000 Å	188000	1.02	4000 Å	770000	1.04
IV	250 Å	550000	1.05	2000 Å	670000	$\leq$ 1.06

The polystyrene of $M_w = 670000$ is purchased from Pressure Chemical Company. All other polymers are purchased from Polymer Laboratories, Ltd.

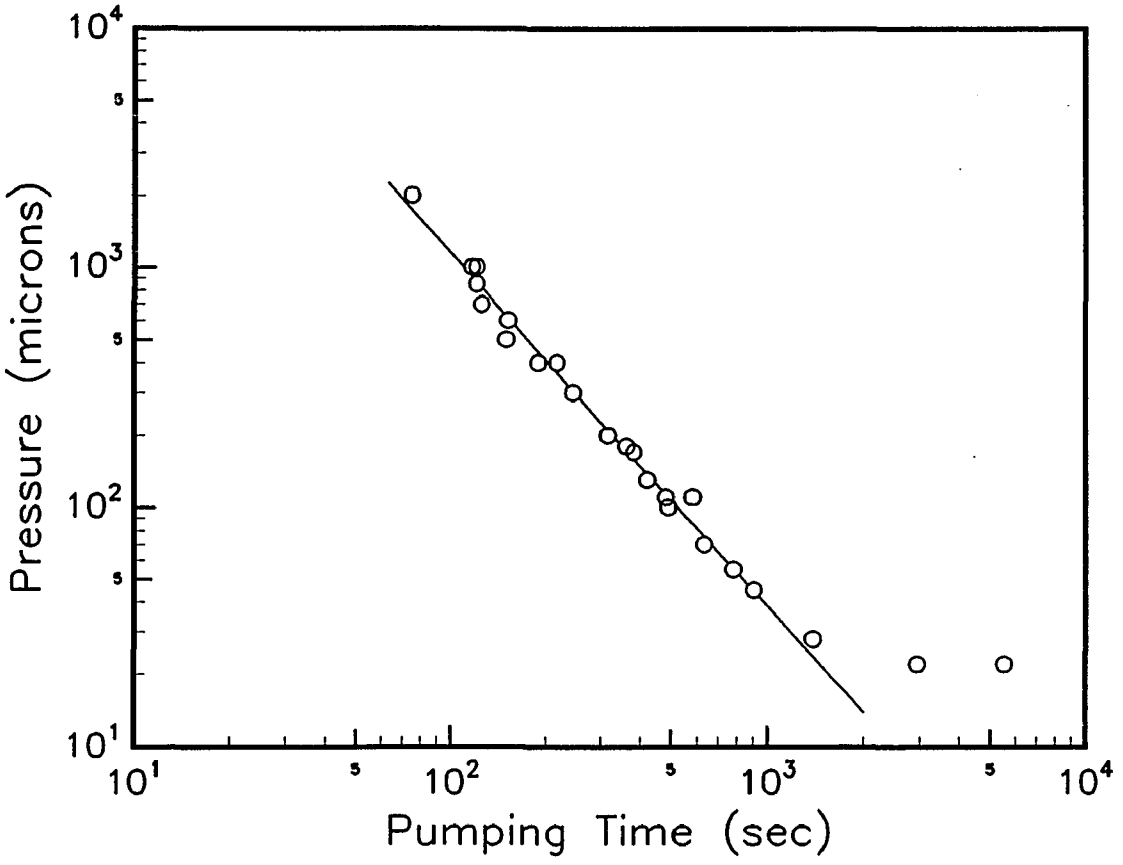

Figure 6.1 The pressure as a function of pumping time in the annealing oven.

distilled water was applied to cool the samples faster. The thickness of individual samples were measured by ellipsometry to reduce the uncertainties in the film thickness due to the thickness variation from the spun film. The mutual-diffusion profiles were then measured using SIMS. The sampling area of SIMS is a square of 0.3 mm in side. In this area the film thickness variation and initial film roughness proves to be much less than 100 Å SIMS resolution. The details of the SIMS technique and data reduction is discussed in Chapter 1.

The mutual-diffusion profiles were compared with calculated profiles using the *fast model* of polymer mutual-diffusion,[8] which predicts that the mutual-diffusion coefficient

D_m as a function of the volume fractions of two polymers is

$$D_m(\phi) = \phi_A^2 \phi_B^2 \left(\frac{N_A}{\phi_A} D^*_A + \frac{N_B}{\phi_B} D^*_B \right) \left(\frac{1}{N_A \phi_A} + \frac{1}{N_B \phi_B} - 2\chi \right), \qquad (6.1)$$

where D^*_A and D^*_B are the tracer diffusion coefficients of polymer A and polymer B, and χ is the interaction parameter between monomers A and B. The tracer diffusion coefficients of dPS and hPS were assumed to be inversely proportional to square of their molecular weights, $D^*_A/D^*_B = N_A^2/N_B^2$. An unfavorable interaction parameter,[9] $\chi = 1.7 \times 10^{-4}$, for dPS and hPS was used.

6.2 MUTUAL-DIFFUSION OF SYMMETRIC BILAYER

For the samples in set I that has near symmetric molecular weights of 188000 for dPS and 220000 for hPS, $D^*_A/D^*_B \approx 1.6$, and the "thermodynamic slowing down" due to the unfavorable χ is less than 0.85, so that D_m is not a strong function of volume fraction. The mutual-diffusion profile calculated using D_m given by equation (6.1) is indistinguishable from an error function, so constant D_m is assumed in the following analysis. For these samples annealed for less than 1 hour, where the effect of the boundary is not yet significant, an error function

$$\phi(x) = \frac{1}{\sqrt{4\pi D t}} \int_{-\infty}^{x} e^{-\frac{\zeta^2}{4Dt}} d\zeta \qquad (6.2)$$

where x is the distance to the initial interface, was used to fit the profile. For those samples annealed for longer times, the diffusion equation with constant diffusion

coefficient subjected to a closed boundary is solved numerically (Appendix A) to fit the experimental profile. The mutual-diffusion coefficient D_m measured from our data is not a constant. Instead, it progressively becomes smaller as the sample is annealed longer (Table IX).

A model independent quantity is the interfacial width which can be conveniently defined as the square root of $D_m t$. $D_m t$ as a function of annealing time is plotted in Figure 6.2 as open circles (○) on a log-log scale. For samples annealed longer than 1 hour, the diffusion is normal with a slope of 0.969. For samples annealed less than 1 hour, the slope obtained from the data is 0.505 ± 0.010. Note in Figure 6.2, the interfacial width is plotted in terms of R_0, the root-mean-square of end-to-end distance of the polymer. The anomalous scaling of the width of the diffusion profile as 1/4 power of diffusion time can not be explained either by reptation model or Rouse model, both predict normal diffusion for distance larger than R_0.

Table IX Summary of the Measured Mutual-Diffusion Coefficients between dPS (188 000) and hPS (220 000) at 160 °C as a Function of Annealing Time

Sample	Time (sec)	D_m (Å^2/sec)
Sample set I	760	287
188 k dPS/220 k hPS	1854	184
	3600	133
	5958	115
	24700	115
	88410	105.5

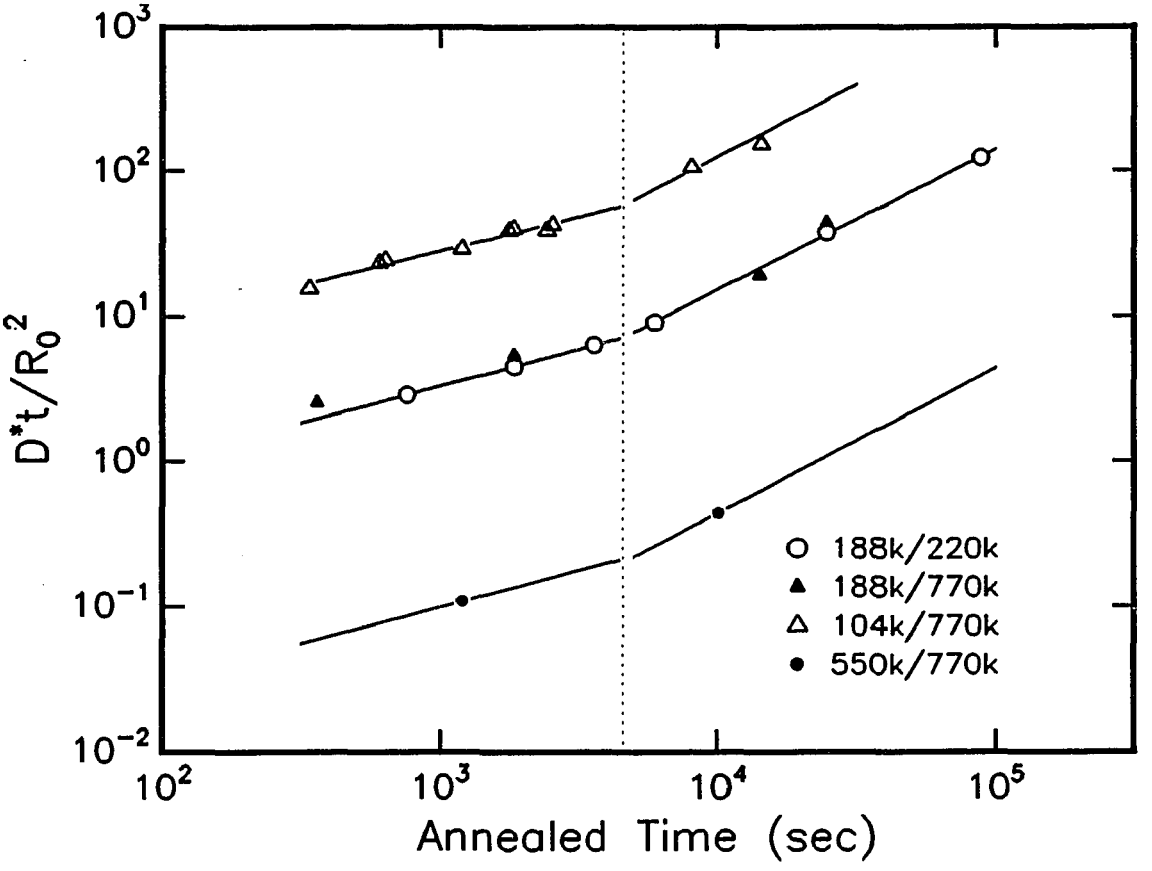

Figure 6.2 The reduced interfacial width, $D^*_s t/R_0^2$, as a function of annealing time for bilayers of different molecular weights.

6.3 MUTUAL-DIFFUSION OF ASYMMETRIC BILAYER

We also measured the mutual-diffusion between polymers with asymmetric molecular weights. The broken curve in Figure 6.3 is the profile of dPS ($M_w = 104\,000$) hPS ($M_w = 770\,000$) bilayer annealed for 26.5 minutes. The profile deviates significantly from the error function due to the strong volume fraction dependence of the mutual-diffusion coefficient. The volume fraction dependence of the diffusion coefficient can be calculated from the profile using the formula[10]

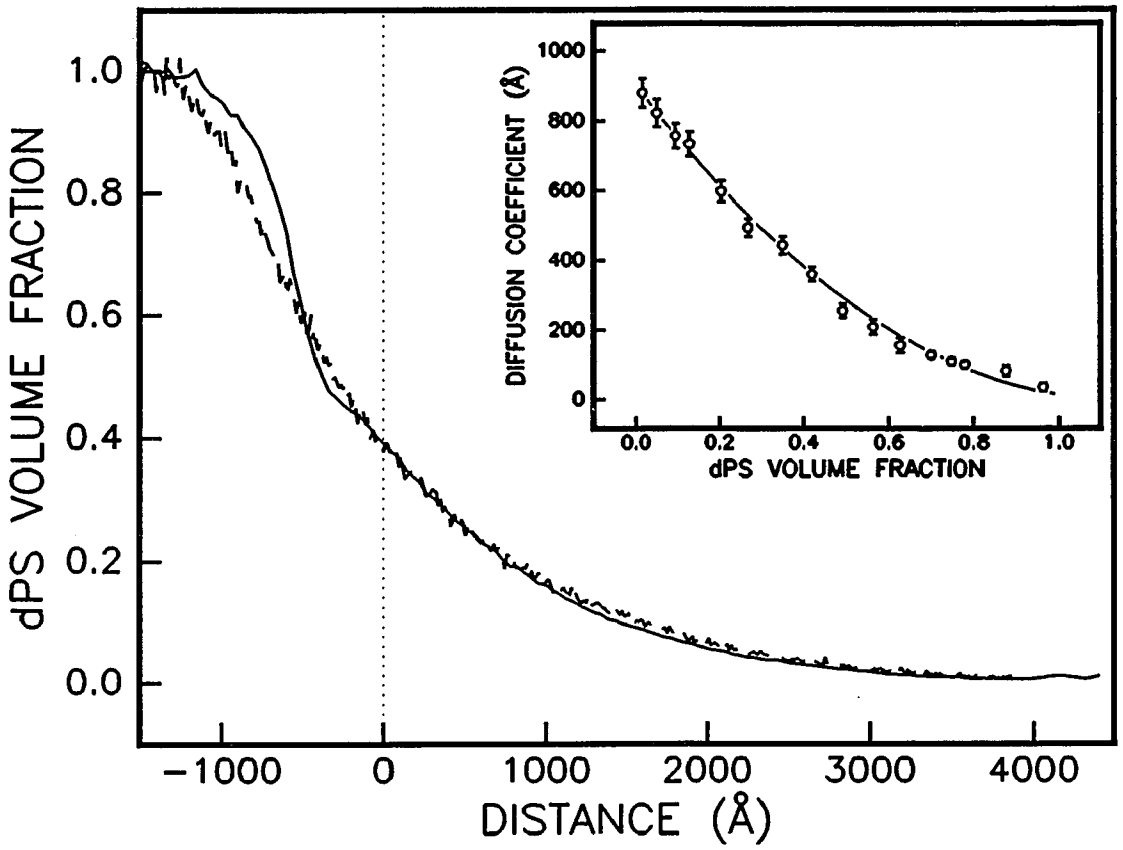

Figure 6.3 The profiles of dPS (104k)/hPS (770k) samples annealed for 26.5 min, with pre-annealed (solid curve) and not pre-annealed (broken curve) hPS layer. The inset is the diffusion coefficient.

$$D_m(\phi) = -\frac{1}{2t}\frac{dx}{d\phi}\int_0^{\phi} x(\phi')\,d\phi' \ . \qquad (6.3)$$

The result obtained by applying equation (6.3) to the profile in Figure 6.3, presented in the inset of Figure 6.3 as open circles (○), agrees well with the curve calculated from equation (6.1), taking D^* for dPS equal to 900 Å/sec^2. Consequently, the volume fraction dependent D_m given in (6.1) was used to fit all profiles and the tracer diffusion coefficient of the shorter chains, D^*_s thus obtained are tabulated in Table X.

Like the symmetric bilayer samples, the profiles of asymmetric bilayer samples also

scale close to 1/4 power of the annealing time for times less than 1 hour, and D^*_s is a function of time. Since the diffusion is controlled by the faster species, the interfacial width can be well characterized by the quantity $D^*_s t$. This characteristic width of profiles is plotted in Figure 6.2.

Since the original film was spun cast out of solution, the structure of the polymer chains could be very different from its relaxed Gaussian configuration. If the chain sizes

Table X Summary of the Measured Tracer Diffusion Coefficient as a Function of Annealing Time at 160 °C for Samples in Sets II, III, and IV

Sample	Time (sec)	D^*_s (Å^2/sec)
Sample set II	338	1916
104 k dPS/770 k hPS	606	1604
	637	1695
	1200	1015
	1784	908
	1854	904
	2430	667
	2550	698
	8114	544
	14400	446
Sample set III	360	535
188 k dPS/770 k hPS	1854	221
	14160	102
	24720	135
Sample set IV	1200	20.2
550 k dPS/670 k hPS	10143	9.6

are smaller and the chains are less entangled initially, one would expect the mutual-diffusion to be faster at early stages and as the chains relax to the Gaussian configuration, the entanglement increases and the diffusion slows down. The possibility that the relaxation of the chains from their initial configuration to Gaussian configuration takes longer than the reptation time can not be ruled out *a priori*. To check such a possibility, a control sample was made, with asymmetric molecular weight of 104000 for dPS and 770000 for hPS, in which the longer chain (hPS of 770000) film was pre-annealed at 160 °C for 4 hours in high vacuum before the bilayer is made. This sample is subsequently annealed together with a sample from set II at 160 °C for 26.5 minutes. If the initial polymer configuration does affect the diffusion of the polymer, the samples will have different profiles. Figure 6.3 compares the mutual-diffusion profiles of samples with pre-annealed (solid curve) and not pre-annealed (broken curve) hPS layer. The profile of the sample with pre-anneal hPS layer shows a kink at the interface, which is typical for a contaminated surface and may be the result of pre-annealing. The diffusion of dPS into hPS is not affected by the pre-annealing.

6.4 MOLECULAR WEIGHT DEPENDENCE

The tracer diffusion coefficients of 188k dPS obtained from the symmetric sample and the asymmetric sample are the same. Together with the good fit of the profile by the calculated profile, the *fast model* of mutual-diffusion is confirmed. Figure 6.4 plots the apparent diffusion coefficient scaled by the inverse of molecular weight squared. The data for short annealing time fall upon one another closely. Although the scattering of

data for long annealing time is unsatisfactory, a lot of previous work is available to indicate that the diffusion coefficient is inversely proportional to the molecular weight squared. This indicates that the transition time between the two scaling regimes occurs at the same annealing time of $t \approx 4500$ seconds for all molecular weights. This result agrees with the previous measurement of mutual-diffusion on dPS/hPS (of molecular weights 660,000 and 725,000 respectively) made by Reiter and Steiner.[6] In their measurement, the transition from 1/4 power to 1/2 power occurred at approximately 8×10^4 minutes at 120 °C, which, using the WLF relation,[11,12] translates to 3000

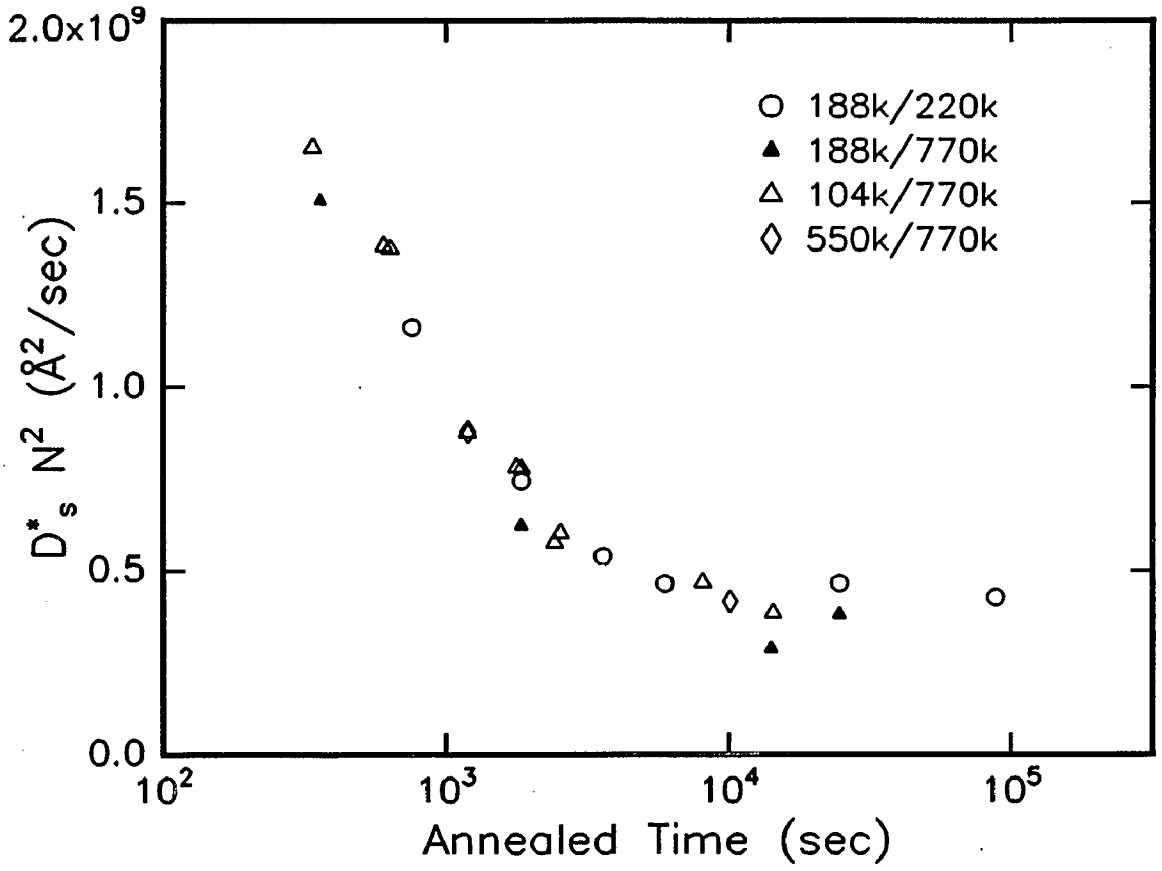

Figure 6.4 The apparent tracer diffusion coefficient as a function of annealing time of the shorter chains, scaled by the inverse square of their degree of polymerization.

seconds at 160 °C. The single transition time also supports our conclusion that the 1/4 power scaling is not caused by the unrelaxed initial chain configurations.

6.5 DISCUSSION

Considering the fact that the mutual diffusion agrees so well with the established theory, with the only exception of changing diffusion coefficient, it is tempting to think that the anomalous behavior is due to some side effects. The time it takes for the sample to heat up, if significant at all, should reduce the diffusion at short time. It could also be the heat flow that enhances the diffusion, but the thermal equilibrium is expected to be achieved in a few minutes at most and the heat comes from either side of the sample. One very plausible explanation is that the solvent hasn't been completely removed before the sample was annealed. As the solvents diffuses out when annealed, the mobility of the monomer is reduced. Combining the square root time dependence of solvent reduction and the square root time dependence of interfacial broadening, it is possible to get a 1/4 power time dependence. However, the amount of residing solvent is expected to be very small unless there is some interaction binding the solvent and polymer together, considering that the samples were kept in high vacuum for several hours before being annealed. The thickness of the samples were also measured before and after the annealing, which gave no noticeable ($< 1\%$) change. It is quite a remarkable thing that itself deserves attention if the voids created by the vanishing amount of solvent can effect the diffusion coefficient by a factor of more than five.

There are several reasons for looking for an explanation at a more fundamental level.

First, the pre-annealed sample does not support the solvent assumption made above. Second, we compared the diffusion profiles between dry samples and samples soaked in water before being annealed and no difference is observed. Finally, similar behavior is also observed in the computer simulation study performed by Jilge *et al.*[13] Jilge *et al.* used the percolation effect[14] to explain the anomalous behavior appearing in the single molecule diffusion but simply stated that the similar anomalous behavior of the chain molecules was the "consequence of the large size of the polymer coils". We think it is possible that the percolation effect also plays a role in polymer diffusion, although the source of obstacles comes from entanglement. Studies of single polymer diffusion in porous media using the percolation method gives an approximately 1/4 power time dependence regime for chain displacement larger than the size of the polymer.[15,16] Obviously an entangled polymer in a melt differs from a single polymer in a porous media in several ways. The distance between entanglement points is smaller than the size of the chain but the volume of the restricted space is small. The obstacles caused by the entanglement are not fixed but evolve with time. By using different lattice sizes for the obstacle and for the polymer and introducing correlation between the obstacles, it is possible to closely represent a polymer chain in a melt.

In Doi and Edwards theory, the tube a polymer chain is confined is quite wide, comparable to the entanglement length. Except for the analytical treatment, a chain with most part being able to make lateral motion except some far apart entangled points seems to be a better picture than a chain confined in a tube. One should not be surprised if the reptation model does not describe well the motion of polymers over small distances.

Whether the observed anomalous behavior is due to a yet unknown side effect or it

actually uncovers the inadequacy of the reptation model is not yet clear based on the information we have now. Temperature dependence measurements, measurements that use different solvent and polymer systems, and pre-annealing of shorter chain film should provide helpful hints. Nevertheless, this experiment demonstrated that the correct measurement of polymer diffusion is far more difficult than it sounds and at least some of the previously reported experiments need to be re-examined.

REFERENCES

1. P. G. de Gennes, *J. Chem. Phys.* **55,** 572 (1971).

2. M. Doi and S. F. Edwards, *J. Chem. Soc., Faraday Trans. II* **74,** 1789; 1802; 1818 (1978).

3. M. Doi and S. F. Edwards, *The Theory of Polymer Dynamics,* (Oxford University Press, Oxford, UK, 1986).

4. T. P. Lodge, N. A. Rotstein, and S. Prager, *Advances in Chemical Physics,* (Edited by I. Prigogine and S. A. Rice), Vol LXXIX, p1 (John Wiley & Sons, Inc., 1990).

5. A. Karim, A. Mansour, G. P. Felcher, and T. P. Russell, *Phys. Rev. B* **42,** 6846 (1990).

6. G. Reiter and U. Steiner, *J. Phys. II* **1,** 659 (1991).

7. W. W. Graessley, *J. Polym. Sci., Polym. Phys. Ed.* **18,** 27 (1980); W. W. Graessley, *Roy. Soc. Chem. Faraday Symposium* **18,** 1 (1984).

8. R. J. Composto, J. W. Mayer, E. J. Kramer, and D. M. White, *Phys. Rev. Lett.* **57,** 1312 (1986).

9. F. S. Bates and G. D. Wignall, *Phys. Rev. Lett.* **57,** 1429 (1986).

10. J. Crank, *The Mathematics of Diffusion,* 2nd ed. (Oxford University Press, New York, 1975).

11. M. L. Williams, R. F. Landel, and J. D. Ferry, *J. Am. Chem. Soc.* **77,** 3701 (1955).

12. D. J. Plazeck, *J. Phys. Chem.* **69,** 3480 (1965).

13. W. Jilge, I. Carmesin, K. Kremer, and K. Binder, *Macromolecules* **23,** 5001 (1990).

14. D. Stauffer and A. Aharony, *Introduction to Percolation Theory,* 2nd ed. (Taylor and Francis, London, 1991).

15. A. Baumgärtner, *Europhys. Lett.* **4,** 1221 (1987).

16. A. Baumgärtner and M. Muthukumar, *J. Chem. Phys.* **87,** 3082 (1987).

APPENDIX A

Numerical Solution of Diffusion Equation with Generalized Linear Boundary Condition

The diffusion equation with a composition dependent diffusion coefficient

$$\frac{\partial u}{\partial t} = \frac{\partial}{\partial x}\left[D(u)\frac{\partial u}{\partial x}\right] , \qquad \textbf{(A.1)}$$

and a generalized linear boundary condition

$$J(x=a) = -D\frac{\partial u}{\partial x}\bigg|_{x=a} = -S\phi(x=a,t) + RU_a + Q \qquad (a \in \{0, l\}) , \quad \textbf{(A.2)}$$

where U_a is the total mass flowed across each boundaries,

$$U_a(t) = -\int_0^t J(a,\tau)\,d\tau + U_a(0) \ , \tag{A.3}$$

is solved numerically in the following way. The values of u at $N+1$ discrete points equally spaced between the boundaries ($\Delta x = l/N$) are calculated. The *Crank-Nicholson*[1] differentiating scheme gives equation (A.6) in the following form

$$\begin{aligned}
&\frac{2(\Delta x)^2}{\Delta t}(u_{j,n+1}-u_{j,n}) = \\
&\frac{1}{2}\{[D(u_{j+1,n+1})+D(u_{j,n+1})](u_{j+1,n}-u_{j,n})-[D(u_{j-1,n+1})+D(u_{j,n+1})](u_{j,n}-u_{j-1,n})\} + \\
&\frac{1}{2}\{[D(u_{j+1,n})+D(u_{j,n})](u_{j+1,n+1}-u_{j,n+1})-[D(u_{j-1,n})+D(u_{j,n})](u_{j,n+1}-u_{j-1,n+1})\} \ .
\end{aligned} \tag{A.4}$$

where $u_{j,n}$, $j = 1, \ldots, N+1$, are the values of u at the jth point at the time $t = n\Delta t$ and $u_{j,n+1}$ are the values at $t = (n+1)\Delta t$. Substituting $D(u_{i,n+1})$ ($i = j$ or $j+1$) by

$$D(u_{i,n+1}) = D(u_{i,n}) + D'(u_{i,n})(u_{i,n+1}-u_{i,n}) \ , \tag{A.5}$$

eqn (A.6) can be linearized as

$$\begin{aligned}
&\left[D_{j-1/2}-\frac{1}{2}D'_{j-1,n}(u_{j,n}-u_{j-1,n})\right]u_{j-1,n+1} + \left[D_{j+1/2}-\frac{1}{2}D'_{j+1,n}(u_{j,n}-u_{j+1,n})\right]u_{j+1,n+1} + \\
&\left[-\frac{2(\Delta x)^2}{\Delta t}+\frac{1}{2}(u_{j+1,n}-2u_{j,n}+u_{j-1,n})D'_{j,n}-(D_{j+1/2}+D_{j-1/2})\right]u_{j,n+1} \\
&= \\
&-\frac{2(\Delta x)^2}{\Delta t}u_{j,n}-\left[D_{j+1/2}-\frac{1}{2}(u_{j+1,n}D'_{j+1,n}+u_{j,n}D'_{j,n})\right](u_{j+1,n}-u_{j,n})- \\
&\left[D_{j-1/2}-\frac{1}{2}(u_{j-1,n}D'_{j-1,n}+u_{j,n}D'_{j,n})\right](u_{j-1,n}-u_{j,n})
\end{aligned} \tag{A.6}$$

where $D_{j\pm1/2} = [D(u_{j,n}) + D(u_{j\pm1,n})]/2$ and $D'_{j,n} = D'(u_{j,n})$.

The boundary condition is incorporated into the *Crank-Nicholson* scheme in the following way: Given that u_0, u_1 are the u values at $x = 0$ and Δx respectively and

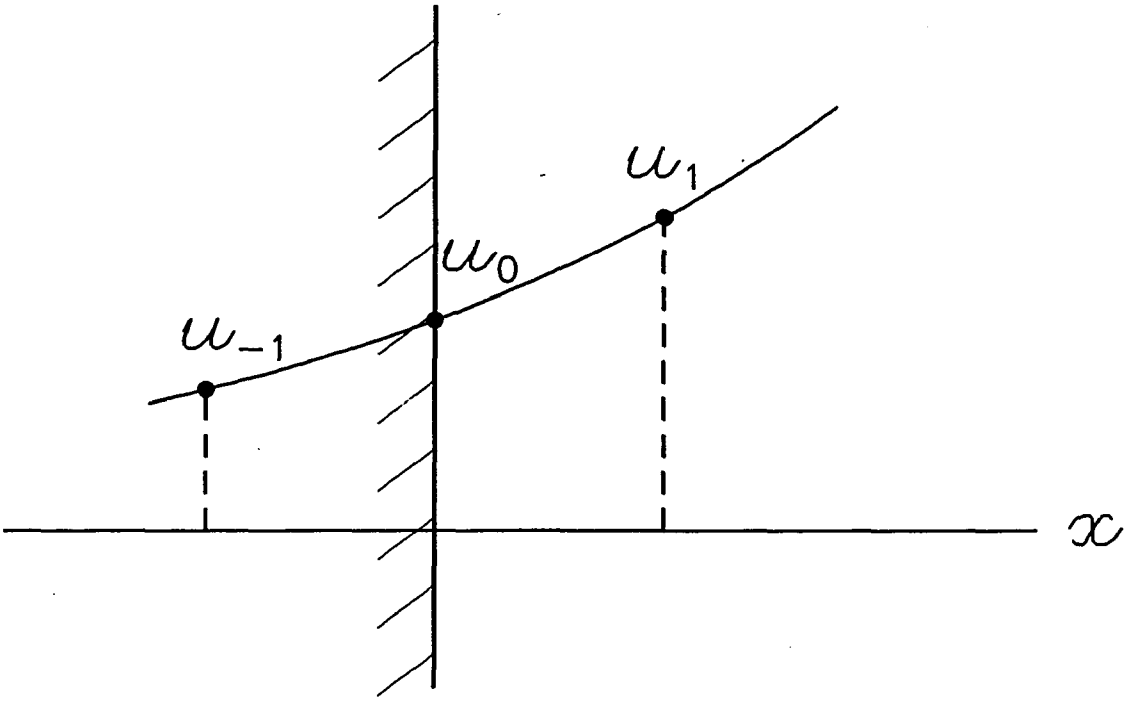

Figure A.1 An imaginary value u_{-1} across the boundary is used to write down appropriate equation for boundary condition.

assuming u_{-1} is the u value at the imaginary point across boundary, $x = -\Delta x$ (Figure A.1), that satisfies the boundary condition

$$D(u_{0,n})\frac{u_{1,n}-u_{-1,n}}{2\Delta x} = Su_{0,n} - RU_n - Q \ , \tag{A.7}$$

or

$$u_{-1,n} = u_{1,n} - \frac{2\Delta x}{D(u_{0,n})}(Su_{0,n}-RU_n-Q) \ , \tag{A.8}$$

the *Crank-Nicholson* formula (A.6) at the boundary ($j = 0$) becomes

$$\left[D_{-1/2}-\frac{1}{2}D'_{-1,n}(u_{0,n}-u_{-1,n})\right]\left[u_{1,n+1}-\frac{2\Delta x}{D_0}(Su_{0,n+1}-RU_{n+1}+Q)\right]+$$
$$\left[D_{1/2}-\frac{1}{2}D'_{1,n}(u_{0,n}-u_{1,n})\right]u_{1,n+1}+$$
$$\left[-\frac{2(\Delta x)^2}{\Delta t}+\frac{1}{2}(u_{1,n}-2u_{0,n}+u_{-1,n})D'_{0,n}-(D_{1/2}+D_{-1/2})\right]u_{0,n+1} \qquad \textbf{(A.9)}$$
$$=$$
$$-\left(\frac{2(\Delta x)^2}{\Delta t}\right)u_{0,n}-\left[D_{1/2}-\frac{1}{2}(u_{1,n}D'_{1,n}+u_{0,n}D'_{0,n})\right](u_{1,n}-u_{0,n})-$$
$$\left[D_{-1/2}-\frac{1}{2}(u_{-1,n}D'_{-1,n}+u_{0,n}D'_{0,n})\right](u_{-1,n}-u_{0,n})$$

Equations (A.6) and (A.9), together with the definition of U

$$\frac{U_{n+1}-U_n}{\Delta t}=S\left(\frac{u_{0,n+1}+u_{0,n}}{2}\right)-R\left(\frac{U_{n+1}+U_n}{2}\right), \qquad \textbf{(A.10)}$$

or

$$\left(1+\frac{R\Delta t}{2}\right)U_{n+1}-\left(\frac{S\Delta t}{2}\right)u_{0,n+1}=\left(1-\frac{R\Delta t}{2}\right)U_n+\left(\frac{S\Delta t}{2}\right)u_{0,n}+Q\,. \qquad \textbf{(A.11)}$$

constitutes a set of simultaneous linear equations which relates U_n and $u_{j,n+1}$ to U_n and $u_{j,n}$. The equation set is tri-diagonal and can be solved easily by the LU decomposition method.

REFERENCES

1. W. H. Press, B. P. Flannery, S. A. Teukolsky, and W. T. Vetterling, *Numerical Recipes: The Art of Scientific Computing*, Chapter 17 (Cambridge University Press, 1986); J. Crank, *The Mathematics of Diffusion*, 2nd ed. (Oxford University Press, New York, 1975).

APPENDIX B

Diffusion Equation with Time Dependent Diffusion Coefficient

A solution having the property of $x \sim t^{1/4}$ can be obtained from the diffusion equation

$$\frac{\partial \phi}{\partial t} = \frac{\partial}{\partial x}\left[D(\phi,t)\frac{\partial \phi}{\partial x}\right] , \tag{B.1}$$

with a phenomenological time dependence of $D(\phi,t)$ as

$$D(\phi,t) = \tilde{D}(\phi)\frac{1}{2\sqrt{t}} . \tag{B.2}$$

Performing a transformation of

$$\sqrt{t} \rightarrow \tau , \tag{B.3}$$

reduces eqn (B.1) to a diffusion equation with a time-independent diffusion coefficient, $D(u)$:

$$\frac{\partial \phi}{\partial \tau} = \frac{\partial}{\partial x}\left[\tilde{D}(\phi)\frac{\partial \phi}{\partial x}\right] . \qquad \textbf{(B.4)}$$

Any boundary condition must be modified accordingly. For a boundary in the form of

$$\frac{\partial z^*}{\partial t} = D(\phi,t)\frac{\partial \phi}{\partial x} = R\phi(0) - Sz^* \qquad \textbf{(B.5)}$$

multiplying τ to both sides of eqn (B.5), we obtain the boundary condition in terms of the new valuable τ as,

$$\frac{\partial z^*}{\partial \tau} = \tilde{D}(\phi)\frac{\partial \phi}{\partial x} = 2\tau R\phi(0) - 2\tau Sz^* \qquad \textbf{(B.6)}$$

The new boundary condition, equation (B.6), though "time" dependent, can easily be implemented to the *Crank-Nicholson* method discussed in Appendix A.

Bibliography

Anderson, H. H. and Ziegler, J. F., *Hydrogen Stopping Power and Ranges in all Elements* (Pergamon Press, New York, 1977).

Auroy, P., Auvray, L., and Leger, L., *Phys. Rev. Lett.* **66,** 719 (1991).

Ballard, D. G., Schelten, J., and Wignall, G. D., *Eur. Polym. J.* **9,** 965 (1973).

Bartell, L. S. and Roskos, R. R., *J. Chem. Phys.* **44,** 457 (1966).

Bates, F. S. and Wignall, G. D., *Macromolecules* **19**, 932 (1986).

Bates, F. S. and Wignall, G. D., *Phys. Rev. Lett.* **57,** 1429 (1986).

Baumgärtner, A., *Europhys. Lett.* **4,** 1221 (1987).

Baumgärtner, A. and Muthukumer, M., *J. Chem. Phys.* **87,** 3082 (1987).

Briggs, D and Hearn, M. J., *Vacuum* **36,** 1005 (1986).

Cohen, M. S. and Muthukumar, M., *J. Chem. Phys.* **90**, 10 (1989).

Composto, R. J., Mayer, J. W., Kramer, E. J., and White, D. M., *Phys. Rev. Lett.* **57,** 1312 (1986).

Cosgrove, T., Heath, T., van Lent, B., Leermakers, F., and Scheutjens, J., *Macromolecules* **20,** 1692 (1987).

Cosgrove, T., *J. Chem. Soc. Faraday Trans.* **86(9),** 1323 (1990).

Cotton, J. P., Decker, D., Benoit, H., Farnowx, B., Higgins, J., Jannick, G., Ober, R., Picot, C., and des Cloizeaux, J., *Macromolecules* **7,** 863 (1974).

Crank, J., *The Mathematics of Diffusion,* 2nd ed. (Oxford University Press, New York, 1975).

de Gennes, P. G., *J. Chem. Phys.* **55,** 527 (1971).

de Gennes, P. G., *Scaling Concepts in Polymer Physics,* (Cornell University Press, Ithaca, N. Y. 1979).

des Cloizeaux, J. and Jannick, G., *Polymers in Solution: Their Modelling and Structure,* (Oxford University Press, New York, 1990).

DiMarzio, E. A. and McCrackin, F. L., *J. Chem. Phys.* **43,** 539 (1965).

Doi, M. and Edwards, S. F., *J. Chem. Soc., Faraday Trans. II* **74,** 1789 (1978).

Doi, M. and Edwards, S. F., *J. Chem. Soc., Faraday Trans. II* **74,** 1802 (1978).

Doi, M. and Edwards, S. F., *J. Chem. Soc., Faraday Trans. II* **74,** 1818 (1978).

Doi, M. and Edwards, S. F., *The Theory of Polymer Dynamics,* (Oxford University Press, Oxford, UK, 1986).

Doolittle, L. R., *Nucl. Intr. and Meth.* **B9,** 344 (1985).

Feldman, L. C. and Mayer, J. W., *Fundamentals of Surface and Thin Film Analysis* (North-Holland, New York, 1986).

Fetters, L. J., Graessley, W. W., Hadjichristidis, N., Kiss, A. D., Pearson, D. S., and Younghouse, L. B., *Macromolecules* **21,** 1644 (1988).

Flory, P., *J. Chem. Phys.* **17,** 303 (1949).

Flory, P., *Principles of Polymer Chemistry,* (Cornell University Press, Ithaca, N. Y. 1971).

Fox, T. G., Jr. and Flory, P. J., *J. Appl. Phys.* **21,** 581 (1950).

Gnaser, H., Hutcheon, I. D., *Phys. Rev. B* **35,** 877 (1987).

Gokan, H., Esho, S., and Ohnishi, Y., *J. Electrochem. Soc.* **130,** 143 (1983).

Graessley, W. W., *J. Polym. Sci., Polym. Phys. Ed.* **18,** 27 (1980).

Graessley, W. W., *Roy. Soc. Chem. Faraday Symposium* **18,** 1 (1984).

Green, P. F. and Kramer, E. J., *J. Mater. Res.* **1,** 202 (1986).

Green, P. F. and Kramer, E. J., *Macromolecules* **19,** 1108 (1986).

Green, P. F. and Doyle, B. L., *Phys. Rev. Lett.* **57,** 2407 (1986).

Hadziioznnou, G., Patel, S., Granick, S., and Tirrell, M., *J. Am. Chem. Soc.* **108,** 2869 (1986).

Halperin, A., *Europhys. Lett.* **8,** 351 (1989).

Halperin, A., *Macromolecules* **22,** 2403 (1989).

Hesslink, F. Th, *J. Phys. Chem.* **73,** 3488 (1969).

Jilge, W., Carmesin, I., Kremer, K., and Binder, K., *Macromolecules* **23,** 5001 (1990).

Jones, R. A. L., Kramer, E. J., Rafailovich, M. H., Sokolov, J., and Schwarz, S. A., *Phys. Rev. Lett.* **62,** 280 (1989).

Jones, R. A. L., Norton, L. J., Kramer, E. J., Composto, R. J., Stein R. S., Russell, T. P., Mansour, A., Karein, A., Felcher, G. P., Rafailovich, M. H., Sokolov, J., Zhao, X., and Schwarz, S. A., *Europhys. Lett.* **12,** 41 (1991).

Karim, A., Mansour, A., Felcher, G. P., and Russel, T. P., *Phys. Rev. B* **42,** 6846 (1990).

Kirste, R. G., Kruse, W. A., and Schlten, J., *Makromol. Chem.* **162,** 299 (1973).

Kramer, E. J., Green, P. F., and Palmstrøm, C. J., *polymer* **25,** 473 (1984).

Kramer, E. J., *Physica B* **173,** 189 (1991).

Kwon, O 'D., Beaglehole, D., Webb, W. W., Widom, B., Schmidt, J. W., Cahn, J. W., Moldover, M. R., and stephenson, B., *Phys. Rev. Lett.* **48,** 185 (1982)

Ligoure C. and Leibler, L., *J. Phys.* France **51,** 1313 (1990).

Lodge, T. P., Rotstein, N. A., and Prager, S., *Advances in Chemical Physics, Vol LXXIX,* Edited by Prigogine, I. and Rice, S. A. (John Wiley & Sons, Inc., 1990).

Mackor, E. L., *J. Colloid Sci.* **6,** 492 (1951).

Mackor, E. L. and van der Walls, J. H., *ibid.* **7,** 535 (1952).

Meier, D. J., *J. Phys. Chem.* **71,** 1861 (1967).

Mills, P. J., Green, P. F., Palmstrøm, C. J., Mayer, J. M., and Kramer, E. J., *Appl. Phys. Lett.* **45,** 957 (1984).

Milner, S. T., Witten, T. A., and Cates, M. E., *Macromolecules* **21,** 2610 (1988).

Milner, S. T., *Science* **22,** 905 (1991).

Milner, S. T., *Macromolecules* **25,** 5487 (1992).

Moelwyn-Hughes, E. A., *Physical Chemistry,* (Pergamon Press, 1964).

Moldover, M. R. and Cahn, J. W., *Science* **207,** 1073 (1980).

Muthukumar, M. and Ho, J. S., *Macromolecules* **22,** 965 (1989).

Nakanishi, H. and Pincus, P., *J. Chem. Phys.* **79,** 977 (1983).

Patel, S. S. and Tirrell, M., *Ann. Rev. Phys. Chem.* **40,** 579 (1989).

Plazeck, D. J., *J. Phys. Chem.* **69,** 3480 (1965).

Pohl, D. W. and Goldburge, W. I., *Phys. Rev. Lett.* **48,** 1111 (1982).

Press, W. H., Flannery, B. P., Teukolsky, S. A., and Vetterling, W. T., *Numerical Recipes: The Art of Scientific Computing,* (Cambridge University Press, 1986).

Rafailovich, M. H., Sokolov, J., Zhao, X., Jones, R. A. L., and Kramer, E. J., *Hyperfine Interact.* **62,** 45 (1990).

Russell, T. P., Deline, V. R., Wakharkar, V. S., and Goulon, G., *Bulletin Mater. Res. Soc.* October, 33 (1989).

Schmidt, I. and Binder, K., *J. Phys.* **46,** 1631 (1985).

Schwarz, S. A., *J. Vac. Sci. Tech. A* **5,** 308 (1987).

Shull, K. R., *J. Chem. Phys.* **94,** 5723 (1991).

Sillescu, H., *Makromol. Chem., Rapid Commun.* **5,** 519 (1984).

Soedervall, O., Odelius, H., Lodding, A., and Engstroem, E. U., *Scanning Mirosc.* **1,** 471 (1987).

Sokolov, J., Rafailovich, M. H., Jones, R. A. L., and Kramer, E. J., *Appl. Phys. Lett.* **54,** 590 (1989).

Stauffer, D. and Aharony, A., *Introduction to Percolation Theory,* 2nd ed. (Taylor and Francis, London, (1991).

Reiter, G. and Steiner, U., *J. Phys. II* **1,** 659 (1991).

Tauton, J. H., Toprakcioglu, C., Fetters, L. J., and Klein, J., *Nature* **333,** 712 (1988).

van Kampen, N. G., *Stochastic Processes in Physics and Chemistry,* (North-Holland, Amsterdam, The Netherland, 1987).

Whitlow, S. J. and Wool, R. P., *Macromolecules* **22,** 2648 (1989).

Williams, D. E. and Davis, L. E., *Characterization of Metal and Polymer Surfaces* (Edited by Lee, L. H.), vol 2, P53, (Academic Press, New York, 1977).

Williams, M. L., Landel, R. F., and Ferry, J. D., *J. Am. Chem. Soc.* **77,** 3701 (1955).

Ziegler, J. F., *Helium stopping powers and ranges in all Elements* (Pergamon Press, New York, 1977).

Autobiography

Xiaofeng Zhao was born in Autumn of 1965. He grew up in the beautiful towns of Choucheng and Puyan, located in the centre of Zhejiang province of the People's Republic of China.

Zhao's father is a teacher of literature, linguistics and logic. His mother also teaches literature and history in high school. The family has a vast collection of books in these areas. Reasoning is made fun by his father through interesting problems. His very caring mother always tries to explain something using her limited scientific knowledge (and the explanation is more often incorrect, but, she is really good at geometry). They are always proud of their son and always encourage him to do better. Because of this, the spirit of confidence and continuous pursuit is deeply implanted in their son's mind. In those times when important decision were to be made, the parents were always there

and gave wise suggestions so that one never had regrets. It is a luxury to be brought up in a family like this, being loved, understood, encouraged but never being pushed.

In September 1982, Xiaofeng Zhao went to the college in Zhejiang University, Hangzhou, one of the leading polytechnic institutes in China, majoring in physics. There was a small, but very competitive student group in physics. The academic standard is highly upheld by the physics department faculty members. Students are encouraged and sometimes required to study subjects considered as at the graduate level in most other universities. Excelling in a competitive examination, Zhao was admitted to Queens College of the City University of New York. On August 20, 1986, he flew across the Pacific Ocean to the United States of America.

Queens College provided a unique opportunity for Zhao to improve his English and learn to communicate with students as a teacher and to interact with professors as a student. Zhao spent his years of graduate study doing experimental research in polymer physics under the supervision of Professor Miriam H. Rafailovich and Dr Jonathan C. Sokolov. His research work is summarized in this thesis.

Also in Queens College, he met Weizhong Zhao, who was at the time also a graduate student from China studying in Queens College towards her doctoral degree in physics. She later joined the same research group and they worked together very well in a lot of experiments. Two years after they met, she became his wife on October 26, 1990.

Zhao is interested in classical and rock music, hanging out together with friends and he is fond of spicy chinese food. What he likes most is reading. This might be inherited from his parents or learned from his older sister. He also has talent in painting.